THE UNIVERSITY OF CHICAGO

# TUMOR SUPPRESSIVE FUNCTIONS OF BNIP3

A DISSERTATION SUBMITTED TO

THE FACULTY OF THE DIVISION OF THE BIOLOGICAL SCIENCES

AND THE PRITZKER SCHOOL OF MEDICINE

IN CANDIDACY FOR THE DEGREE OF

DOCTOR OF PHILOSOPHY

COMMITTEE ON CANCER BIOLOGY

BY

APARAJITA HOSKOTE CHOURASIA

CHICAGO, ILLINOIS

JUNE 2016

DEDICATION

To my beloved parents, Madhu and Anil Hoskote (1940–2013).

To my dearest husband, Amit Chourasia.

TABLE OF CONTENTS

List of Figures……...ix

Acknowledgements……xii

Abbreviations……..xiv

Abstract……...xvii

1. INTRODUCTION……..1

Mitochondrial dysfunction in cancer……..1

BNIP3: function, regulation and role in cancer……..12

Overview of breast cancer and pancreatic ductal adenocarcinoma mouse models……19

2. MATERIALS AND METHODS……24

Mice……..24

Genotyping……..25

Cell lines and Tissue culture……26

Reagents……..28

Stable overexpression……...28

Stable knockdowns……29

Growth curves……29

Three-dimensional spheroid assay……..29

Immunofluorescence……..30

Quantitative PCR……30

Protein extraction……32

Immunoblotting……33

Histology and Immunohistochemistry……33

Antibodies……33

Flow cytometry……34

Transmission electron microscopy……..35

Magnetic Resonance Imaging (MRI)/microPET/CT Imaging……..35

Metabolomics analyses……35

Measurement of oxygen consumption rate……37

ATP Assay……...37

The Cancer Genome Atlas (TCGA) and other human data……38

Statistical Analysis……38

3. BNIP3 LOSS INCREASES PRIMARY MAMMARY TUMOR GROWTH, INVASION AND INCIDENCE OF LUNG METASTASES IN MMTV-PYMT MOUSE MAMMARY TUMOR MODEL……...39

Introduction……..39

Loss of BNip3 increases primary tumor growth *in vivo* and tumor cell proliferation *in vitro*……...41

Loss of BNip3 promotes primary tumor cell migration and invasion *in vitro*…….48

BNip3 null mice exhibit accelerated lung metastasis with significantly reduced latency……..52

BNIP3 is deleted in human triple negative breast cancer……54

Conclusion……...56

4. LOSS OF BNIP3 LEADS TO DYSFUNCTIONAL MITOCHONDRIA AND DEREGULATED TUMOR CELL METABOLISM……..57

Introduction……..57

BNip3 null tumor cells have reduced mitophagy……...58

Loss of BNip3 is associated with increased mitochondrial mass *in vitro* and *in vivo*……62

BNip3 null tumor cells exhibit reduced mitochondrial function……69

Loss of BNip3 is associated with increased glucose uptake and aerobic glycolysis *in vitro* and *in vivo*……72

BNip3 null tumor cells have markedly reduced oxidative metabolism……...79

Conclusion……...81

5. INCREASED ROS PRODUCTION IN BNIP3 NULL TUMORS CONTRIBUTES TO HIF STABILIZATION……...82

Introduction……..82

Loss of BNip3 is associated with increased Hif-1α levels and activity *in vitro* and *in vivo*…….....83

Loss of BNip3 is associated with increased levels of ROS *in vitro* and *in vivo*…92

Treatment of BNip3 null mice with BHA reduces ROS associated levels of Hif-1α, tumor growth and metastasis……96

Conclusion……101

6. BNIP3 NULL TUMOR CELLS RELY ON AUTOPHAGY FOR SURVIVAL……102

Introduction……102

Inhibition of glycolysis with 2DG treatment reduces cell growth in BNip3 null tumor cells……103

Inhibition of glycolysis and autophagy with 2DG and bafilomycin increases cell death in BNip3 null tumor cells……..105

Conclusion……109

7. BNIP3 LOSS INCREASES PRIMARY TUMOR GROWTH AND REDUCES LATENCY OF LIVER AND LUNG METASTASIS IN PDX-1-CRE;LSL-KRASG12D MOUSE MODEL OF PDAC……110

Introduction……110

Generation of BNip3 null mice in PDX-1-Cre;LSL-$KRAS^{G12D}$ mouse model…..111

Loss of BNip3 increases tumor growth and reduces overall survival *in vivo*…..112

BNip3 loss reduces latency of lung metastasis……...121

Conclusion……123

8. LOSS OF BNIP3 INCREASES CELL GROWTH AND IS ASSOCIATED WITH INCREASED C-MYC PROTEIN LEVELS IN HUMAN PANCREATIC CANCER CELL LINES……..124

Introduction……124

Exogenous expression and stable knockdown of BNIP3 in human pancreatic cancer cell lines……125

BNIP3 reduces cell growth and c-Myc levels in pancreatic cancer cell lines independent of its mitophagy function……..130

BNIP3 associated decrease in c-Myc protein level is not transcriptionally regulated……137

Conclusion……142

9. DISCUSSION……...143

References……153

LIST OF FIGURES

Figure 1. Mitochondrial ROS generated by electron transport chain……3

Figure 2. Schematic summary of autophagy……6

Figure 3. Schematic summary of regulation of BNIP3……..16

Figure 4. Loss of BNip3 protein expression during mammary tumor progression in MMTV-PyMT mice……..42

Figure 5. BNip3 protein expression in wild-type and BNip3 null mammary tumors..43

Figure 6. Loss of BNip3 promotes mammary tumor growth……43

Figure 7. Loss of BNip3 increases growth rate of primary mammary tumor cells…45

Figure 8. Loss of BNip3 increases proliferation of primary mammary tumor cells…47

Figure 9. Loss of BNip3 does not affect cell survival……47

Figure 10. Loss of BNip3 promotes early progression to carcinoma……49

Figure 11. Loss of BNip3 promotes migration and invasion in vitro……..50

Figure 12. Loss of BNip3 promotes growth in 3D……51

Figure 13. Loss of BNip3 increases lung metastases……53

Figure 14. BNip3 is deleted in human triple negative breast cancer……55

Figure 15. Loss of BNip3 decreases mitophagy in MECs……..60

Figure 16. Loss of BNip3 increases mitochondrial mass in MECs……63

Figure 17. Loss of BNip3 increases mitochondrial mass in mammary tumors……65

Figure 18. Loss of BNip3 increases mitochondrial mass in MECs……67

Figure 19. Transmission electron micrographs of wild-type and BNip3 null primary tumors……..68

Figure 20 BNip3 null mammary tumor cells exhibit reduced mitochondrial function.....71
Figure 21 BNip3 loss increases glucose uptake and lactate output……74
Figure 22 Loss of BNip3 induces aerobic glycolysis in MECs……..76
Figure 23 Loss of BNip3 induces aerobic glycolysis in MECs……..78
Figure 24 Loss of BNip3 suppresses oxidative phosphorylation in MECs……..80
Figure 25 Loss of BNip3 increases Hif-1α levels……85
Figure 26 Loss of BNip3 promotes Hif-1α activity……...87
Figure 27 BNip3 loss promotes angiogenesis……88
Figure 28 Echinomycin treatment reduces cellular growth rate and Hif-1α activity in BNip3 null MECs……90
Figure 29 BNIP3 loss predicts reduced metastasis free survival in TNBC……91
Figure 30 Loss of BNip3 increases levels of ROS in mammary tumors……..93
Figure 31 BNip3 loss increases levels of ROS *in vitro*……...95
Figure 32 Effect of BHA diet on BNip3 null tumor growth and metastasis……..97
Figure 33 Effect of BHA diet on BNip3 null tumors……98
Figure 34 BHA diet supplementation reduces Hif-1α activity in BNip3 null tumors……100
Figure 35 BNip3 null MECs do not rely on glycolysis for survival……..104
Figure 36 Analysis of autophagy in wild-type and BNip3 null mammary tumors….106
Figure 37 BNip3 null MECs exhibit increased dependency on autophagy for survival……...108

Figure 38 Immunohistochemical analysis of 3 month old wild-type and BNip3 null pancreas……113

Figure 39 Immunohistochemical analysis of 4.5 month old wild-type and BNip3 null pancreas……117

Figure 40 BNip3 loss reduces survival in PDX1-Cre;LSL-$KRAS^{G12D}$ mice……...120

Figure 41 BNip3 loss reduces latency of lung metastasis in PDX1-Cre;LSL-$RAS^{G12D}$ mice…….....122

Figure 42 BNIP3 expression in human pancreatic cancer cell lines……..126

Figure 43 Generation of MiaPaca-2 cell lines stably expressing empty-vector control and wild-type BNIP3……128

Figure 44 Generation of CFPAC-1 cell lines with stable knockdown of BNIP3……129

Figure 45 BNIP3 reduces cellular growth rate, but not via mitophagy……..131

Figure 46 BNIP3 reduces cellular growth rate……...132

Figure 47 Loss of BNIP3 promotes c-Myc activity……134

Figure 48 Loss of BNIP3 promotes c-Myc protein levels……136

Figure 49 c-Myc is not transcriptionally regulated by BNIP3……..138

Figure 50 BNIP3 promotes proteasomal degradation of c-Myc……..140

Figure 51 BNIP3 does not promote proteasomal degradation of c-Myc via phosphorylation at Threonine58……141

Figure 52 Schematic summary of the role BNIP3 in suppressing tumor progression and metastasis in the MMTV-PyMT mouse model of mammary tumorigenesis……149

ACKNOWLEDGEMENTS

I would like to begin by thanking my advisor, Dr. Kay Macleod, who has been extremely supportive of me as a graduate student. She has led by example and highlighted the importance of critical thinking and evaluation in research, be it of articles published in peer-reviewed journals or of our own data in the lab. I am grateful for her encouragement, especially during the difficult days that are an inevitable part of graduate school. I appreciate her belief in me in allowing me to delve into different projects while simultaneously guiding me as needed. I would also like to thank my thesis committee members, Dr. Geoffrey Greene, Dr. Hedy Kindler and Dr. Donald Vander Griend, who helped me to identify and address the most relevant questions in my thesis projects.

I would like to thank the administrative staff of the Biomedical Sciences Cluster and the Ben May Department for Cancer Research as well as the scientific staff at the Human Tissue Resource Center, the microscopy core facility and the biophysics core facility for all their technical assistance.

I want to thank my classmate, Daniel Rabe, for being a great friend throughout the last five years. I also want to thank my peers, Marina Sharifi, Michelle Boland, Lauren Drake, Erin Mowers and Maya Springer, all of who started out as labmates, but ended up becoming great friends over time. I really appreciate their love and sisterly support, especially when I was pregnant with my daughter, Aria. They made my long days in lab so much more comfortable by being there for me whenever I needed any help. I am truly grateful and will cherish their friendships for life.

Last, but not the least, I want to thank my family. I thank my parents for bringing me up with great belief in my abilities. I have always looked up to my mother as a role model and admired her grit in the toughest of situations in life. I have admired my father for the passion with which he brought up his children and the courage with which he fought a long and arduous battle with multiple myeloma. Their virtues have given me the strength and resolve to regroup myself in difficult times, especially in the last few years of graduate studies. As I complete my Ph.D. dissertation and prepare to graduate, I feel relieved that I have been able to fulfill my father's last wish. I would also like to thank my mother-in-law and father-in-law for their keen interest in my thesis project and encouragement throughout the last five years.

I would like to end by thanking my husband, Amit, who has been my pillar of strength during my graduate school journey. It is said that behind every successful man there is a woman. However, I would like to acknowledge that behind all of my achievements in the last five years, I have had the unflinching support of my husband. From working remotely from Chicago, giving me academic advice, to taking care of all home chores so that I could focus on my research, his contribution towards my goals has been immense. I will be eternally grateful to him for making this a truly memorable journey.

# ABREVIATIONS

| | |
|---|---|
| ALT | alternative lengthening of telomeres |
| AMPK | AMP dependent kinase |
| ATG | autophagy related |
| BNIP3 | Bcl-2/adenovirus E1B 19-kDa-interacting protein 3 |
| COX | cytochrome oxidase |
| CREB | cAMP response element binding protein |
| CSC | cancer stem cell |
| CSF-1 | colony stimulating factor-1 |
| CYTB | cytochrome b |
| Cyt c | cytochrome c |
| DCIS | ductal carcinoma *in situ* |
| ER | estrogen receptor |
| ERK | extracellular signal regulated kinase |
| ERR$\alpha$ | estrogen related receptor alpha |
| ERR$\beta$ | estrogen related receptor beta |
| ERR$\gamma$ | estrogen related receptor gamma |
| GCN5 | histone acetyltransferase |
| HIF-1 | hypoxia inducible factor-1 |
| IHC | immunohistochemistry |
| LC-MS | liquid chromatography–mass spectrometry |
| MEK | mitogen activated protein kinase kinase (MAPK kinase) |

| | |
|---|---|
| Mfn-2 | mitofusin2 |
| MIN | mammary intraepithelial neoplasia |
| MITF | melanocyte-specific transcription factor |
| MRI | magnetic resonance imaging |
| mtDNA | mitochondrial DNA |
| mTOR | mammalian target of rapamycin |
| ND1 | NADH dehydrogenase subunit 1 |
| NMR | nuclear magnetic resonance |
| NRF1 | nuclear respiratory factor 1 |
| NRF2 | nuclear respiratory factor 2 |
| OXPHOS | oxidative phosphorylation |
| PanIN | pancreatic intraepithelial neoplasia |
| PDAC | pancreatic ductal adenocarcinoma |
| PE | phosphatidylethanolamine |
| PET/CT | positron emission tomography/ computed tomography |
| PGC-1$\alpha$ | PPAR$\gamma$ co-activator-1 alpha |
| PGC-1$\beta$ | PPAR$\gamma$ co-activator-1beta |
| PI3P | phosphatidylinositol-3-phosphate |
| PKA | protein kinase A |
| POLRMT | mitochondrial RNA polymerase |
| PPAR$\alpha$ | peroxisome-proliferator activator receptor alpha |
| PPAR$\delta$ | peroxisome-proliferator activator receptor delta |
| PPAR$\gamma$ | peroxisome-proliferator activator receptor gamma |

| | |
|---|---|
| PR | progesterone receptor |
| PRC | PGC-1 related co-activator |
| qRT-PCR | quantitative real-time PCR |
| ROS | reactive oxygen species |
| SOD | superoxide dismutase |
| TCA | tricarboxylic acid cycle |
| Tfam | mitochondrial transcription factor A |
| TFB1M | mitochondrial transcription factor B1 |
| TFB2M | mitochondrial transcription factor B2 |
| TOM20 | translocase of outer membrane 20 |
| ULK1 | unc-51-like autophagy-activating kinase 1 |
| Vdac1 | voltage-dependent anion channel-1 |
| VEGF | vascular endothelial growth factor |
| YY1 | yin yang 1 |

# ABSTRACT

BNIP3 is a mitochondrial protein that targets mitochondria for autophagosomal degradation or mitophagy. It is induced under physiological stresses such as hypoxia and nutrient starvation and functions to eliminate damaged mitochondria in order to maintain the overall mitochondrial integrity of the cell. BNIP3 is a bona fide HIF-1 target and is also regulated by RAS, pRB/E2F, p53, NFκB and FoxO3. While BNIP3 is up-regulated at pre-malignant stages of various human cancers including DCIS and PanINs, it is down-regulated by deletion or promoter hypermethylation in invasive breast cancer, PDAC, hematological malignancies, hepatocellular carcinoma, gastric and lung cancer, thus indicating that loss of BNIP3 may be critical to disease progression. However, while the role of BNIP3 in mitophagy has been well characterized, its function in tumor initiation and progression is not well understood.

In order to assess the function and mechanism of BNip3 in tumor growth and progression to metastasis, we crossed BNip3 null mice to MMTV-PyMT mouse model of mammary tumorigenesis and the PDX1-Cre;LSL-KRAS$^{G12D}$ mouse model of pancreatic tumorigenesis. Our results show that loss of BNip3 significantly promotes primary tumor growth and metastasis in both tumor models, demonstrating that BNip3 functions to suppress tumor progression to metastasis. BNip3 null mammary tumor cells exhibit significantly reduced mitophagy with a concomitant increase in dysfunctional mitochondria. While loss of BNip3 results in significant increase in mitochondrial mass, it reduces mitochondrial function and oxidative metabolism. However, BNip3 null mammary tumor cells show significantly elevated levels of glycolysis, indicating that

defective mitochondria due to inefficient mitophagy can induce the Warburg effect. Notably, loss of BNip3 increases levels of ROS, which in turn promotes stabilization and activity of Hif-1$\alpha$, thus demonstrating that BNip3 applies brakes on Hif-1$\alpha$ levels and activity in mammary tumor cells. We also show that BNip3 null mammary tumor cells rely on autophagy for survival, thus highlighting that effects of mitophagy inhibition are not the same as effects of inhibition of global autophagy.

In the pancreatic tumor model, we show that loss of BNip3 increases primary tumor growth and reduces the latency to metastasis as well as overall survival. Using human pancreatic cancer cell lines, we also show that BNIP3 reduces cell growth, which is associated with reduced levels of c-Myc protein. However, the effect of BNIP3 on c-Myc is independent of its function of mitophagy. Overall, we have shown that BNip3 functions as tumor suppressor that inhibits progression to metastasis by mitophagy dependent and mitophagy independent pathways.

# INTRODUCTION

## 1.1. Mitochondrial dysfunction in cancer

In 1927, Otto Warburg had observed that cancer cells exhibited aerobic glycolysis in comparison to normal cells in the body, thus bringing mitochondrial metabolism to the forefront of cancer research (1,2). However, 80 years since his discovery, a lot of work has been done to understand the role of mitochondria in cancer with emphasis on mutations in mitochondrial genome, mitochondrial enzymatic defects, ROS production, oncogenic regulation of mitochondrial function and mitochondrial retrograde signaling (3-17). Our current understanding highlights that no single bioenergetic change is common to all cancers and just as there are tumor cells that rely on aerobic glycolysis (now also known as “Warburg effect”), there are those that depend equally on functional oxidative metabolism (18-20).

Mitochondria, known as “powerhouses” of the cell are key to energy production and cellular metabolism (21,22). Mitochondria are composed of two highly specialized and functionally distinct membranes, the outer mitochondrial membrane (OMM) and the inner mitochondrial membrane (IMM), which together create the intermembrane space (IMS) and the mitochondrial matrix. The OMM consists of large number of transport proteins called porins that are permeable to molecules of 5000 daltons or less, including small proteins. On the other hand, the IMM is highly selective to movement of molecules, permeable mainly to molecules that are required for the TCA cycle, beta-oxidation and OXPHOS in the matrix and at the IMS. The mitochondrial matrix is also home to a circular genome made up of mtDNA that comprises of 16,569 base pairs and

is organized into nucleoids. Each mitochondrion can have thousands of copies of mtDNA that encode for 13 OXPHOS proteins, 22 tRNAs, and 12S and 16S rRNAs.

Mitochondria have diverse functions including ATP generation, modulation of redox status, generation of ROS, generation of biosynthetic precursors, regulation of calcium levels and initiation of apoptosis. One function that is the most integral to the cell is generation of ATP via OXPHOS. The same process also generates ROS, which are known to have physiological (cell proliferation and differentiation) and pathophysiological (lipid peroxidation, DNA damage, protein modification) consequences (23).

Mitochondrial ROS and HIF

Mitochondrial electron transport chain is the dominant source of ROS in cells. In the TCA cycle, oxidation of acetyl CoA results in generation of NADH and $FADH_2$. During OXPHOS, NADH and $FADH_2$ transfer electrons to complex I and II of the electron transport chain, respectively, from where they are transferred to complex III and are ultimately used to reduce molecular oxygen to water at complex IV (Figure 1). During this process, there is a simultaneous extrusion of protons from the mitochondrial matrix into the IMS that produces an electrochemical gradient required for generation of ATP by complex V. However, electrons in complex I, II and III can prematurely reduce oxygen to form superoxide anions (24). ROS exist in other forms including hydrogen peroxide, hydroxyl radicals and hypochlorus acid and can also be generated by other systems including NADPH oxidase complex, lipoxygenase, cycloxygnase and peroxisomes in cells. While some amounts of ROS exist in cells under normal

physiological conditions, there is a propensity for their levels to increase in rapidly proliferating cells owing to the dramatic increase in oxygen demand and ATP. Increased levels of ROS are seen also due to reduced scavenging of ROS as well as due to oncogene induced replicative stress (22,25).

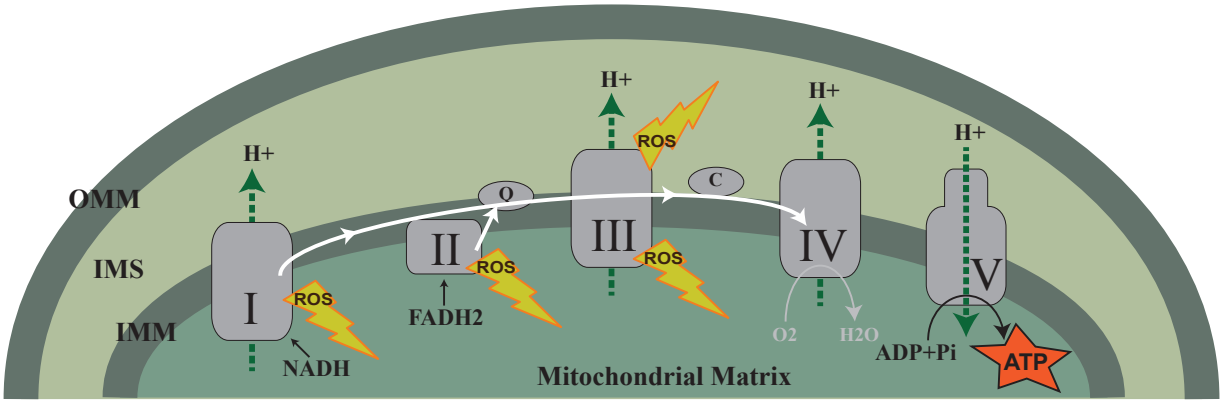


**Figure 1. Mitochondrial ROS generated by electron transport chain.** NADH and $FADH_2$ transfer electrons to the electron transport chain at complex I and II, respectively. Electrons are then transferred via ubiquinone (Q) to complex III, which transfers them to complex IV via cytochrome c (C). At complex IV, the electrons reduce molecular oxygen to water. Protons are extruded from the mitochondrial matrix into the intermembrane space (IMS) generating a proton motive force required for generation of ATP from ADP and inorganic phosphate (Pi) by complex V or ATP synthase. Superoxide anions (ROS) generated by incomplete reduction of molecular oxygen at complex I and II are released into the mitochondrial matrix while ROS generated at complex III are released into the matrix as well as IMS.

Tumor cells adapt to high levels of ROS by reprograming their metabolism and a key way in which they do so is by increasing levels of HIF-1 (26-28). Under conditions of low oxygen, HIF-1$\alpha$ gets stabilized as it escapes hydroxylation by prolyl hydroxylases and its subsequent proteasomal degradation by von Hippel-Lindau protein (pVHL). Stabilized HIF-1$\alpha$ can then translocate to the nucleus where together with HIF-1$\beta$, it modulates gene expression for several targets involved in processes including cellular metabolism, angiogenesis, invasion and metastasis, epithelial to mesenchymal transition and mitophagy. Key metabolic targets of HIF-1$\alpha$ are glucose transporter, hexokinase, pyruvate dehydrogenase kinase, phosphofructokinase, and lactate dehydrogenase, all of which are involved in glycolysis (29). Thus elevated levels of HIF-1$\alpha$ often result in increased aerobic glycolysis, which supports tumor cells in meeting their energy demand under conditions of oxygen stress (30). HIF-1$\alpha$ also induces expression of angiopoietins and VEGF, which promote angiogenesis in order to overcome the oxygen depletion (31,32). Interestingly, HIF-1$\alpha$ also induces expression of BNIP3 and BNIP3L (herein, NIX) that target mitochondria for autophagosomal degradation, thus limiting ROS in cells (22). However, while the role of VEGF, angiopoietins and metabolic targets of HIF are well defined in tumor progression, not much is known about the role of BNIP3 in tumor initiation and progression and thus, will be the main focus of this study.

Mitophagy

Macroautophagy (herein, autophagy) is a self-degradative process in which cytosolic cargo is sequestered within double-membraned vesicles called

autophagosomes and degraded upon fusion with the lysosome (Figure 2). Autophagosomes originate from nucleation and expansion of phagophores that are derived mainly from the endoplasmic reticulum, but may also be derived from mitochondria or the Golgi apparatus (33,34). A “preinitiation” complex or the ULK complex consists of ULK1, FIP200 and ATG13 activates the “initiation” complex or the class III PI3K kinase (VPS34) complex including VPS34 and Beclin1 to produce PI3P which is an essential lipid for phagophore biogenesis. Phagophore initiation is followed by an elongation reaction that consists of maturation of the growing phagophore and eventual closure of the double-membrane structure called autophagosome. The elongation reaction relies on ubiquitin-like protein conjugation systems involving E1and E2 ligases that catalyze conjugation of ATG5-ATG12-ATG16L1complex as well as linkage of phosphatidylethanolamine to LC3I to form LC3II. Both these complexes integrate into the elongating phagophore with LC3II integrated into the internal as well as external membrane of the phagophore. Upon formation of the autophagosome, while the ATG5-ATG12-ATG16L1 complex dissociates from the membrane, LC3II remains stably integrated, and hence is used as a reliable marker to study autophagic flux in cells. Once formed, autophagosomes fuse with lysosomes to form autolysosomes in which cellular cargo is degraded before release into cytoplasm for recycling.

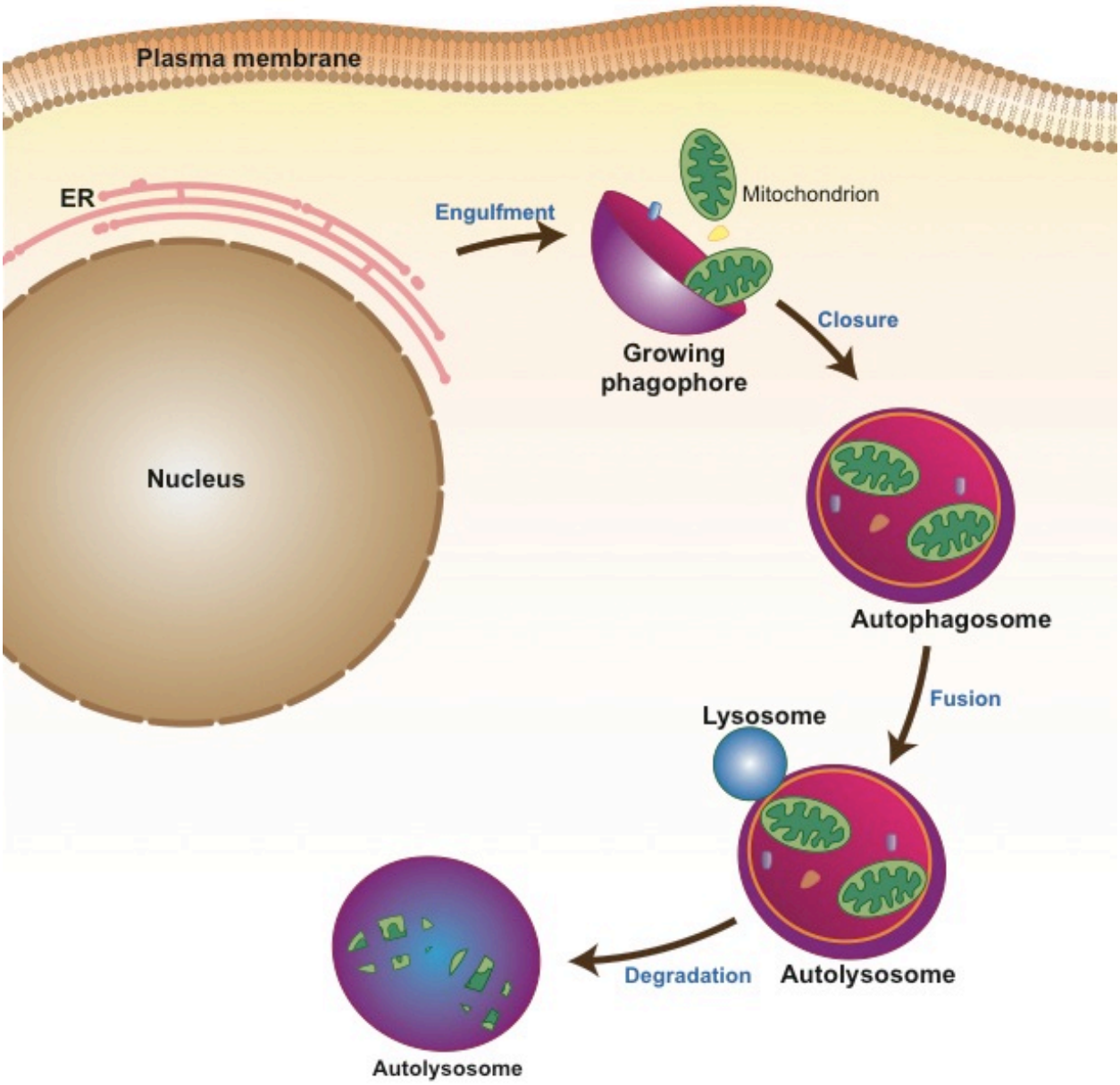


**Figure 2. Schematic summary of autophagy.**

Cytosolic cargo can range from protein aggregates and damaged cellular organelles to pathogens and dead cells that may be targeted for autophagic degradation in a non-selective or selective manner (35). Non-selective or general autophagy can be triggered by nutrient stress arising from low levels of ATP, growth factors and amino acids that may require bulk replenishment of essential metabolites. On the other hand, selective autophagy can be triggered by environmental stresses such as hypoxia that may require removal of damaged organelles, or by physiological factors such as cellular differentiation that may require removal of mitochondria and ribosomes from maturing reticulocytes.

Mitochondrial autophagy or mitophagy is an example of selective autophagy where dysfunctional mitochondria are targeted for autophagosomal degradation (36,37). Mitochondria are highly dynamic and frequently undergo cycles of fusion and fission. Studies have shown that upon undergoing fission, mitochondria with lower membrane potential and reduced fusion protein, Opa-1, undergo autophagic degradation thus limiting oxidative damage in cells (38). On the other hand, under conditions of nutrient starvation, mitochondria undergo fusion to form elongated networks with increased cristae, ATP synthase activity and energy production and ultimately avoid autophagic degradation (39,40). However, while mitochondrial dynamics may influence the priming of mitochondria for autophagic degradation, mitophagy is regulated by molecular adaptors including Parkin, PINK1, BNIP3, NIX, and more recently, FUNDC1, that specifically target mitochondria for autophagic degradation (36).

Parkin is an E3 ubiquitin ligase that localizes to the OMM to ubiquitinate mitochondrial proteins including VDAC, Mfn-2 and Miro (41-44). PINK1 is

serine/threonine kinase that gets degraded in the matrix of healthy mitochondria, but translocates to the OMM of depolarized mitochondria. Once at the OMM, PINK1 is known to phosphorylate Parkin, ubiquitin as well as Parkin substrates such as Mfn-2 in order to facilitate recruitment of Parkin to the mitochondria (45,46). In turn, Parkin mediated ubiquitination of mitochondrial proteins results in recruitment of p62 that serves as an adaptor molecule to recruit LC3 containing growing phagophores to the mitochondria (47,48). Interestingly, while pro-apoptotic proteins including Puma, Noxa, Bim and Bad promote mitophagy; anti-apoptotic proteins including Bcl-$X_W$, Mcl-1 and Bcl-$X_L$ inhibit it by preventing Parkin mediated ubiquitination of its mitochondrial targets (49).

The tumor suppressive function of mitophagy is highlighted by the fact that Parkin is frequently deleted or down-regulated in breast and ovarian tumors and in lung adenocarcinoma cell lines (36,50,51). Moreover, Parkin null mice exhibit increased hepatocyte proliferation and hepatic tumors (52). Parkin is also induced by p53 in order to limit Warburg effect and enhance oxidative metabolism in tumors, thus mediating the function of p53 in energy metabolism (53). This is consistent with the fact that Parkin is recruited to depolarized mitochondria that may have compromised oxidative metabolism. More recently, Parkin has also been shown to regulate stability of CDK4 and G1/S cyclins, cyclin D and cyclin E, by targeting them for degradation, thus exhibiting a tumor suppressive role that is independent of mitophagy (54).

The two other important regulators of mitophagy, BNIP3 and NIX, are also known to have tumor suppressive functions (discussed in detail Chapter 1.2), thus further supporting the premise that mitophagy is anti-tumorigenic.

Mitochondrial biogenesis and MYC

Mitochondrial biogenesis is controlled in cells by several factors such as response to cellular stresses (nutrient supply, reactive oxygen species, hypoxia), oncogenes and tumor suppressors (MYC, HIF-1, p53, BRAF) and entry into cell cycle (22,55). The process is mainly regulated at the transcriptional level by transcription factors including NRF1, NRF2, ERRα, ERRβ, ERRγ, PPARα, PPARγ, PPARδ, and co-activators including PGC-1α, PGC-1β and PRC.

NRF1 and NRF2 induce key components of mtDNA transcription and replication machinery including Tfam, TFB1M, TFB2M and POLRMT (56). NRFs are also required for transcription of nuclear genes involved in electron transport chain (complexes I-V, cytochrome c), mitochondrial translation (ribosomal proteins, tRNA synthetases) and mitochondrial protein import and assembly (Tom20, Tom70, COX17) (57,58).

PPARs are mainly required for transcription of genes involved in oxidation of fatty acids to acetyl-coA (beta-oxidation) in the mitochondrial matrix, but are not known to associate with expression of any OXPHOS or TCA cycle genes. ERRs regulate genes involved in beta-oxidation too. However, upon binding to co-activators PGC-1α and PGC-1β, they also regulate genes involved in OXPHOS, TCA cycle, mitochondrial transcription and translation machinery as well mitochondrial transport proteins.

All of the above-mentioned transcription factors require co-activators PGC-1α, PGC-1β and PRC. These co-activators recruit CBP/p300 and histone acetyltransferases to promote transcription during mitochondrial biogenesis. PGC-1α gets transcriptionally and post-translationally regulated in response to the nutrient and energy status of cells. While it is induced by PPARs, mTOR (via YY1), CREB (activated by PKA) and MITF,

and repressed by p53, PGC-1α is activated by AMPK mediated phosphorylation and inhibited by GCN5 mediated acetylation (57).

BRAF/MAPK pathway driven melanomas have lower levels of PGC-1α, MITF and reduced oxidative metabolism (59). However, not only does BRAF inhibition with small molecules result in cell-cycle arrest and apoptosis, but it also induces PGC-1α via MITF, increases mitochondrial biogenesis and shifts the energy dependency to OXPHOS. Given that PGC-1α is a key regulator of mitochondrial biogenesis, PGC-1α positive melanoma tumors exhibit increased oxidative metabolism and ROS scavenging capacity, thus decreasing their sensitivity to ROS-inducing drugs (60). Predictably, knocking down PGC-1α in melanoma cell lines decreases their oxidative metabolism and increases their sensitivity to ROS-inducing drugs, thus triggering apoptosis. These studies suggest that BRAF driven melanoma tumors as well as PGC-1α positive melanomas may benefit from treatment with inhibitors of mitochondrial biogenesis or oxidative metabolism.

Interestingly, mitochondrial biogenesis has also been reported as a highly common phenotype of CSCs in several cancers including breast, lung, prostate, ovarian, pancreatic, melanoma and glioblastoma. When tumor spheres from 12 human cancer cell lines were treated with 5 different classes of mitochondrial antibiotics including erythromycins and chloramphenicol (target 39S large mitochondrial ribosome), tetracyclines and glycylcyclines (target 28S small mitochondrial ribosome) and pyrvinium pamoate (targets mitochondrial OXPHOS), a significant decrease in tumor spheres was observed with each class of antibiotic (61).

Telomere dysfunction is known to activate tumor suppressor, p53, resulting in growth arrest, senescence and apoptosis (62). PGC-1$\alpha$ is transcriptionally repressed by p53 in response to telomere dysfunction, which in turn reduces mitochondrial biogenesis by decreasing mitochondrial DNA content. Telomerase inhibition has also been shown to induce ALT-dependent tumor resistance, which exhibits increased levels of PGC-1$\beta$ and its targets (TFAM, NRF2, SOD2), mitochondrial biogenesis and ROS scavenging (63). Given that these tumors are highly sensitive to PGC-1$\beta$ and SOD2 knockdown, these studies highlight the importance of mitochondrial biogenesis and function for tumor sustenance.

A key driver of mitochondrial biogenesis is the oncogene, MYC (64,65). Some of the key MYC targets involved in mitochondrial biogenesis are PGC-1$\beta$, NRF1, TFAM, Pol$\gamma$, NRF2, PRC, ERR-$\alpha$ and PPAR$\alpha$ (66,67). MYC null cells show significantly reduced mitochondrial mass compared with cells expressing MYC. Also, cells expressing MYC have been shown to rely more on oxidative metabolism and are more sensitive to OXPHOS inhibitors as compared to MYC null cells (68-70). Interestingly, mitochondrial biogenesis is negatively regulated by HIF-1, which promotes MXI-1-dependent inhibition of MYC transcriptional activity and proteasome-dependent degradation of MYC protein (71). Not only does MYC regulate mitochondrial biogenesis, but MYC transformed cells also exhibit increased glycolysis and glutaminolysis and anabolic synthesis of macromolecules such as lipids, proteins and nucleotides (72-78). Apart from regulating biogenesis and metabolism in cancer cells, MYC oncoprotein also regulates cell cycle, cell adhesion, cytoskeleton and miRNAs, resulting in a broad and significant impact on tumor initiation and progression (79).

MYC is found deregulated in 70% of human malignancies due to gene amplification, chromosomal translocation, overexpression, or protein stabilization (77,80). MYC overexpression and protein stabilization can occur by activation of growth factors and their receptors, Ras/MAPK pathway, PI3K/Akt pathway, Wnt/β-catenin signaling and Notch pathway, whereas MYC degradation occurs mainly by GSK-3β mediated phosphorylation and subsequent proteasomal degradation (81). While MYC regulates mitochondrial metabolism and biogenesis, it is not known if there exists a retrograde signaling from mitochondria to the nucleus i.e., from mitochondria to MYC, affecting its regulation, and is one of the key components of this study.

### 1.2. BNIP3: function, regulation and role in cancer

BNIP3 (Bcl-2/E1B-19kDa-interacting protein 3) and BNIP3L (NIX) are key mitochondrial modulators of mitophagy (36,82). BNIP3 interacts with antiapoptotic protein Bcl-2 and was isolated from a yeast two-hybrid screen in order to identify the cellular targets of E1B-19kDa protein which could be functionally substituted by Bcl-2, hence the name BNIP3 (83,84). NIX shares a 55% sequence homology with BNIP3 and was also isolated from a similar yeast two-hybrid screen (85). Both BNIP3 and NIX have a weakly conserved BH3 domain and Bcl-2 mutants that could not bind BNIP3 were also found to be defective in cell death suppression, hence BNIP3 and NIX came to be known as cell death inducing or pro-apoptotic BH3-only proteins. However, it is now well-established that the BH3 domain is only weakly conserved in these proteins and that both, BNIP3 and NIX, are strongly expressed in several normal tissues in the body

without causing cell death, thus highlighting the fact that they are not true BH3-only proteins (86).

Function of BNIP3 in mitophagy

Both, BNIP3 and NIX, homodimerize into the OMM owing to critical glycine zipper present in their transmembrane domain at the carboxyl terminal. Homodimerization of BNIP3 is required for its ability to induce autophagy since mutant BNIP3 forms that can not dimerize failed to induce this function (87-89). Interestingly, BNIP3 dimerizes not just into the OMM, but also at the endoplasmic reticulum (ER) resulting in autophagy of the ER (ERphagy) (90). Once dimerized into the OMM, the remainder protein that includes the LC3 interacting region (LIR) at the unstructured amino terminal extrudes into the cytosol. The LIR motif is a short peptide sequence containing the core motif [WxxL] that enables proteins to directly bind to LC3 (90). Thus, similar to ATG32, but unlike Parkin that requires interaction of ubiquitinated mitochondrial proteins with p62 to target them to the autophagosomes, BNIP3 and NIX can directly tether the mitochondria for autophagic degradation (91,92). Since, BNIP3 interacts with Bcl-2 and Bcl-XL through the same amino terminal region that has the LIR motif, it is believed that these interactions in turn can regulate its mitophagy function (93,94). Both, BNIP3 and NIX, interact with Rheb, a Ras-related small GTPase, at the mitochondria (95). However, BNIP3 has been shown to inhibit Rheb-mTOR mediated cell growth in response to hypoxia, consistent with its growth suppressive function (discussed in detail below). BNIP3 has also been shown to compete with Beclin in order to bind Bcl-2, thus releasing Beclin for induction of mitophagy under hypoxic conditions. Lastly, BNip3 also

plays a role in mitochondrial dynamics as its overexpression results in mitochondrial fragmentation that has been ascribed to translocation of dynamin-related protein 1 (Drp1) to the mitochondria as well as to inhibition of mitochondrial fusion by interaction with optic atrophy 1 (OPA1) (96-98). This may be a way for BNIP3 to prime mitochondria for autophagic degradation.

Thus, while the function of BNIP3 as a key modulator of mitophagy has been well established, to what extent this plays a role in promoting or suppressing tumor growth has not been characterized. Previous work in our lab had highlighted the importance of BNip3 mediated mitophagy in maintenance of mitochondrial integrity (99). We had shown that BNip3 lacking liver had increased mitochondrial mass, reduced mitochondrial function and increased lipid synthesis, which are also characteristics of mitochondrial dysfunction in cancer. Thus, we investigated the impact of BNip3 mediated mitophagy in the MMTV-PyMT mouse model of mammary tumorigenesis.

Regulation of BNIP3

BNIP3 is a hypoxia inducible gene containing HIF-1 response element (HRE) in its promoter that can be strongly activated by hypoxia or increased HIF-1$\alpha$ expression in several normal and cancer cell lines (Figure 3) (100-103). Our lab has shown that while BNIP3 is essential for hypoxia-induced autophagy, it is transcriptionally repressed by RB/E2F to prevent autophagic cell death (104). We showed for the first time that BNIP3 promoter had E2F binding site that interacted functionally with HRE to suppress BNIP3 induction by HIF-1$\alpha$. In Rb null MEFs or with inhibition of prolyl hydroxylases in Saos-2 cells, BNIP3 induced autophagic cell death, which switched to necrosis upon BNIP3

knockdown in these cells. BNIP3 is also transcriptionally repressed by NF-kB and p53 (105,106). NF-kB has been shown to compete with E2F for binding to BNIP3 promoter and silencing BNIP3 expression (107). This effect gets abrogated in cardiac cells and human pancreatic cancer cell lines that knocked down for pRB or E2F and are deficient for NF-kB. However, BNIP3 is transcriptionally induced by FoxO3 in skeletal muscle to mediate its effect on autophagy (108). Importantly, BNIP3 is also regulated by RAS, which indirectly induces BNIP3 by activation of MEK/ERK pathway, which in turn activate Hif-1$\alpha$ and result in expression of BNIP3. Inhibition of MEK/ERK using MEK specific inhibitor, U0126, or mutation in HRE on BNIP3 promoter, both abrogated up-regulation of BNIP3 by RAS (109-111).

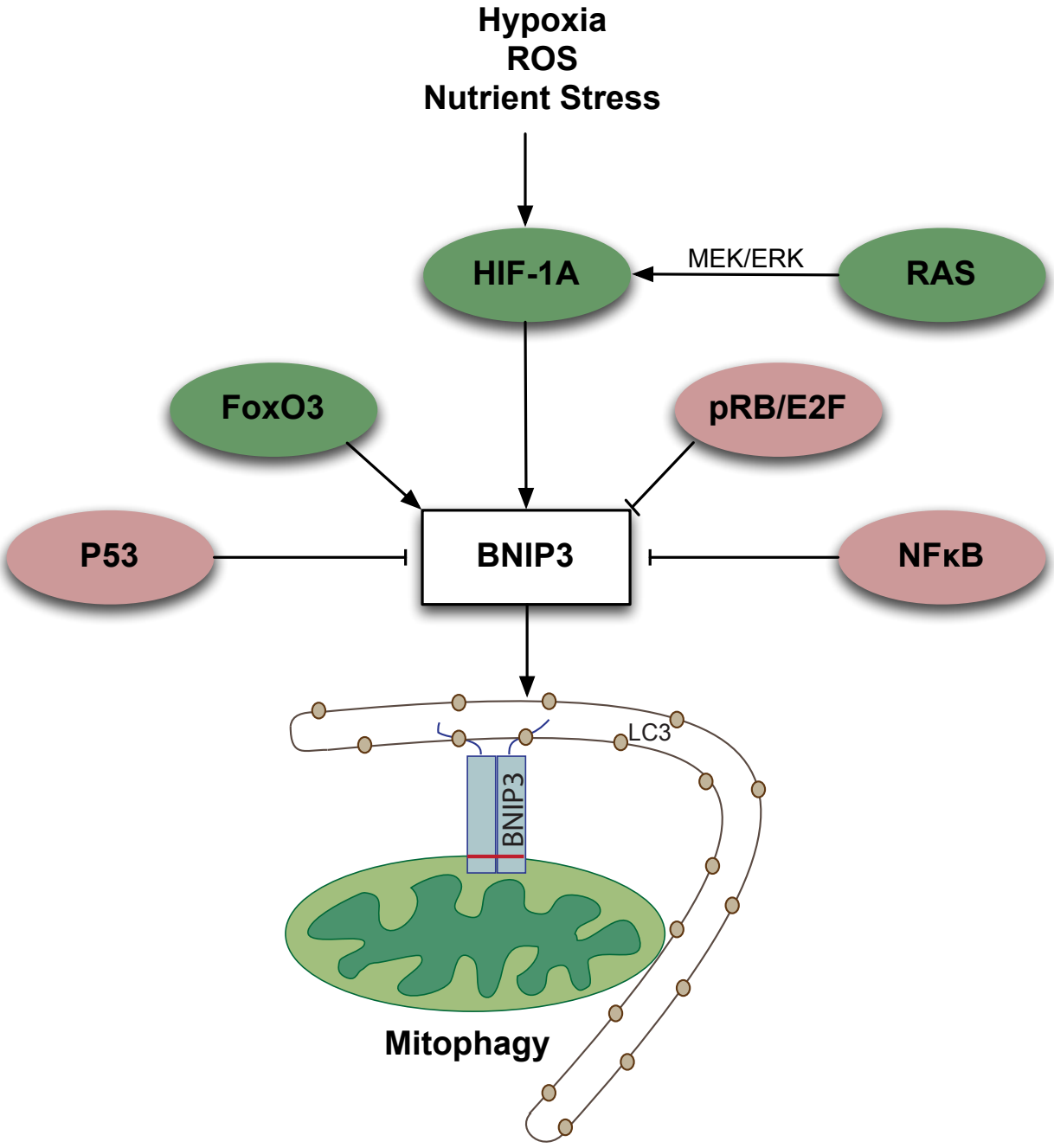


**Figure 3. Schematic summary of regulation of BNIP3.**

Role of BNIP3 in cancer

BNIP3 expression has been found up-regulated during initial stages of tumor formation such as DCIS which is an early, non-invasive lesion in the breast. In a study that analyzed 56 samples of DCIS for BNIP3 and NIX expression levels, both were strongly expressed in a subset of DCIS (112). However, BNIP3 expression in DCIS also correlated with high grade and necrotic lesions, which was not the case for NIX. Interestingly, investigation of invasive breast cancer has shown loss of BNIP3 expression in patients that significantly correlated with lymph node metastases and high mitotic index, thus establishing loss of BNIP3 as a poor prognostic indicator for the disease (113). Consistent with these findings in human breast cancer, BNIP3 loss has also been shown to increase tumor growth and metastasis in a model of murine breast cancer cell lines (114). 4T1, 4T07 and 67NR were used to examine levels of BNip3 and it was observed that BNip3 expression inversely correlated with the metastatic potential of these cell lines. Thus, while BNip3 expression was the highest in 67NR cell line, which is a non-metastatic cell line, it was lowest in 4T1, which is highly metastatic to the lungs, liver, bone and brain. Knockdown of BNip3 in 4T07 cell line, which had intermediate metastatic potential, increased their primary tumor growth and metastatic potential, suggesting that BNip3 loss was critical for tumor progression.

However, overexpression of BNIP3 in human breast and lung carcinoma cell lines has shown to increase tumor growth in a xenograft model whereas its knockdown was shown to impair tumorigenicity (115). Moreover, BNIP3 is also the target of p53-miR-145 regulation in prostate cancer and was found to be up-regulated with tumor

progression, thus suggesting that BNIP3 has a pro-tumorigenic role (116). However, a more in-depth analysis of BNIP3 literature suggests otherwise.

BNIP3 is also silenced by promoter hypermethylation during stages of cancer progression in hematological, gastric, colorectal, lung and hepatocellular malignancies (117-120). Treatment of acute lymphocytic leukemia cell lines with DNA methyltransferase inhibitor, 5-aza-2'-deoxycytidine or decitabine reversed the epigenetic silencing of BNIP3 and concomitantly reduced their cell viability. These studies suggest that BNIP3 has an anti-tumorigenic function. A similar trend with BNIP3 expression has been reported in pancreatic cancer as well, where BNIP3 expression was found to be high in PanIN lesions, but significantly reduced in PDAC patient samples (121). The study also reported that patients with BNIP3 loss had a significantly reduced median survival compared to their BNIP3 expressing counterparts. Loss of BNIP3 is also found to result in chemoresistance to 5-fluorouracil and gemcitabine in human pancreatic cancer cell lines (122-123). BNip3 loss in pancreatic cancer cell lines is the result of gene silencing due to promoter hypermethylation, an effect that is relieved by decitabine treatment resulting in reduced cellular viability (124). Conversely, higher expression of BNIP3 in pancreatic cancer is associated with longer overall survival (125).

While the above-mentioned studies suggest a tumor suppressive function of BNIP3, neither do they report an in-depth analysis of the consequence of BNIP3 deletion in mouse models nor do they address the mechanism by which BNIP3 may be exerting tumor suppression. Thus in order to understand the exact function of BNIP3 in cancer, we investigated the consequences of BNip3 deletion in the MMTV-PyMT mouse model of mammary tumorigenesis. Given that BNIP3 is a bona fide regulator of mitophagy, we

also examined the functional consequences of impaired mitophagy resulting from BNip3 loss in this mouse model in order to tease out the mechanism by which BNip3 may suppress tumor growth and metastasis.

Moreover, given that KRAS is the most frequently and early activated oncogene in pancreatic cancer and that BNIP3 is a target for KRAS mediated upregulation, the above-mentioned evidence suggested that BNIP3 may play a tumor suppressive role in PDAC, where upregulation of BNIP3 in early stages may suppress tumor progression (126). Thus, we examined the tumor suppressive function of BNIP3 by employing human pancreatic cancer cell lines and a physiologically relevant mouse model of PDAC.

### 1.3. Overview of breast cancer and pancreatic ductal adenocarcinoma mouse models

MMTV-PyMT mouse model of mammary tumorigenesis

Breast cancer is not only the most frequently diagnosed cancer in women accounting for 29% of estimated new cases, but it is also the second leading cause of cancer deaths in women in US (127). Almost all of the breast cancer deaths occur due to metastatic disease which arises from dissemination of breast cancer cells from the primary site into the lymphatic or vascular circulation and eventually lodging in lymph nodes, lungs, bone, liver or the brain to form metastatic lesions (128,129). A key component in studying the disease effectively is the use of a mouse model that can mimic the disease as it occurs in humans. The MMTV-PyMT mouse model of mammary

tumorigenesis, with high penetrance and spontaneous metastasis to the lungs, is one such well-defined tumor model that is widely used and accepted in the field (130,131).

The MMTV-PyMT transgenic mice exhibit mammary gland specific expression of oncoprotein, polyoma middle T antigen (PyMT) under the control of promoter/enhancer of mouse mammary tumor virus (MMTV) resulting in formation of multifocal mammary adenocarcinomas independent of pregnancy. Tumor formation in this model occurs in four distinct stages of hyperplasia, adenoma/MIN, and early and late carcinoma. Mice develop hyperplastic lesions by about 6 weeks of age and MIN by about 8-9 weeks of age. Adenoma/MIN are premalignant mammary lesions with highly proliferative cellular masses filling the acini and ducts, but exhibiting minimal cytological atypia. Early carcinoma starts to develop by 10-11 weeks of age and is marked by cytological atypia, loss of basement membrane, stromal invasion and leukocyte infiltration. This stage in PyMT mice is morphologically similar to DCIS with early stromal invasion in humans. Late carcinoma begins to develop by 11-13 weeks of age and resembles invasive ductal carcinoma in humans. This stage exhibits very high cellular and nuclear atypia and high mitotic index. The tumors are made of sheets of malignant cells with complete loss of acinar structure and high fibroinflammatory component comprising of fibroblasts, macrophages and eosinophils. The mice also begin to show lung metastasis by this stage of late carcinoma.

At the molecular level, the MMTV-PyMT tumors show a gradual loss of ER, PR and β1-integrin with an overexpression of ErbB2 and cyclin D1 from the stage of adenoma/MIN to late carcinoma indicating that the more aggressive and hormone independent tumor cells transition to a malignant disease. This is consistent with human

data where loss of receptor status or overexpression of ErbB2 correlates with poor patient prognosis.

PDX1-Cre;LSL-KRAS$^{G12D}$ mouse model of pancreatic tumorigenesis

Pancreatic cancer is an aggressive malignancy that is estimated to result in 42,000 deaths in 2016, making it the fourth leading cause of cancer deaths in the US (127). It is characterized by not only early dissemination of cancer cells with rapid peritoneal and perineural metastasis, but also exhibits resistance to chemotherapy and radiation (126,132-134). Additionally, the fact that majority of pancreatic cancer cases get detected at advanced stages makes the disease almost invariably fatal. This highlights the need to understand the disease biology better in order to identify potential early disease markers.

Extensive research in the last decade has highlighted key molecular alterations in oncogenes such as KRAS and tumor suppressors such as p16/CDKN2A, TP53 and SMAD45 (134-136). While alterations in KRAS and P16/CDKN2A occur in early PanIN lesions, alterations in TP53 and SMAD4 are seen in later stages of advanced PanIN and invasive carcinoma. KRas is activated not only in early PanIN stages, but also in chronic pancreatitis, thus making it difficult to apply it as an early disease marker (137,138). Thus, it becomes important to study key molecular alterations and signaling pathways downstream of KRas that may result in progression from precursor PanIN lesions to invasive carcinoma.

There are several mouse models for pancreatic cancer that are vary in reproducibility of human disease and effectiveness in clinical approach (139-141). The

Pdx1-Cre;KRas$^{G12D}$ GEMM for pancreatic cancer is quite accurate in recapitulating the disease as it occurs in humans progressing from precursor PanIN lesions to invasive PDAC and has been used extensively to study the effect of loss of tumor suppressor genes such as TP53, P16/INK4A and P14/ARF on pancreatic tumor progression (142-145). Thus, it stands out as the prime choice for studying the effect of BNip3 loss in pancreatic tumor initiation and progression.

This model utilizes the LoxP-flanked STOP element inserted into mutant KRas knock-in allele (KRasG12D) that results in the mutant allele remaining silent (142,143). However, excision of the STOP element in the Lox-STOP-Lox (LSL) cassette activated by Pdx1 promoter driven Cre recombinase results in activation of the mutant allele. Pdx1 is a transcription factor integral to pancreatic development and is expressed around embryonic day 8.5 in the fetal mouse, while its expression is restricted to the islet cells in an adult mouse. The model shows development of early stage PanIN-1A lesions with a few weeks of birth, though progression to PDAC can take upto 12 months. PanIN-1A and 1B show development of papillary ductal lesions without loss of apical polarity or nuclear atypia. The pancreatic acini and islets appear normal with the organ retaining its architecture. However, PanIN-2 starts to show moderate nuclear atypia, which becomes severe by PanIN-3 along with complete loss of polarity. Late PanIN stage also shows cluster of cells pinched off into the ductal lumen along with mucin secreting goblet cells and fibroinflammatory reaction showing desmoplastic regions as in human disease progression. Progression to PDAC shows glandular pattern of differentiation and metastatic lesions are seen in liver, lungs, peripancreatic lymph nodes and nervous plexus as seen in human PDAC. Thus, Pdx1-Cre;KRas$^{G12D}$

mouse model of PDAC was a major breakthrough in transgenic mice used for PDAC, primarily since it recapitulated development of PanIN lesions that progressed to invasive and metastatic PDAC. Also, this model has become the basis of plethora of GEMMs for PDAC by introducing additional genetic alterations, which help researchers to study their effect on PDAC development and progression.

# CHAPTER 2

# MATERIALS AND METHODS

## Mice

MMTV-PyMT mice: MMTV-PyMT mice (Jackson Laboratories) were bred to BNip3 null mice (146) to generate compound MMTV-PyMT;BNip3$^{+/+}$ or MMTV-PyMT;BNip3$^{-/-}$ mice on a >99% pure FVB/N background. Tumor studies were performed on virgin female progeny. Mice were monitored routinely for tumor burden and were euthanized when tumors began to impede movement and affect quality of life. Mice were sacrificed at time points of day35, day50, day65 and day80 to collect mammary tumors and lungs. Tumor size was measured using electronic calipers and tumor volume was calculated using the formula, L x $W^2$ (L=length, W=width). Mammary tumors and lungs collected at the time of necropsy were fixed in 10% neutral buffered formalin for 24 hours followed by transfer to 70% ethanol. Formalin fixed tissues were embedded in paraffin and sectioned for histology. Tissues were sectioned at 5 um thickness. Lung metastases were quantified using 6 serial sections 25 um apart. Slides were cut and stained with hematoxylin and eosin and metastases were counted per section. For butylated hydroxyanisole (BHA) studies, indicated cohorts of mice were fed 7 mg/kg BHA provided through custom chow (Harlan-Teklad, TD-110712).

PDX-1-Cre;LSL-KRAS$^{G12D}$ mice: PDX-1-Cre and LSL-KRAS$^{G12D}$ mice (Jackson Laboratories) were bred separately to BNip3 null mice to generate PDX-1Cre;BNip3$^{-/-}$

and LSL-KRAS$^{G12D}$;BNip3$^{-/-}$ mice on a C57BL/6 background. These were then bred together to generate PDX-1-Cre;LSL-KRAS$^{G12D}$;BNip3$^{+/+}$ and PDX-1-Cre;LSL-KRAS$^{G12D}$;BNip3$^{-/-}$ mice. Mice were monitored routinely for signs of cachexia and lethargy were euthanized when quality of life deteriorated. Mice were sacrificed at time points of 3 and 4.5 months to collect pancreas, spleen, liver, lungs, diaphragm and intestines. Weight of mouse and pancreas was measured at necropsy. All tissues and organs were fixed in 10% neutral buffered formalin for 24 hours followed by transfer to 70% ethanol. Formalin fixed tissues were embedded in paraffin and sectioned for histology. Tissues were sectioned at 5um thickness.

**Genotyping**

For isolation of genomic DNA, mouse-tail snips were incubated overnight at 55$^{o}$C in tail lysis buffer (100 mM Tris pH 8.0, 5 mM EDTA pH 8.0, 0.2% SDS, 200 mM NaCl) containing 100 nM proteinase K. DNA was run on 2% agarose gels. A list of primers and size of products obtained for BNip3, PyMT, Cre, and KRAS$^{G12D}$ PCRs is given below.

<u>BNip3</u>

BNip3 WT: 5'-TGT GGC TGA GAG TCA GTG GTC-3'

BNip3 GT2: 5'-TTG CAA GTC TAG GAG TCA GTT-3'

BNip3 NTKV: 5'-GTG GAT GTG GAA TGT GTG CG-3'

BNip3 wild-type: 435 bp, BNip3 null: 220 bp

<u>PYMT</u>

Transgene FWD: 5'-GGA AGC AAG TAC TTC ACA AGG G-3'

Transgene REV: 5’-GGA AAG TCA CTA CTA GGA GCA GGG-3’

PYMT transgene: 566 bp

Cre

Forward: 5’-GGACATGTTCAGGGATCGCCAGGC-3’

Reverse: 5’-CGACGATGCAGCATGTTTAGCTG-3’

Cre: 225 bp

$KRAS^{G12D}$

Primer 1: 5'-GTC TTT CCC CAG CAC AGT GC-3’

Primer 2: 5'-CTC TTG CCT ACG CCA CCA GCT C-3’

Primer 3: 5’-AGC TAG CCA CCA TGG CTT GAG TAA GTC TGC-3’

Wild-type: 622 bp, LSL cassette: 500 bp and 1 lox (recombined): 650 bp

**Cell lines and Tissue Culture**

For primary MECs, mammary tumors were collected into sterile petri dish and minced with razor blade to less than 1 mm pieces. Minced tissue was transferred to falcon tube with 40 ml digestion solution (serum-free DMEM, 3 mg/ml collagenase A, 1 mg/ml hyaluronidase, 2 U/ml DNase I) and shaken at 150 rpm for 1 hour at 37$^{o}$C. To stop digestion, 5 ml of fetal calf serum was added. Digest was strained through 70 um strainer and centrifuged at 1200 rpm for 3 hours. Cell pellet was resuspended in 10-15 ml media and plated in a 10 cm dish. MECs were cultured in DMEM/F12 media (Invitrogen 21041-025) with 5% defined fetal bovine serum (heat inactivated), 10 ng/ml epidermal growth factor (Sigma E9644), 5 µg/ml insulin (Invitrogen 12585-014), 0.5 µg/ml hydrocortisone (Sigma H0135-1mg), 10 µg/ml gentamycin (Invitrogen 15710-064)

and 1% penicillin/streptomycin (Invitrogen 15140-163). Lentiviral infected exogenous expression cell lines were selected and maintained in 1.5 ug/ml puromycin (Sigma P8833).

MiaPaca-2 cells were obtained from ATCC (ATCC CRL-1420) and cultured in DMEM (Invitrogen 11995) with 10% fetal bovine serum (heat inactivated), 2.5% horse serum and 1% penicillin/streptomycin (Invitrogen 15140-163). Exogenous BNIP3 expression clones were selected and maintained in 1.5 mg/ml G418 (ALX-380-013-G005). CFPAC-1 cells were kindly provided by Dr. Deborah Lang and cultured in IMDM (Invitrogen 12440-061) with 10% fetal bovine serum (heat inactivated) and 1% penicillin/streptomycin (Invitrogen 15140-163). Lentiviral infected control and BNIP3 shRNA cell lines were selected and maintained in 2 ug/ml puromycin (Sigma P8833). Saos-2 cells were cultured in RPMI (Invitrogen 11875-119) with 10% fetal bovine serum (heat inactivated) and 1% penicillin/streptomycin (Invitrogen 15140-163). Empty-vector and BNIP3 overexpression cell lines were maintained in 500 ug/ml G418. RKO cells were cultured in DMEM (Invitrogen 11995) with 10% fetal bovine serum (heat inactivated) and 1% penicillin/streptomycin (Invitrogen 15140-163). Empty-vector and BNIP3 overexpression cell lines were maintained in 1 ug/ml puromycin. All cell lines were maintained in incubators at 20% $O_2$, 5% $CO_2$ and 95% $N_2$. For hypoxia, cells were maintained at 1% $O_2$ condition in humidified Tissue Culture Glove Box (Coy Laboratory Products).

**Reagents**

Echinomycin (Sigma SML0477-1mg) used at 10 ng/ml, 2-deoxyglucose (Sigma D8375-1G) used at 5 mM, BafilomycinA1 (Enzo Life Sciences BML-CM110-0100) used at 100nM, MG132 (Enzo Life Sciences BML-PI102-005) used at 50 uM, Hydroxychloroquine (Sigma H0915) used at 50 μM.

**Stable overexpression**

Lentivirus (pGIII-CMV-GFP-2A-Puro) expressing mouse BNip3 (ABM LV534527) was purchased from Applied Biological Materials and used to stably infect BNip3 null MECs using manufacturer's protocol. Empty-vector and BNip3 expressing cell lines were selected and maintained in puromycin.

pcDNA3.1 plasmids containing control-HA and human BNIP3-wild-type-HA were transfected overnight into MiaPaca-2 cells using Lipofectamine 2000 (Invitrogen 11668-019) in Opti-MEM reduced serum medium (Invitrogen 31985-088). Selection of stable clones with G418 was started 48 hours after transfection. Stable clones were expanded in order to validate overexpression by immunoblot.

pBabe-puro-MycERT2 plasmid was used for standard PCR mutagenesis to generate phospho-mutant Myc at T58A which was transfected overnight into MiaPaca-2 cells using Lipofectamine 2000.Stable clones were selected with puromycin (3 ug/ml) and expanded to validate overexpression by immunoblot.

**Stable knockdowns**

Lentivirus (pLKO-puro) expressing non-targeting control and human BNIP3 shRNA targeting coding sequence (Sigma TRCN0000280253) and 3'-UTR (Sigma TRCN0000280255) were purchased from Sigma and used to stably infect CFPAC-1 cells using manufacturer's protocol. Control and BNIP3 shRNA cell lines were selected and maintained in puromycin.

**Growth curves**

2 x $10^4$ cells were plated in 6-well plates on day1 with media change on day2. Cells were counted from day3 till day8. Additional media changes or compound additions were done on day 5. Cells were counted using hemocytometer and experiments were done in triplicates.

**Three-dimensional (3D) spheroid assay**

5 x $10^3$ cells were plated on day1 in assay medium containing 2% matrigel (BD No. 354230 from BD Biosciences) and 5 ng/ml epidermal growth factor on eight-well glass chamber slides that were coated with matrigel (147). Cells were re-fed with assay medium containing 2% matrigel and 5 ng/ml epidermal growth factor every alternate day and 3D spheres were imaged on day5 and day10 using Zeiss Axiovert 100TV microscope. 5 representative images were taken per genotype per condition and spheres per image were counted to obtain an average of total number of 3D spheres.

**Immunofluorescence**

Immunofluorescence staining for mitophagy was performed on cells fixed in 4% paraformaldehyde, permeabilized in 100% methanol at -20°C, blocked in 2%FBS/1% Goat Serum/PBS and incubated 1:200 with anti-LC3B (Cell Signaling #2775) and 1:500 with anti-cyclophilin D (MitoSciences MSA04) at 4$^{o}$C overnight. Cells were imaged using Olympus DSU spinning disk confocal microscope with a Hamamatsu model C9100 EM-CCD camera run by SlideBook v5.0 software. Image deconvolution was performed with Openlab software and image analysis was performed using ImageJ software.

**Quantitative PCR**

For genomic DNA isolation, MECs were seeded in 6-well plates. At the time of DNA isolation, cells were washed once with phosphate buffered saline or PBS (Invitrogen) and collected in 500 ul PBS, centrifuged at 1200 rpm for 3 minutes at room temperature in order to resuspend cell pellet in lysis buffer (100 mM Tris pH 8.0, 5 mM EDTA pH 8.0, 0.2% SDS, 200 mM NaCl) containing 100 nM proteinase K. Relative mitochondrial to nuclear genome ratios were determined using TaqMan real-time PCR primers specific to mitochondrial genome encoded NADH dehydrogenase subunit 1 or Nd1 (Applied Biosystems Mm04225274_s1) and cytochrome b or Cytb (Applied Biosystems Mm04225271_g1) and to nuclear genome encoded β-globin (Applied Biosystems AIY9ACV). 5 ng of genomic DNA was used per well. Each sample was assayed in triplicate, normalized to endogenous control of b-globin and quantified using the comparative CT method.

For RNA isolation, cells seeded in 6-well plates or pulverized tumors were homogenized using 1 ml TRIzol reagent (Invitrogen) followed by addition of 200 ul chloroform to obtain a TRIzol:chloroform ratio of 5:1. Samples were vortexed for 15 seconds followed by 5-minute incubation at room temperature. Samples were centrifuged at 12000 x g for 15 minutes at 4$^{o}$C in order to collect the aqueous phase containing RNA in to a fresh tube followed by addition of 1 volume of 70% ethanol. The RNA-ethanol mix was dissolved well by pipetting several times followed by clean-up using the Qiagen RNeasy kit. cDNA synthesis from total RNA was performed using the High Capacity RNA-to-cDNA master mix (Applied Biosystems). mRNA levels were quantified using TaqMan real-time PCR primers for specific genes. 250 ng of cDNA was used per well. Each sample was assayed in triplicate, normalized to endogenous control of b-actin and quantified using the comparative CT method.

List of TaqMan gene expression primers from Applied Biosystems

b-actin (mouse): 4352341E, BNip3 (mouse): Mm00833810_g1, Pdk1 (mouse): Mm00554300_m1, Pgk1 (mouse): Mm00435617_m1, Slc2a1 (mouse): Mm00441473_m1, Hk2 (mouse): Mm00443385_m1, Vegfa (mouse): Mm00437306_m1, Ang2 (mouse): Mm00545822_m1, Flt1 (mouse): Mm01210866_m1

b-actin (human): 4352935- 0908022, BNIP3 (human): Hs00969291_m1 BNIP3, c-Myc (human): Hs00153408_m1 MYC, CDKN1A (human): Hs00355782_m1, CCND2 (human): Hs00153380_m1, FASN (human): Hs01005622_m1, PPARGC1B (human): Hs00991676_m1, CAD (human): Hs00983188_m1, ODC1 (human): Hs00159739_m1

**Protein extraction**

Cells were plated in 10-cm plates for whole cell extracts and in 15-cm plates for nuclear extracts. Extraction/lysis buffers contained protease inhibitors (0.5 mM PMSF, 1 ug/ml aprotinin, 1 ug/ml leupeptin), phosphatase inhibitors (1 mM Na3VO4 and Halt phosphatase inhibitor cocktail from Fisher #78420) and DTT. For whole cell extracts, cells were lysed in RIPA (10 mM Tris pH 8.0, 140 mM NaCl, 1% sodium deoxycholate, 0.1% SDS and 1% NP40). Cells were washed once with ice-cold PBS and collected in about 500 ul PBS, centrifuged at 1200 rpm for 3 minutes at 4$^{o}$C followed by resuspension of cell pellet in equal volume of RIPA. Lysates were incubated on ice for 15 minutes (vortexing every 5 minutes) followed by centrifugation at 13200 rpm for 15 minutes at 4$^{o}$C. Clarified lysates were transferred to new tubes and protein concentration was determined using the DC protein assay from Biorad.

For nuclear extracts, cells were resuspended in lysis buffer (50 mM Tris pH 7.5, 5 mM $MgCl_2$, 0.4% NP-40) and incubated on ice for 5 minutes followed by centrifugation at 4000xg for 4 minutes at 4$^{o}$C. Supernatant containing the cytoplasmic fraction was transferred to a new tube and the nuclear pellet was washed twice in 500 ul lysis buffer followed by centrifugation at 4000xg for 4 minutes at 4$^{o}$C. After the final wash, the nuclear pellet was lysed in Buffer C (10 mM HEPES pH 7.9, 0.5 mM EDTA, 0.5 mM EGTA and 400 mM NaCl) and incubated on ice for 15 minutes followed by centrifugation at 13200 rpm for 15 minutes at 4$^{o}$C. Clarified lysates were transferred to new tubes and protein concentration was determined using the DC protein assay from Biorad.

**Immunoblotting**

Depending on the molecular weight of protein being investigated, proteins (50ug – 100ug of protein/well) were loaded onto 8%, 10%, 13% or 15% SDS-PAGE gels and run at 90V for stacking (approximately 30 minutes) followed by 120V for running (1 hour and 30 minutes) gels. Proteins were transferred onto nitrocellulose or PVDF membranes, blocked in milk or bovine serum albumin for 30 minutes at room temperature followed by overnight incubation in primary antibody at 4$^{o}$C. The next day, membranes were washed and incubated in HRP-conjugated secondary antibodies (Dako) followed by detection by chemiluminescence. All proteins less than 25 kDa in weight were run on 15% gels and transferred onto PVD membranes. b-actin and PARP were used as loading controls for whole cell and nuclear lysates, respectively.

**Histology and Immunohistochemistry**

Mouse tumors and organs were formalin fixed and submitted for paraffin embedding, sectioning and immunohistochemistry to the Human Tissue Resource Center at the University of Chicago. Stained sections were digitized using a ScanScope XT automated slide scanning system (Aperio) and quantified using the Spectrum Plus image analysis software (Aperio).

**Antibodies**

Primary antibodies used for immunohistochemistry and Immunoblotting are listed below. Ki67 (Labvision #RM-9106), BNIP3 (Sigma #HPA003015), Vdac1 (BioVision #3594-100), CoxIV (Cell Signaling #4844), ER-α (Santa Cruz sc-542), TOM20 (Santa Cruz sc-

11415), Hif-1α (Abcam ab2185), laminin-α1 (Abcam ab11575), CD31 (Santa Cruz sc-1506), α-SMA (Abcam ab5694), LC3B (Nanotools 0231-100/LC3-5F10), 8-hydroxy-guanine (Santa Cruz sc-66036), c-Myc (Abcam ab32072), CK-19 (Abcam ab52625), pancreatic amylase (Abcam ab21156), BNip3 (Cell Signaling #3769), Hif-1α (Abcam ab2185), Vdac1 (BioVision #3594-100), CoxIV (Cell Signaling #4844), LC3B (Novus NB600-1384), p62/Sqstm1 (Progen CP-62C), β-actin (A1978), PARP (Santa Cruz sc7150), cyclophilin D (Mitosciences MSA04), Nrf2 (Santa Cruz sc722), Nix (Sigma N0399), HSP60 (Cell Signaling #4870), HA (Cell Signaling #3724), BNIP3 (Sigma B7931), 4E-BP1 (Cell Signaling #9644), phospho-4E-BP1 (Cell Signaling #2855)

**Flow cytometry**

Cell viability was measured by propidium iodide (PI) exclusion assay. Mitochondrial membrane potential and superoxide anion levels were measured using 50 nM TMRE (Invitrogen T69) and 5 uM MitoSOX (Invitrogen M36008). Glucose uptake was measured using 2-NBDG. On the day of the assay, cells seeded in 6-well plates were incubated with the above-mentioned dyes for 15-20 minutes after which they were rinsed with PBS and trypsinized. Trypsinized cells were resuspended and washed twice in 2% FBS-PBS. Finally, cells were centrifuged at 1400 rpm for 4 minutes at 4$^{o}$C and resuspended in 500 ul 2%FBS-PBS. Flow cytometry analysis was performed on LSR II (BD Biosciences) and subsequent analysis of data was carried out using FlowJo software.

**Transmission electron microscopy**

Small pieces of tumors were fixed in 2.5 % gluteraldehyde and sections were analyzed using a Philips CM120 transmission electron microscope.

**Magnetic Resonance Imaging (MRI)/microPET/CT Imaging**

MRI experiments were performed in a 9.4T Bruker (Billerica, MA) small animal scanner with 11.6 cm inner diameter, actively shielded gradient coils (maximum constant gradient strength for all axes: 230 mT/m). Whole-body scanning was performed to study all of the mammary glands. Two interleaved sets of axial high resolution multi-slice RARE (Rapid Acquisition with Relaxation Enhancement) spin echo T2-weighted (T2W) images were acquired (TR/TEeffective = 4000/20.3 ms, FOV = 25.6 mm, matrix size = 2562, slice thickness = 0.5 mm, slice gap = 1 mm, number of slices = 41, NEX = 2, RARE factor = 4) with fat suppression and respiratory gating. MicroPET/CT Imaging was performed using a FLEX Triumph™ microPET/SPECT/CT system (Trifoil Imaging, Northridge, CA). Animals were fasted overnight and100 µCi of $^{18}$F-FDG were injected into the tail vein. MicroCT images for anatomical reference were first acquired (60kV, 140 µA) and microPET acquisition was started 30 minutes after $^{18}$F-FDG administration. A static acquisition was performed for 30 minutes. (Method from Chourasia et al, 2015)

**Metabolomics analyses**

Measurement of total and $^{13}$C-labeled metabolites by LC-MS: Cells were seeded in 10-cm plates in regular growth media and used at approximately 80% confluence. Cells were rinsed with 15 ml PBS and incubated in DMEM base media (Sigma D5030 pH to

7.4 with sodium bicarbonate, 5% dialyzed serum, EGF, hydrocortisone, insulin and gentamycin) for 30 minutes to deplete them of all unlabeled glucose and glutamine (148). Cells were then labeled for 6 hours with DMEM base media containing uniformly labeled D-glucose (10 mM U-$^{13}$C-glucose from Cambridge isotope Laboratories, CLM 1396) or D-glutamine (2 mM U-$^{13}$C-glutamine from Cambridge isotope Laboratories, CLM 1822). After labeling, media was aspirated and 80% methanol (cooled at -80$^{o}$C) was added onto cells with plates maintained on dry ice. Plates were incubated at -80$^{o}$C for 15 minutes followed by scraping cells/methanol mix into 15 ml conical tubes on dry ice and spinning at full speed for 5 minutes at 4$^{o}$C to pellet cell debris and proteins. The supernatant was transferred into 50 ml conical tubes on dry ice while 500 ul of 80% methanol (cooled at -80$^{o}$C) was added to 15 ml conical tubes to resuspend the pellet again. Resuspended pellet was vortexed vigorously, transferred to 1.5 ml eppendorf tubes and centrifuged at full speed for 5 minutes at 4$^{o}$C in order to transfer the supernatant in to the 50 ml conical tube. This extraction step was repeated thrice and after pooling the three extractions, the samples were completely dried using a speedVac. Dried pellets in 1.5 ml eppendorf tubes were submitted to Beth Israel Deaconess Medical Center, Boston, MA, for analysis by LC-MS. Samples were prepared in biological and technical triplicates.

Lactate was quantified from cells grown in $^{13}$C2-glucose-labeled media by $^{13}$C edited $^{1}$H NMR spectra. All NMR spectra were acquired on a Bruker AVANCE III HD NMR spectrometer operating at 600.13 MHz 1H and 150.9 MHz 13C. 2k complex points were acquired over a sweep width of 10 ppm with 13C decoupling for an acquisition time of 341 ms.

**Measurement of oxygen consumption rate**

Seahorse Bioscience models XF24 and XF96 were used to measure the oxygen consumption rate (OCR) (149). 5 x $10^4$ and 2 x $10^4$ cells were seeded in 500 ul and 200 ul growth media for XF24 and XF96, respectively. On the day of the assay, cells were rinsed with PBS, DMEM assay media (Sigma D5030 with 4.5 g/L glucose and/or 2 mM glutamine and/or 1mM sodium pyruvate and pH 7.35 with 0.1N HCl and 0.1N NaOH) was added and cells were incubated in a non-$CO_2$ incubator for 1 hour. OCR was measured using 1 uM oligomycin (port A), 1 uM FCCP (port B) or 5 uM antimycin A (port C). The instruments were calibrated with three cycles of 3 minutes of mix, 15 seconds of wait and 3-4 minutes of measure time. OCR was standardized for total protein concentration after the assay was completed.

**ATP assay**

ATP Bioluminescence Assay Kit CLS II (Roche) was used to measure cellular ATP levels as per manufacturer's protocol. Firefly luciferase utilizes ATP present in samples on D-luciferin to emit light at 562 nm, which is used as readout for ATP levels. Cells were trypsinized and counted on hemocytometer. 2 x $10^5$ cells per sample were boiled with 9 volumes of100 mM Tris, 4mM EDTA at pH 7.75 for 2 minutes. Samples were centrifuged at 1000xg for 1 minute in order to collect 100 ul of supernatant to measure ATP levels. 100 ul of luciferase reagent was added to each sample and ATP levels were measured after 5 seconds of integration. ATP standard was diluted to concentrations of 1.0 x $10^{-6}$ M to 1 x $10^{-10}$ M ATP. All samples and standards were

measured in duplicates ATP concentration calculated from a log- log plot of the standard curve.

**The Cancer Genome Atlas (TCGA) and other human data**

All analyses were performed in R v.3.0.1. TCGA BNIP3 data for RNAseq mRNA estimates and CNV were extracted using the 'cgdsr' package (150). Clinical annotation of TCGA data was downloaded separately from http://gdac.broadinstitute.org and matched to the data in the 'cgdsr' package using R code provided in the supplementary methods. Enrichment of copy number loss was identified using a fisher exact test comparing counts of CNV < 0 in TNBC and non-TNBC samples. Stratification of metastasis-free survival (MFS) was tested in expression array data from 101 breast tumor samples identified as TNBC out of a total of 871 samples in a combined cohort consisting of publically available data sets reposited in Gene Expression Omnibus (GEO) (151). Significant differences in MFS were determined using the log-rank test.

**Statistical Analysis**

Results were expressed as mean ± SEM. Data was analyzed using GraphPad Prism. Significance was determined by Student's t-test for 2 group comparisons and one way ANOVA for >2 group comparisons. Significance for survival curves was determined by Log-rank (Mantel-Cox) and Gehan-Breslow-Wilcoxon test. *p<0.05, **p<0.01, ***p<0.001, ****p<0.0001

# CHAPTER 3

# BNIP3 LOSS INCREASES PRIMARY MAMMARY TUMOR GROWTH, INVASION AND INCIDENCE OF LUNG METASTASES IN MMTV-PYMT MOUSE MAMMARY TUMOR MODEL

## 3.1. Introduction

Breast cancer is not only the most frequently diagnosed cancer in women accounting for 29% of estimated new cases, but it is also the second leading cause of cancer deaths in women in US (127). Almost all of the breast cancer deaths occur due to metastatic disease which arises from dissemination of breast cancer cells from the primary site into the lymphatic or vascular circulation and eventually lodging in lymph nodes, lungs, bone, liver or the brain to form metastatic lesions (128).

Breast tumors are known to contain hypoxic regions that stabilize and activate HIFs, HIF-1 and HIF-2. Overexpression of HIF-1$\alpha$ is indicative of poor prognosis and is associated with increased mortality in lymph node positive patients (152,153). Using the MMTV-PyMT model of mammary tumorigenesis, it has been shown that Hif-1$\alpha$ promotes primary mammary tumor growth and metastasis (154). HIF-1$\alpha$ has also emerged as a promoter of the invasive and metastatic phenotype of triple-negative breast cancer (TNBC) (155). BNIP3 is transcriptionally induced by HIF-1 and targets mitochondria for autophagic degradation under physiological conditions of oxygen and nutrient stress, thus it functions to eliminate damaged or dysfunctional mitochondria and maintain the overall mitochondrial health of the cell (102-104). HIF targets such as glycolysis enzymes including hexokinase, phosphofructokinase, pyruvate

dehydrogenase kinase and lactate dehydrogenase have an established role of driving aerobic glycolysis in tumors (29,30). Other HIF targets including vascular endothelial growth factor, angiopoietins and lysyl oxidases are essential for tumor progression owing to their role in angiogenesis and extracellular matrix remodeling (156,157). However, the function of BNIP3 in cancer is not well established. Given that recent studies have highlighted the reliance of tumor cells on oxidative metabolism, it becomes imperative to study the processes such as mitophagy that are crucial for maintaining healthy mitochondria and promoting efficient OXPHOS (18-20,22,36). Thus, we investigated the function of BNip3 mediated mitophagy on tumor growth and progression by employing the MMTV-PyMT mouse model of mammary tumorigenesis. The MMTV-PyMT model exhibits high penetrance and spontaneous metastasis to the lungs (130,131). It resembles human breast cancer and is a well-defined tumor model that is widely used and accepted in the field.

In this chapter, we have assessed changes in BNip3 expression during the growth and progression of mammary tumors with the MMTV-PyMT model and investigated the significance of its down-regulation with disease progression. We have studied the effect of BNip3 loss on mammary tumor growth and latency and have examined whether loss of BNip3 promotes progression from adenoma/MIN stage to malignant carcinoma. In order to gain a detailed insight into whether the *in vivo* phenotype is recapitulated *in vitro*, we have also assessed tumor cell growth, survival, migration, and invasion and growth in three-dimensional matrigel on cultured mammary epithelial cells. Lastly, we have also assessed the effects of BNip3 loss on tumor metastasis to lungs.

### 3.2. Loss of BNip3 increases primary tumor growth *in vivo* and tumor cell proliferation *in vitro*

IHC analysis of BNip3 in MMTV-PyMT mammary tumors performed previously in the lab had shown a gradual loss of BNip3 from early carcinoma to late-stage and metastatic carcinoma indicating that there was a selective pressure to lose BNip3 during mammary tumor progression (Figure 4). Thus, in order to examine the effect of BNip3 loss on tumor growth and metastasis, MMTV-PyMT mice were crossed with mice carrying a targeted deletion of BNip3 to generate MMTV-PyMT;BNip3$^{+/+}$ (wild-type) and MMTV-PyMT;BNip3$^{-/-}$ (BNip3 null) mice. Loss of BNip3 was confirmed by IHC staining on wild-type and BNip3 null tumors (Figure 5). While loss of BNip3 had no effect on tumor latency, once formed, BNip3 null tumors grew significantly faster than the wild-type tumors as shown by MRI of age-matched wild-type and BNip3 null mice over time (Figure 6).

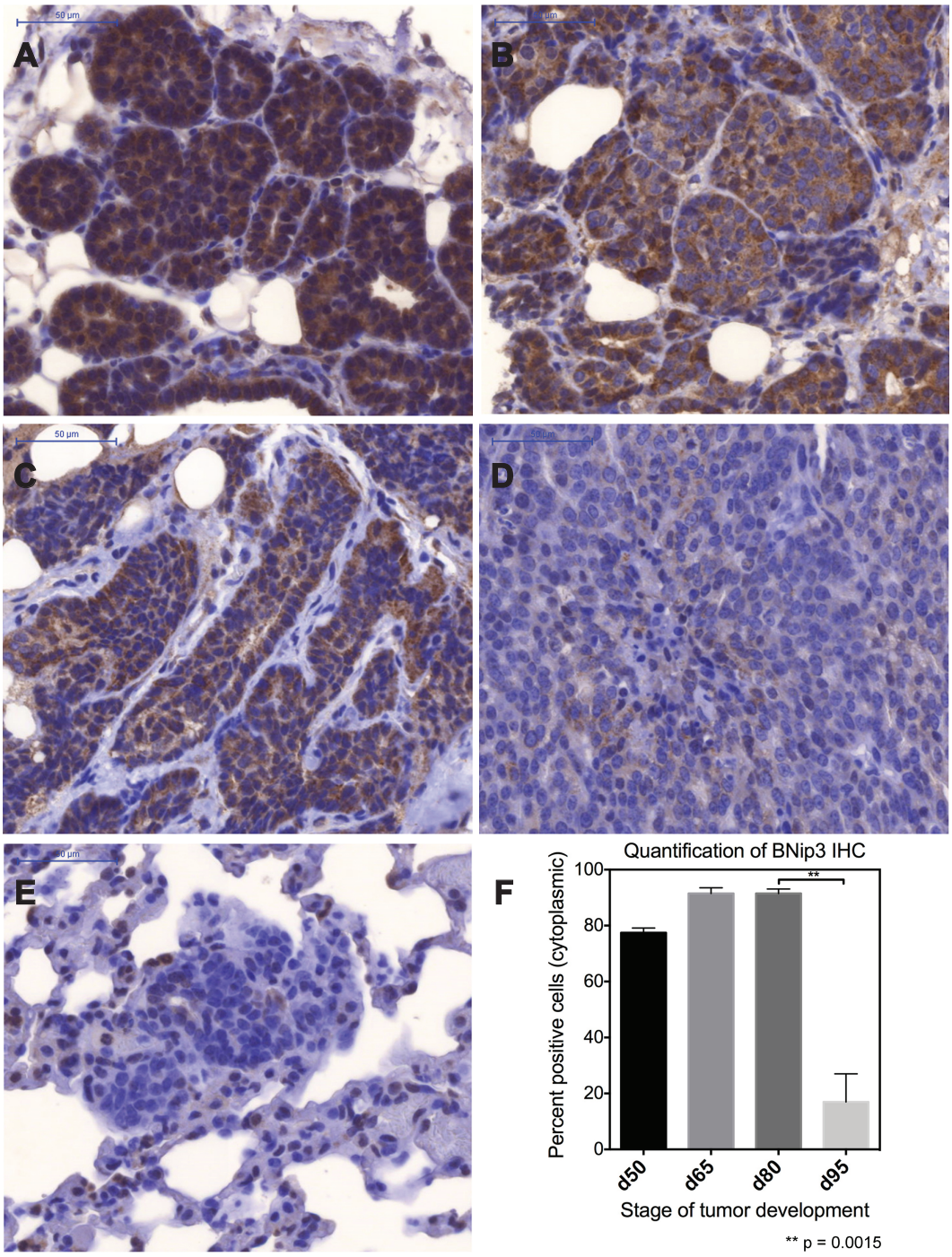


**Figure 4. Loss of BNip3 protein expression during mammary tumor progression in MMTV-PyMT mice.** (A) BNip3 IHC at the stage of adenoma/MIN stage (day50-day65, n=4). (B) BNip3 IHC at the stage of early carcinoma (day65-day80, n=4). (C) BNip3 IHC at the stage of late carcinoma (day80-day95, n=4). (D) BNip3 IHC at the stage of metastatic carcinoma (day95-day105, n=4). (E) BNip3 IHC in lung metastases (day95-day105, n=4). (F) Quantification of BNip3 IHC at adenoma/MIN, early carcinoma, late carcinoma and metastatic carcinoma (p=0.0015). (Data from Kristin Tracy)

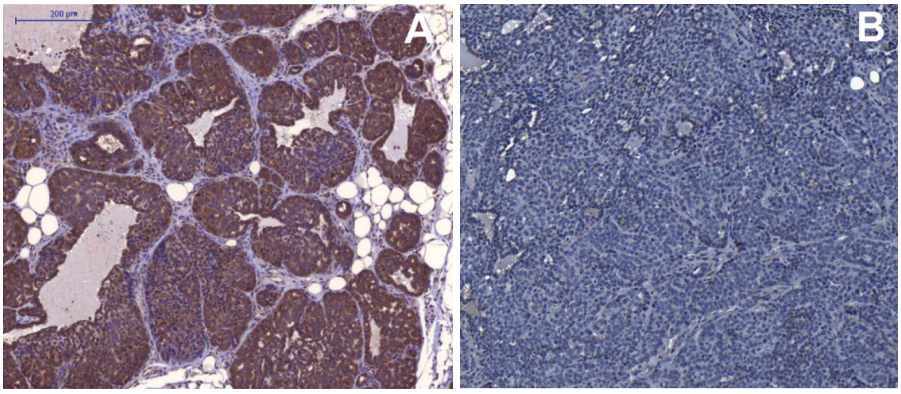


**Figure 5. BNip3 protein expression in wild-type and BNip3 null mammary tumors.** (A) BNip3 IHC of wild-type tumor at day65. (B) BNip3 IHC of BNip3 null tumor at day65. (Data from Kristin Tracy)

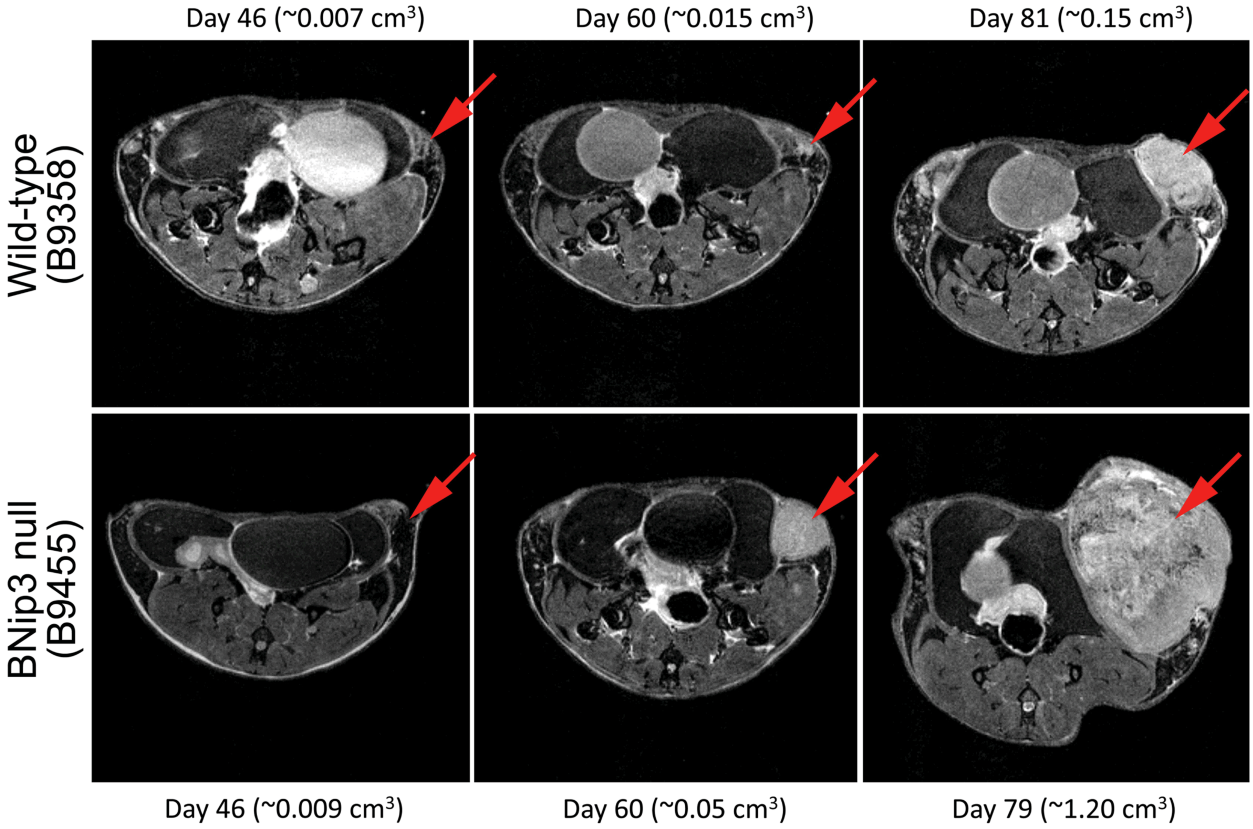


**Figure 6. Loss of BNip3 promotes mammary tumor growth.** MRI images of mammary tumors for wild-type and BNip3 null mice at imaging resolution of 117mm and slice thickness of 0.5mm (red arrows indicate presence of tumor).

In order to examine the growth phenotype of primary mammary epithelial cells (MECs) in vitro, we isolated MECs from wild-type and BNip3 null tumors and measured their growth rate at atmospheric oxygen (20% oxygen) and under hypoxic (1% oxygen) conditions. BNip3 protein expression in wild-type and BNip3 null MECs was confirmed by immunoblot (Figure 7A). BNip3 null MECs had a significantly faster growth rate as compared to wild-type cells under both the conditions (Figure 7B). However, BNip3 null MECs grew slower under hypoxia when compared to their growth rate at atmospheric oxygen. Upon re-expression of exogenous mouse BNip3 into BNip3 null MECS, the growth phenotype was reversed with the BNip3 rescued MECs growing slower than parental BNip3 null MECs or those infected with a control empty-vector (Figure 7D), thus reinstating the growth suppressive function of BNip3 in mammary tumorigenesis. Exogenous expression of empty-vector and mouse BNip3 into BNip3 null MECs was confirmed by immunoblot (Figure 7C).

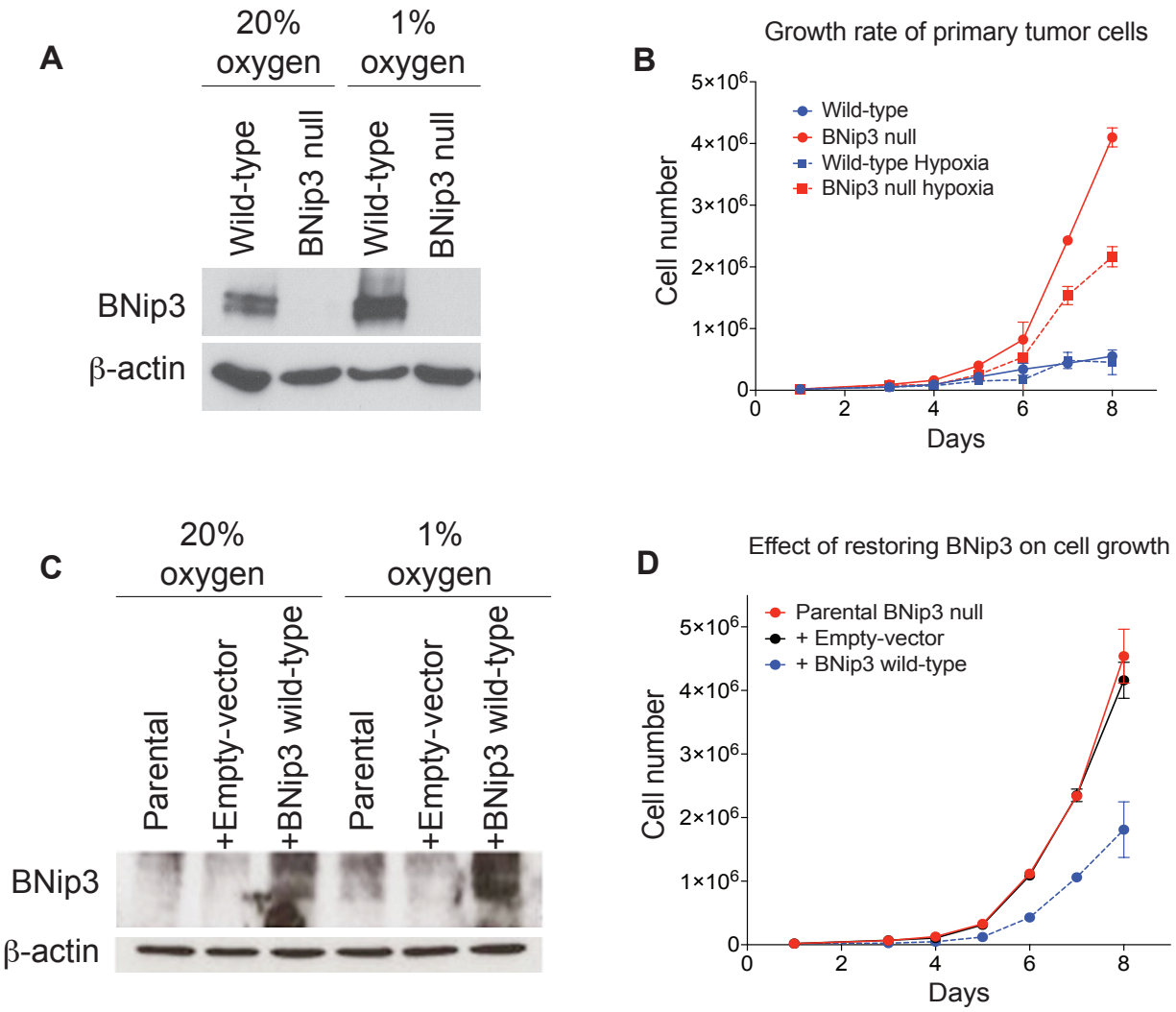


**Figure 7. Loss of BNip3 increases growth rate of primary mammary tumor cells.** (A) BNip3 protein levels of wild-type and BNip3 null MECs at 20% oxygen and 1% oxygen. (B) Growth rate of wild-type and BNip3 null MECs at 20% oxygen (bold line) and under hypoxia (dotted line) measured in triplicate experiments. (C) BNip3 protein levels of parental BNip3 null MECs or expressing empty-vector (+Empty-vector) or wild-type BNip3 vector (+BNip3 wild-type) at 20% oxygen and 1% oxygen. (D) Growth rate of parental BNip3 null MECs or expressing empty-vector or wild-type BNip3 vector at 20% oxygen measured in triplicate.

Increased growth rate of cells can occur due to increased cellular proliferation or decreased cell death or both. In order to determine whether the increased growth rate of BNip3 null MECs *in vitro* was consistent with increased proliferation, we performed the BrdU (5-Bromo-2'-Deoxyuridine) incorporation assay to measure cells entering the S-phase in a 5 hour labeling experiment. We observed significantly increased BrdU uptake in BNip3 null MECS compared to wild-type cells (Figure 8). Given that earlier studies on BNIP3 had suggested that the protein can induce programmed cell death, we examined if the increased growth rate of BNip3 null MECs was a result of decreased cell death by performing propidium iodide (PI) uptake. However, we did not detect any significant difference in cell death by PI staining between wild-type and BNip3 null MECs (Figure 9). Together, these results indicate that increased growth rate of BNip3 null MECs compared to wild-type cells is due to increased cellular proliferation and not reduced cell death.

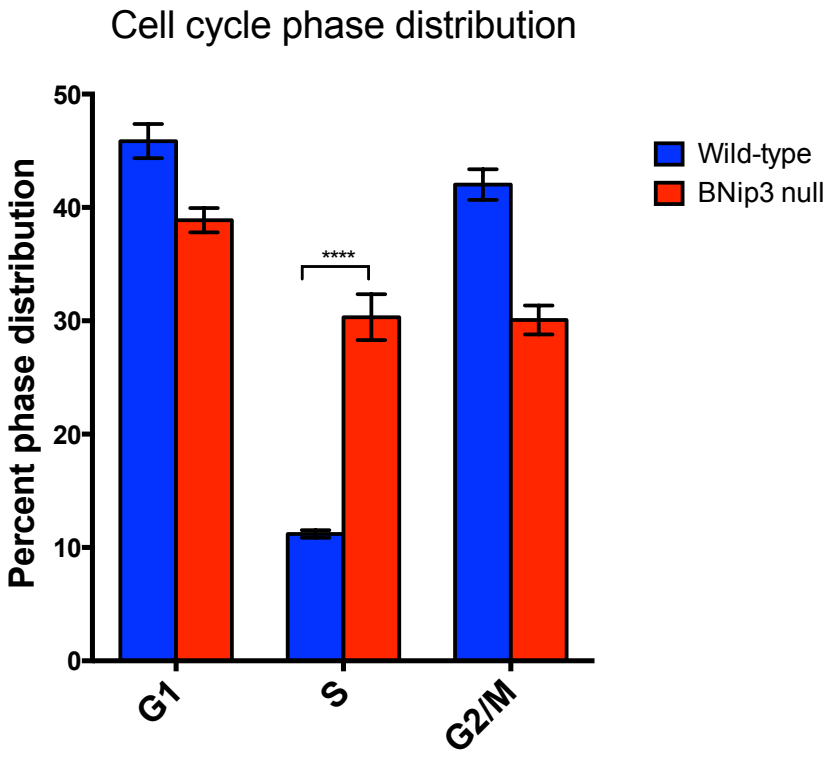


**Figure 8. Loss of BNip3 increases proliferation of primary mammary tumor cells.** Cell cycle phase distribution of wild-type and BNip3 null MECs measured in triplicate experiments by BrdU labeling over 5 hours in culture followed by labeling of fixed cells with α-BrdU and PI.

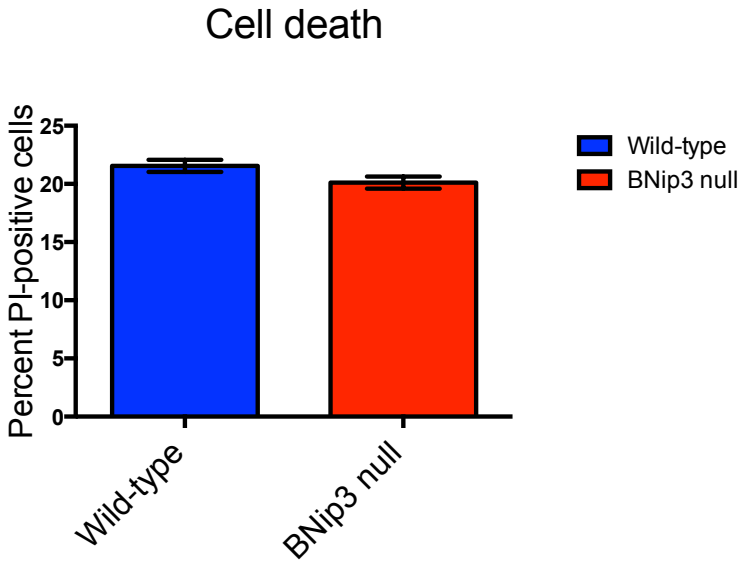


**Figure 9. Loss of BNip3 does not affect cell survival.** Cell survival measured by PI staining of wild-type and BNip3 null MECs.

### 3.3. Loss of BNip3 promotes primary tumor cell migration and invasion *in vitro*

Histological examination of wild-type and BNip3 null tumors performed previously in the lab had shown that BNip3 null tumors exhibited higher nuclear grade with atypical mitotic figures as well as accelerated nuclear pleomorphism as compared to age-matched wild-type tumors (Figure 10). IHC staining for ERα showed that while wild-type tumors retained strong ERα expression by day65, BNip3 null tumors showed a significantly accelerated loss of the steroid receptor for the same time point. H&E analysis and IHC for laminin-α1 also showed an accelerated loss of basement membrane integrity in BNip3 null tumors as compared to age-matched wild-type tumors. These results suggested that BNip3 null tumors progressed more rapidly towards being invasive as compared to wild-type tumors.

In order to compare the migratory and invasive phenotype of wild-type and BNip3 null MECs *in vitro*, we performed Boyden chamber assays for cell migration and invasion. BNip3 null MECs showed significantly higher migration (Figure 11A) as well as invasion through collagen (Figure 11B) when compared to their wild-type counterparts. Furthermore, in order to compare invasiveness of these cells under conditions that mimic the complex extracellular environment found *in vivo,* we performed a three dimensional (3D) spheroid growth assay *in vitro*. MECs were plated on matrigel and the resultant organoids were counted and analyzed (147). Not only did BNip3 null MECs form a significantly higher number of organoids under 20% oxygen compared to wild-type MECs, but the BNip3 null organoids were also highly disorganized (Figure 12) and exhibited loss of spherical architecture that was observed in wild-type organoids. These

results suggest that loss of BNip3 increases invasiveness of MECs *in vitro*, under 2D and 3D growth conditions.

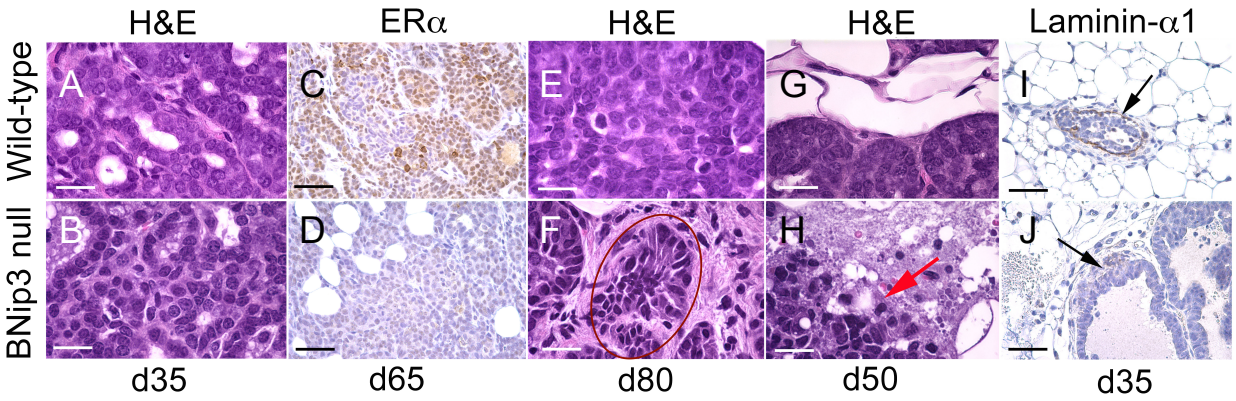


**Figure 10. Loss of BNip3 promotes early progression to carcinoma.**
(A-B) Primary mammary tumors in wild-type and BNip3 null mice at d35 showed increased nuclear grade (grade 3) compared to wild-type (grade 2). (C-D) Expression of estrogen receptor-alpha (ER-α) at d65 shows reduced expression in BNip3 null tumors compared to wild-type. (E-F) Increased pleomorphism and evidence of EMT in BNip3 null tumors at d80 but not in wild-type. (G-H) Loss of basement membrane integrity in BNip3 null tumors at d65. (I-J) Laminin-α1 staining confirms loss of basement membrane integrity in BNip3 null tumors at earlier stages than for wild-type. (Data from Kristin Tracy)

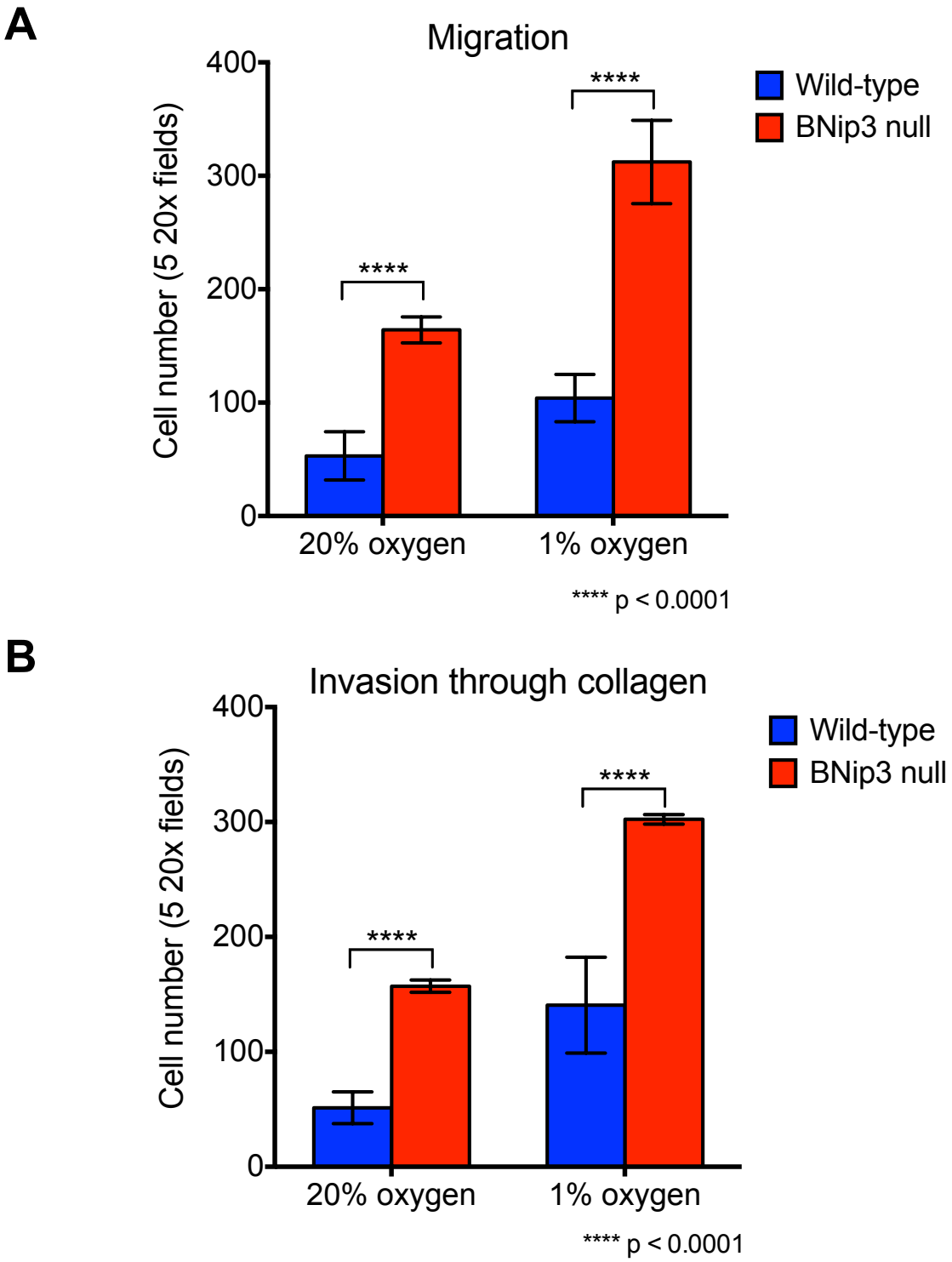


**Figure 11. Loss of BNip3 promotes migration and invasion *in vitro*.**
(A) Migration and (B) Invasion assays in Transwell assays.

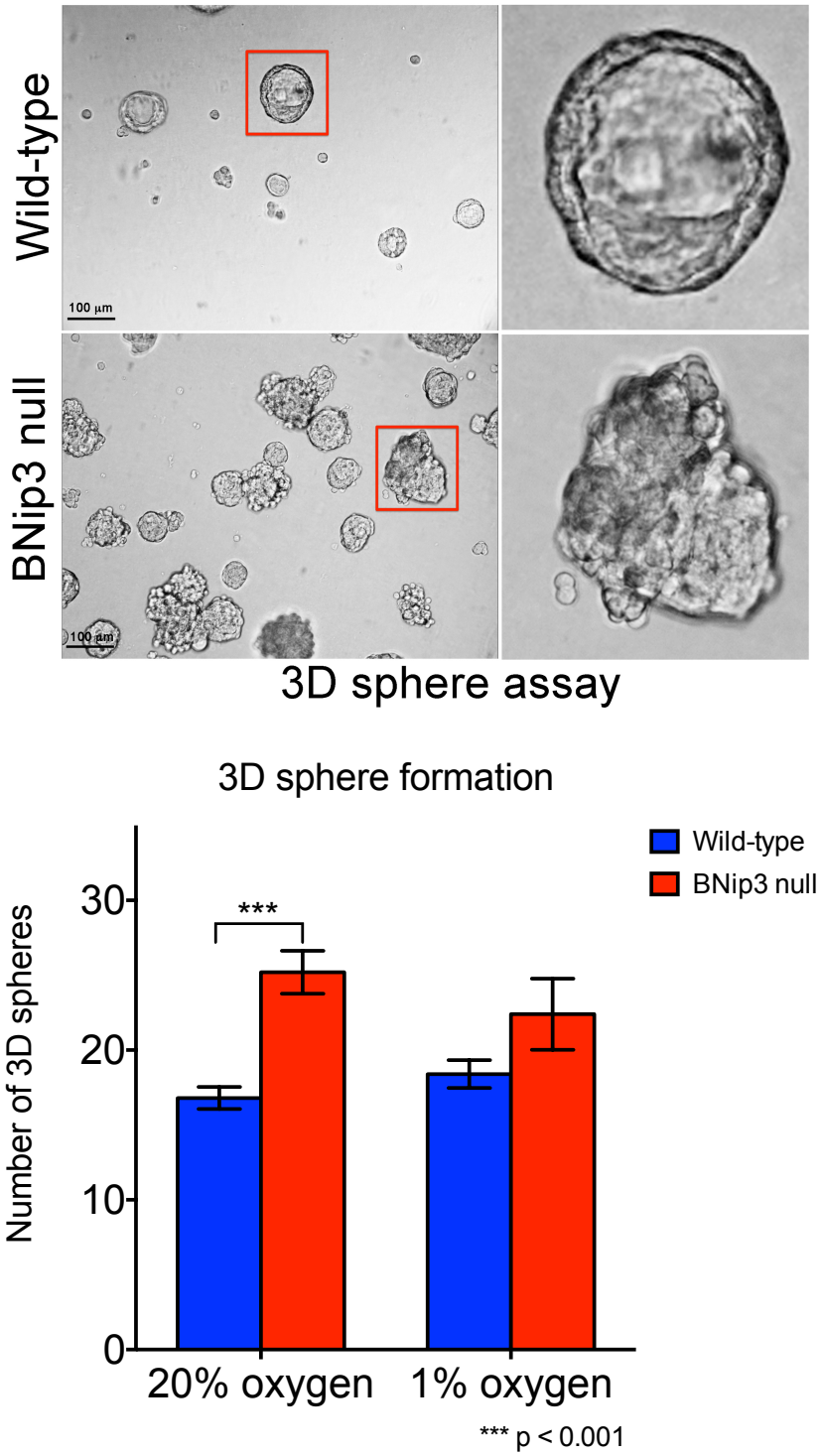


**Figure 12. Loss of BNip3 promotes growth in 3D.**
(Top) Growth of wild-type and BNip3 null 3D spheres in Matrigel at 20% oxygen performed in triplicates. (Bottom) Quantification of 3D spheres in Matrigel at 20% oxygen and 1% oxygen.

### 3.4. BNip3 null mice exhibit accelerated lung metastasis with significantly reduced latency

In order to determine whether the invasive properties of BNip3 null tumor cells affected their ability to metastasize *in vivo*, we compared the latency of lung metastasis and metastatic burden in wild-type and BNip3 null mice. We observed a marked reduction in latency of overt lung metastases in BNip3 null mice compared to their wild-type counterparts. At day80, BNip3 null mice had significant numbers of readily detectable overt lung metastases. On the other hand, wild-type mice had very few, if any overt lung metastases detected at day 80 (Figure 13A-B). Together these results indicate that loss of BNip3 accelerates mammary tumor progression to metastasis in MMTV-PyMT mice.

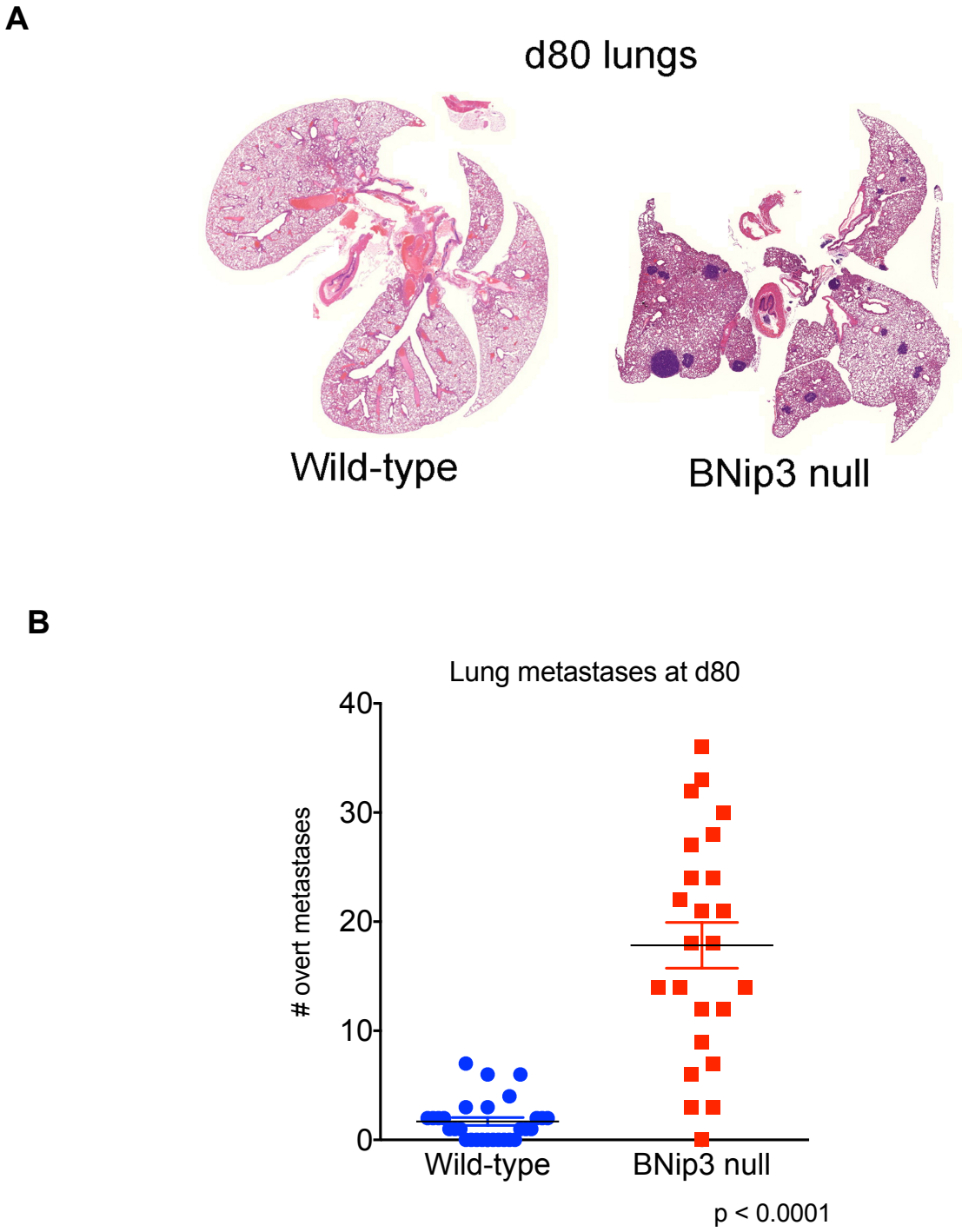


**Figure 13. Loss of BNip3 increases lung metastases.**
(A) Increased lung metastases at d80 in BNip3 null mice (n = 21) compared to wild-type (n = 24). (B) Quantification of lung metastases at d80. (Data from Kristin Tracy)

### 3.5. BNIP3 is deleted in human triple negative breast cancer

Our data revealed that loss of BNip3 in MMTV-PyMT driven mammary tumorigenesis leads to a significant increase in tumor growth, invasion and lung metastases. Studies have shown that BNIP3 is up-regulated at pre-malignant stages of various cancers including DCIS in breast cancer and PanINs in PDAC (112,113,121). However, it is down-regulated as the tumors progress to invasive carcinoma as in invasive ductal carcinoma of the breast and in PDAC. The importance of BNIP3 loss during tumor progression is highlighted by the fact that there is selective pressure to epigenetically silence it in hematological malignancies and cancers of the pancreas, liver and lung (117-120). Our data coupled with these studies prompted us to investigate whether BNIP3 was deregulated in human breast cancer. We examined the cancer genome atlas (TCGA) database for copy number variation (CNV) and changes in expression levels of BNIP3 in breast cancer. Interestingly, we found that TNBC had a significant increase in BNIP3 copy number loss, which was not the case for non-TNBCs or receptor positive breast cancers (Figure 14A-B). While changes in BNIP3 expression levels were observed in non-TNBC patient population, they did not strongly associate with BNIP3 CNV (Figure 14C). However, in case of TNBC patient population, we observed a much stronger association between BNip3 expression levels and CNV (Figure 14D). These results further reinstate the significance of BNIP3 loss in breast cancer, specifically in TNBC.

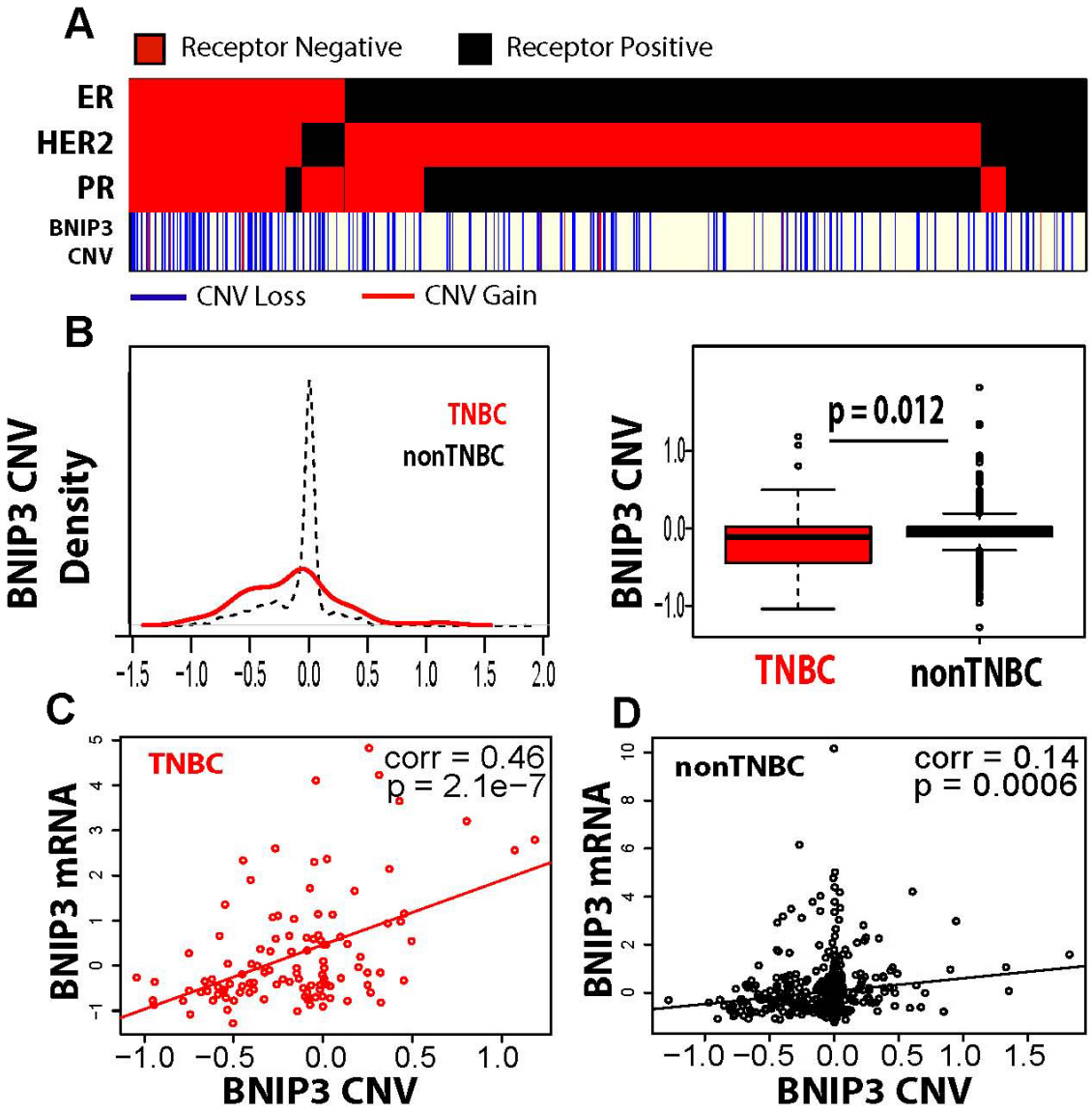


**Figure 14. BNip3 is deleted in human triple negative breast cancer.**
(A) Hormone receptor status (red = negative, black = positive) and chromosomal copy number variation (CNV) of BNip3 (red = gain, blue = loss, white = unchanged) from n = 689 patient samples in The Cancer Genome Atlas (TCGA) breast cohort where status is unambiguously assigned for all three hormone receptors. Relative frequency of copy number variation (CNV) of BNip3 in triple negative breast cancer (TNBC; red, n = 113) and non-TNBC (black, n = 576) in TCGA breast cohort. (C) TCGA TNBC breast tumors (red, n = 113) show a significantly more chromosomal loss than non-TNBC tumors (black, n = 576). (D) RNAseq derived mRNA expression levels of BNip3 in TNBC correlated to chromosomal copy number variation of BNip3 in TNBC samples of the TCGA breast cancer cohort (n = 113). (E) mRNA expression levels of BNip3 correlated to chromosomal copy number variation of BNip3 in non-TNBC samples of TCGA breast cancer cohort (n = 576). (Data from Casey Frankenberger)

## 3.6. Conclusion

In this chapter, we have shown that BNip3 is down-regulated with tumor progression in the MMTV-PyMT, suggesting that it may be inhibiting this process. To understand the significance of this down-regulation, we deleted BNip3 in the tumor model and observed that its loss increases primary tumor growth and tumor cell proliferation with no difference in cell death. BNip3 null tumors show a more rapid progression to carcinoma and consistently, BNip3 null tumor cells are highly migratory and invasive in nature and show increased and disorganized growth when cultured in three-dimensional matrigel. Lastly, BNip3 null tumors exhibit reduced latency for lung metastasis and show increased lung metastases. The above-mentioned data indicates that BNip3 functions to suppress tumor growth and progression to metastasis.

# CHAPTER 4

# LOSS OF BNIP3 LEADS TO DYSFUNCTIONAL MITOCHONDRIA AND DEREGULATED TUMOR CELL METABOLISM

## 4.1. Introduction

Recent studies have highlighted the importance of functional mitochondria and oxidative metabolism in tumor cell survival and proliferation (18-20). Investigation of cancer cell lines cultured under low glucose to mimic the nutrient starvation conditions present in tumors showed that cancer cells relied heavily on oxidative phosphorylation to proliferate under nutrient stress. Oncogene ablation resistant tumor cells have also showed a dependence on oxidative metabolism for their survival. Yet, we have tumors that exhibit dysfunctional mitochondria and a reliance on aerobic glycolysis for energy demands and anabolic processes such as nucleic acid and fatty acid synthesis (22,29,36). Given this dichotomy, it becomes imperative to understand the functional consequences of defective mitophagy, a guardian of mitochondrial health and integrity, on tumor cells.

BNip3 is a bona fide regulator of mitophagy. We and others have shown that loss of BNip3 results in reduced mitochondrial mass and mitochondrial membrane potential along with accumulation of ROS and have shown its importance in maintaining the overall mitochondrial health in cells (22,36,99). However, this has not been investigated in the context of tumor growth and progression. Given that our data showed that BNip3 functions to suppress tumor growth and metastasis, we delved into the mechanism of

how it may be doing so by first investigating the functional status of wild-type and Bnip3 null tumor mitochondria.

In this chapter, we have assessed the effect of BNip3 loss on the overall levels of mitophagy in mammary tumor cells. Since, mitophagy is known to regulate mitochondrial mass and maintain mitochondrial function, we have investigated the effect of BNip3 loss on these functional aspects of mitophagy. Given that mitochondria play a key role in cellular metabolism and that glucose and glutamine are the two essential substrates that govern cellular metabolic reactions, we have examined the effect of loss of BNip3 on glucose and glutamine metabolism in tumor cells. Lastly, we have assessed if loss of BNip3 affects mitochondrial respiration by comparing levels of oxidative phosphorylation between the two genotypes.

### 4.2. BNip3 null tumor cells have reduced mitophagy

Given that mitophagy is one of the main functions of BNip3, we investigated the effect of loss of BNip3 on mitophagy in mammary tumor cells. We performed coimmunofluorescence assay for endogenous LC3 and cyclophilin D to determine levels of mitophagy in wild-type and BNip3 null MECs. While LC3, present in the inner and outer membrane of the autophagosome is a widely accepted marker for autophagy, cyclophilin D is mitochondrial matrix protein that regulates mitochondrial permeability transition pore and, hence is used as mitochondrial marker (33,158). Expectedly, BNip3 null MECs had significantly reduced overlap of LC3 positive autophagosomes and cyclophilin D positive mitochondria as compared to wild-type MECs under untreated conditions of 20% oxygen (Figure 15A-B). Since, BNip3 is strongly induced by hypoxia

and autophagy is inhibited by bafilomycin, we also tested for changes in mitophagy at 1% oxygen (hypoxia) and 1% oxygen + bafilomycin (hypoxia + bafilomycin). However, while we observed a significant increase in mitophagy in wild-type MECs under the above-mentioned conditions, there was no increase in mitophagy in BNip3 null MECs under the same conditions. To further confirm that the significant decrease in mitophagy in BNip3 null MECs was indeed due to the absence of BNip3, we rescued BNip3 null cells by expression of empty-vector and exogenous BNip3-wild-type vector under the above-mentioned conditions. As expected, we observed a significant increase in mitophagy by in exogenous BNip3-wild-type infected cells, but not in empty-vector infected or BNip3 null parental MECs. These results confirmed that mitophagy is effectively reduced by loss of BNip3 in mammary tumor cells.

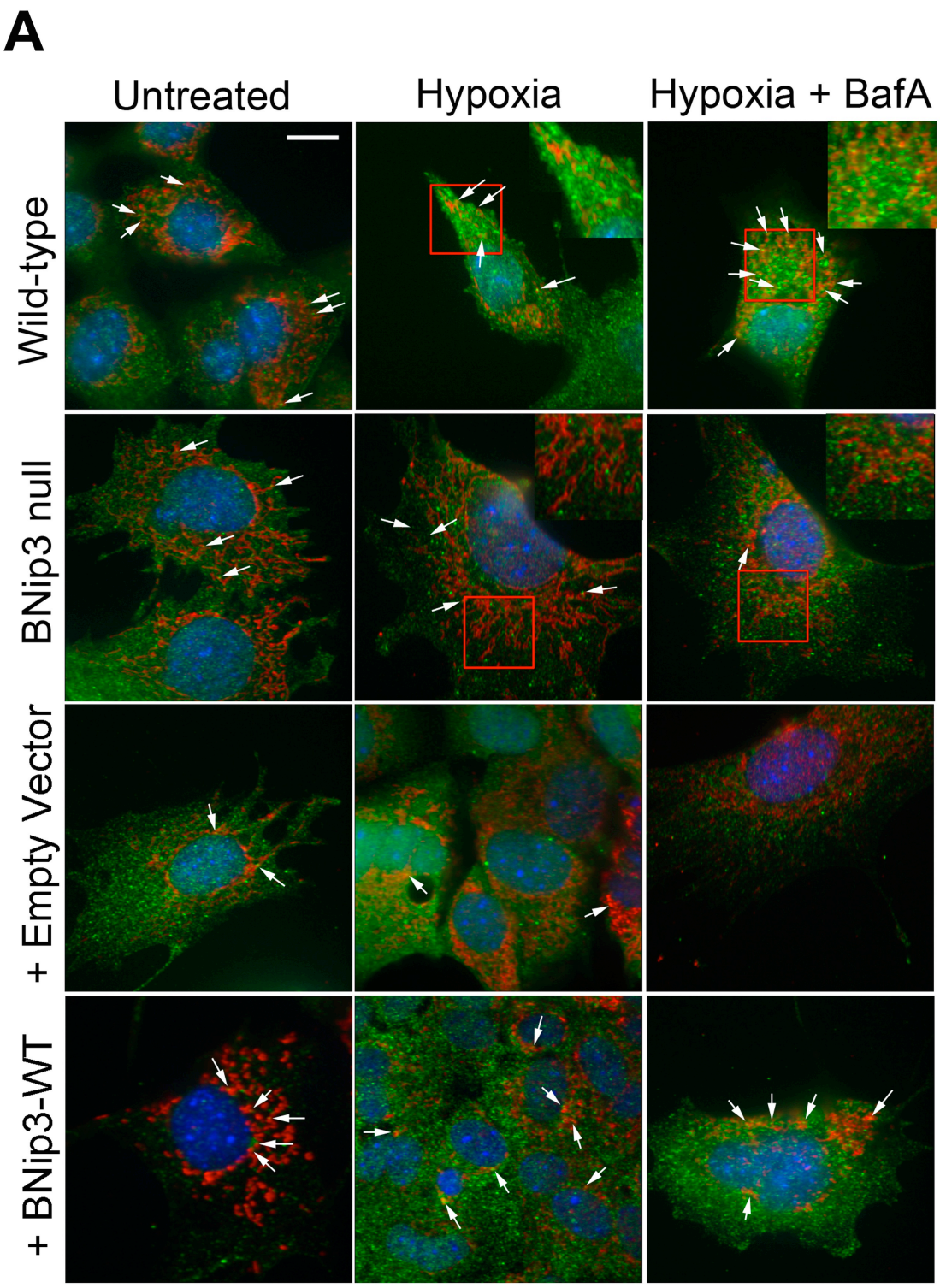


**Figure 15. Loss of BNip3 decreases mitophagy in MECs.**

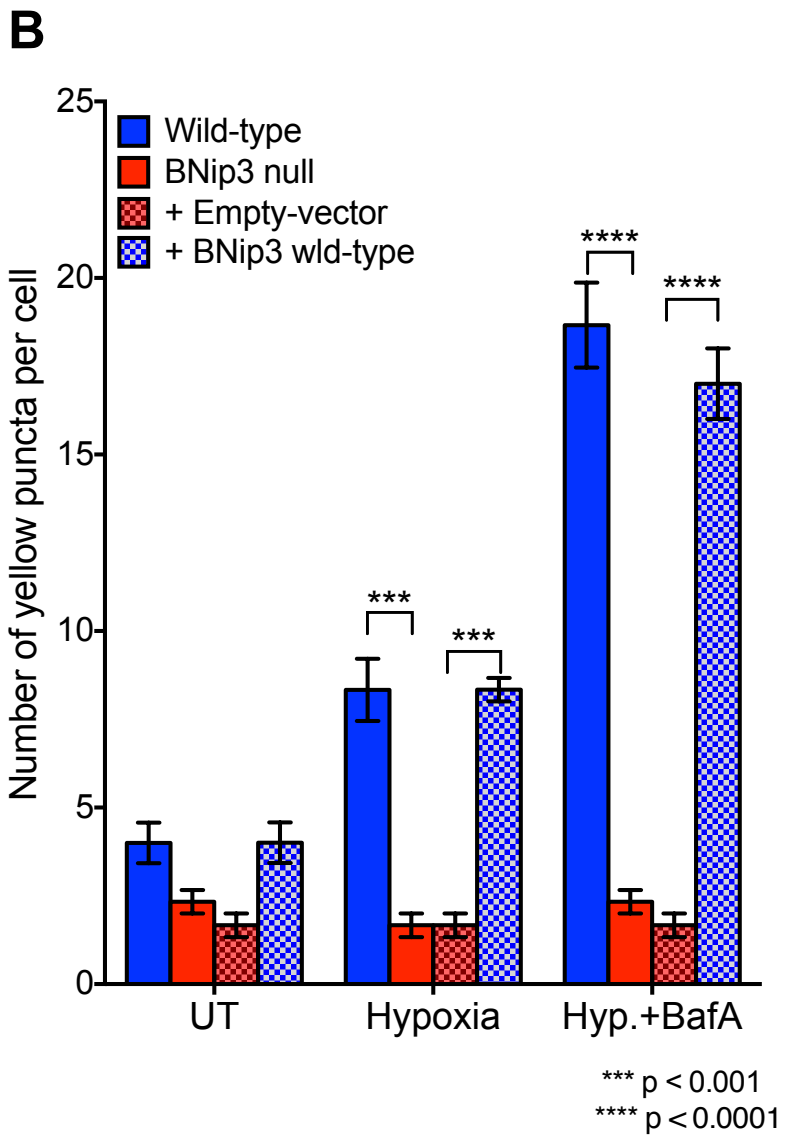


**Figure 15. Loss of BNip3 decreases mitophagy in MECs.**
(A) Co-immunofluorescence for endogenous LC3 (green, autophagosomes) and cyclophilin D (red, mitochondria) to examine the levels of mitophagy in wild-type and BNip3 null MECs determined as the number of yellow puncta arising due to overlap of mitochondria and autophagosome (indicated by white arrows). This was examined at 20% oxygen (untreated), 1% oxygen (hypoxia) and 1% oxygen + bafilomycin A1 (hypoxia + BafA) and in BNip3 null MECs expressing either empty vector control or exogenous BNip3. Scale bar is 20 um. (B) Quantification of number of yellow puncta per 63 x field. n > 4 for all treatments.

### 4.3. Loss of BNip3 is associated with increased mitochondrial mass *in vitro* and *in vivo*

Given that changes in mitophagy can affect the overall quantity and quality of mitochondria in cells, we investigated the effect of BNip3 loss on mitochondrial mass in mammary tumor cells. In order to study the changes in mitochondrial mass, we analyzed mitochondrial:nuclear genome ratio in wild-type and BNip3 null MECs by qRT-PCR for mitochondrial genome-encoded Nd1 and Cytb standardized to nuclear genome-encoded β-globin. Both, Nd1 and Cytb are genes for mitochondrial respiratory chain proteins with Nd1 encoding for NADH dehydrogenase subunit 1 (part of complex I) and Cytb encoding for cytochrome b (part of complex III) (99). We observed a significant increase in mitochondrial:nuclear genome ratio in BNip3 null MECs as compared wild-type cells which was rescued when BNip3 null MECs were infected with exogenous BNip3-wild-type vector, but not empty-vector (Figure 16).

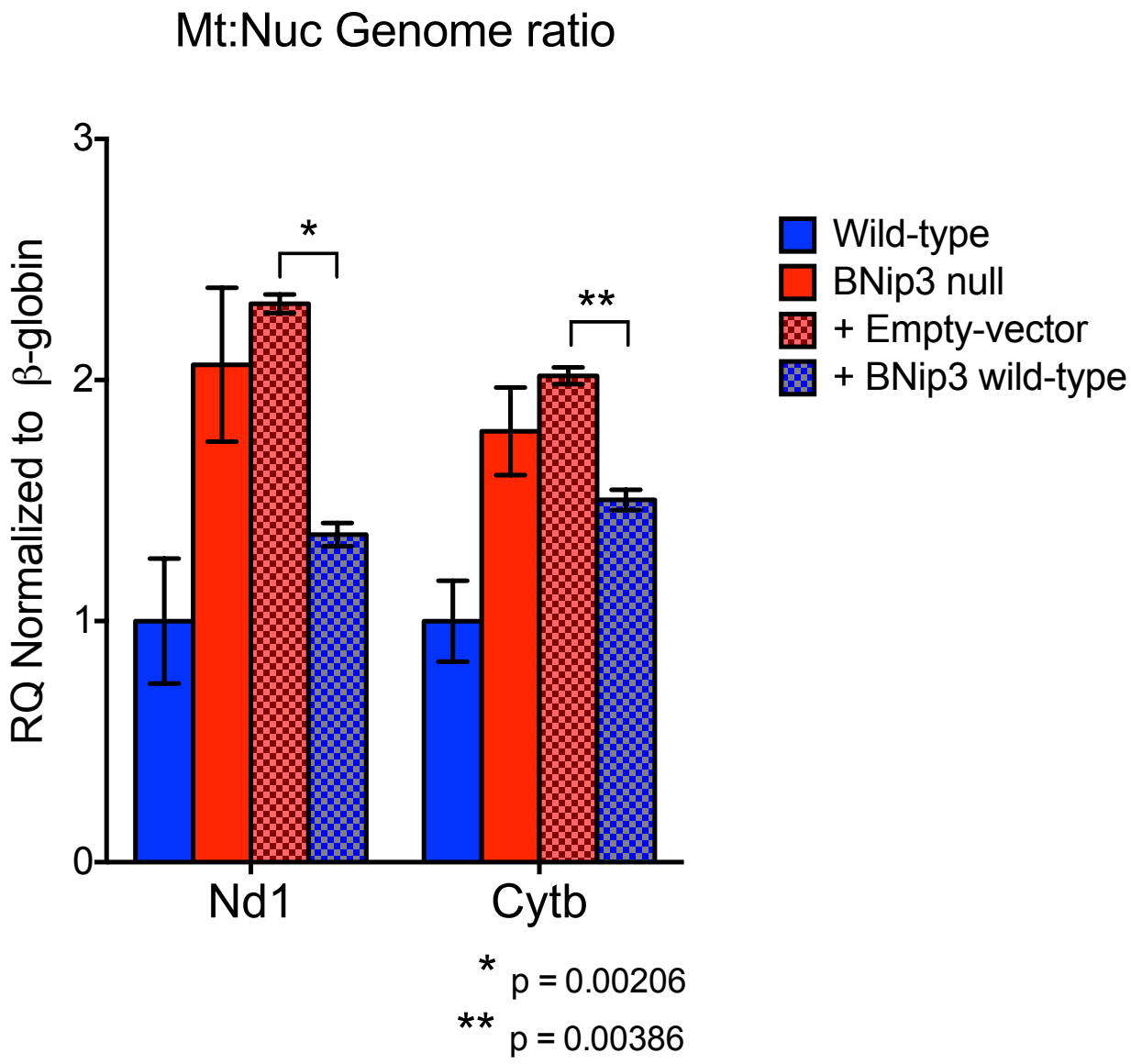


**Figure 16. Loss of BNip3 increases mitochondrial mass in MECs.**
qPCR for mitochondrial genome-encoded Nd1 and Cytb standardized to nuclear encoded b-globin in wild-type MECs, BNip3 null MECs, BNip3 null MECs expressing empty-vector control or BNip3 exogenous BNip3 wild-type for three independent experiments performed in triplicates.

Given the above findings, we investigated if loss of BNip3 had affected other key mitochondrial proteins as a marker for increased mitochondrial mass. IHC analysis of key mitochondrial proteins such as CoxIV, Vdac1 and TOM20 in mammary tumors at day65 showed significantly increased staining for these proteins in BNip3 null tumors as compared to wild-type tumors (Figure 17A-B). While CoxIV is a subunit of cytochrome c oxidase in the mitochondrial respiratory chain, Vdac1 or voltage dependent anion channel 1 is a key channel for calcium ion and ATP transport across the OMM (2,159). TOM20 is a part of the TOM (translocase of outer membrane) receptor complex that recognizes and translocates mitochondrial proteins generated in the cytosol. Furthermore, mitochondrial proteins such as Nix, Vdac1 and CoxIV were also elevated in BNip3 null tumor cells in vitro when examined by immunoblot of whole cell lysates of wild-type and BNip3 null MECs at atmospheric oxygen as well as hypoxia (Figure 18). Interestingly, transmission electron microscopy of wild-type and BNip3 null tumors at day35 showed higher density of mitochondria, many of which appeared abnormally shaped with pinched-off ends, in BNip3 null tumors (Figure 19). Together, these results suggest that loss of BNip3 in mammary tumors results in increased mitochondrial mass due to defective mitophagy.

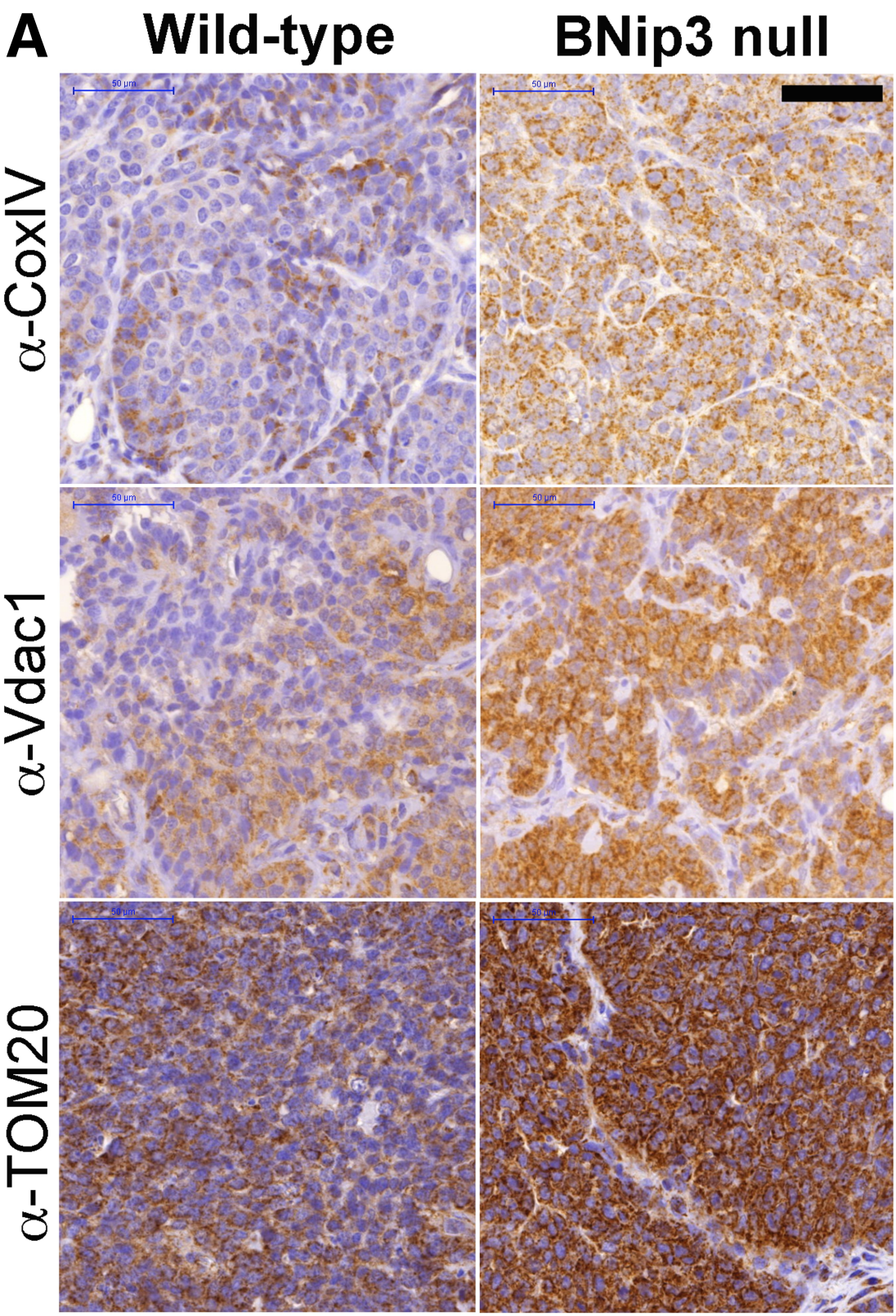


**Figure 17. Loss of BNip3 increases mitochondrial mass in mammary tumors.**

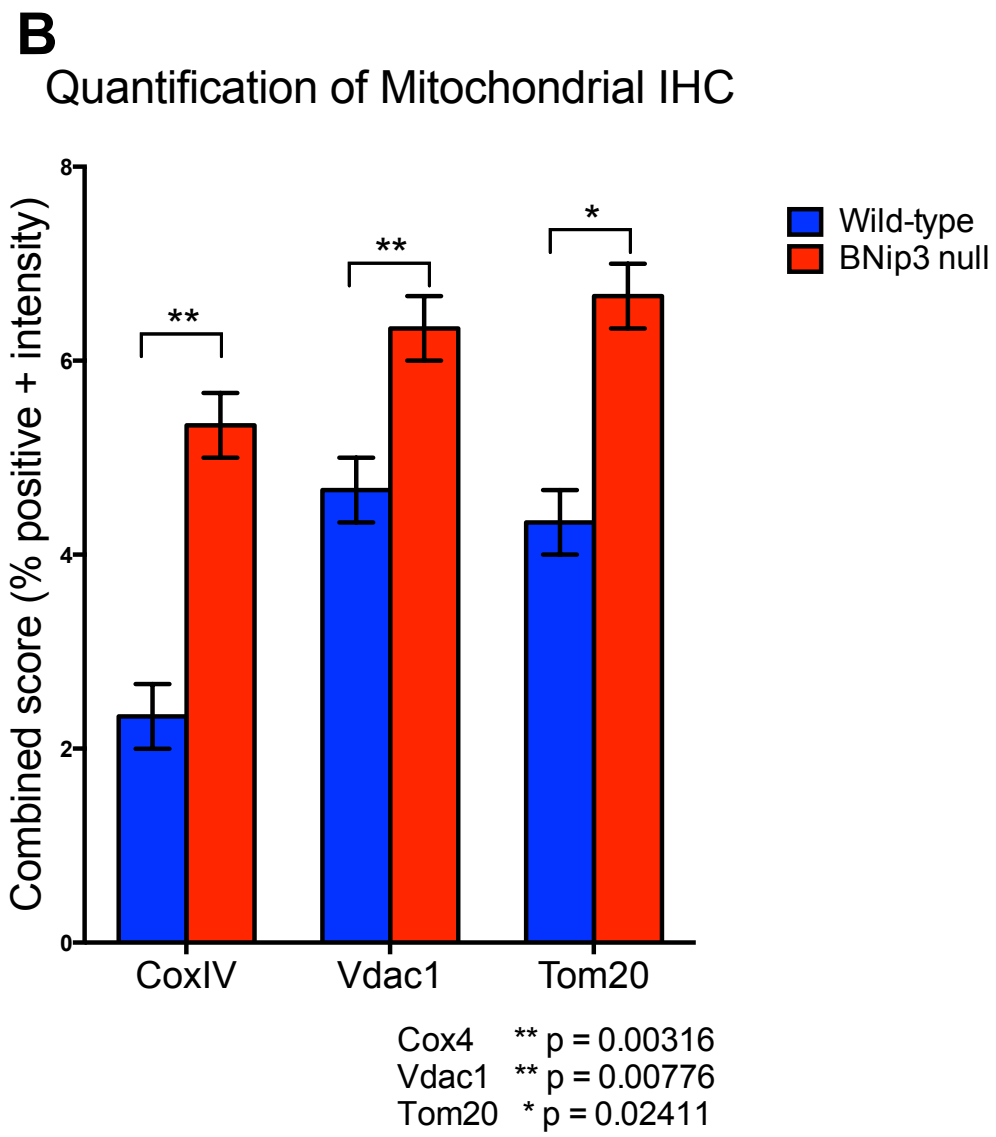


**Figure 17. Loss of BNip3 increases mitochondrial mass in mammary tumors.** (A) Immunohistochemical staining for expression of cytochrome c oxidase-IV (CoxIV), voltage dependent anion channel-1 (Vdac1) and TOM20 on sections from wild-type (n = 4) and BNip3 null (n = 4) tumors at d65. (B) Quantification of IHC staining using the Aperio system. Scale bar is 50 um.

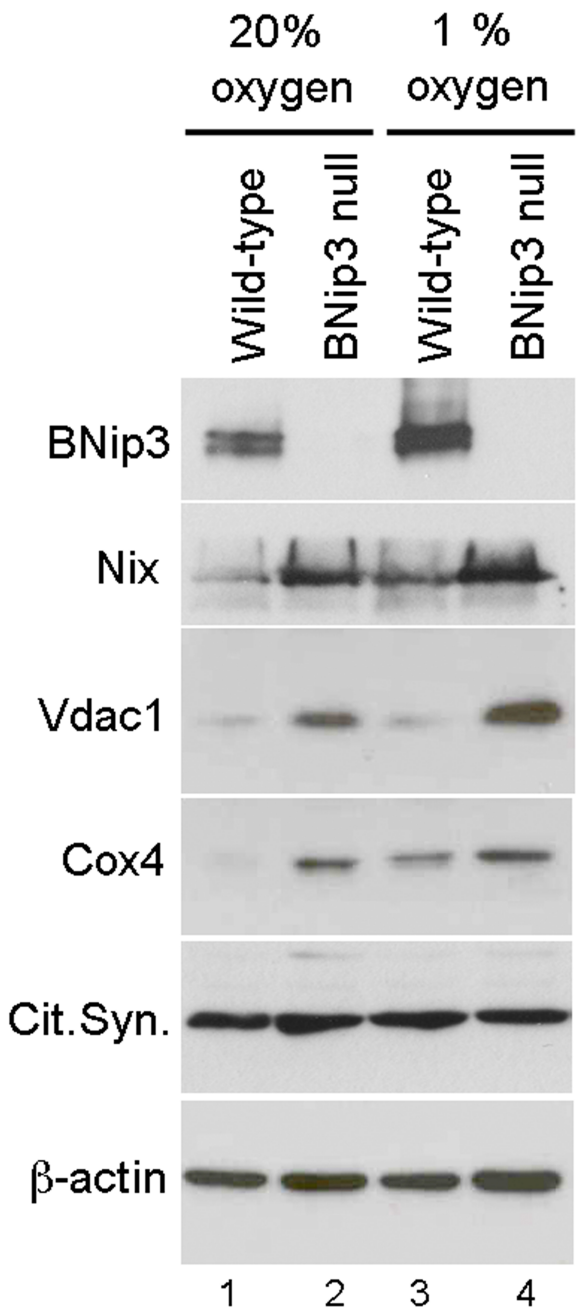


**Figure 18. Loss of BNip3 increases mitochondrial mass in MECs.**
Western blot analysis for expression of mitochondrial proteins in extracts from wild-type and BNip3 null MECs grown at 20% and 1% oxygen.

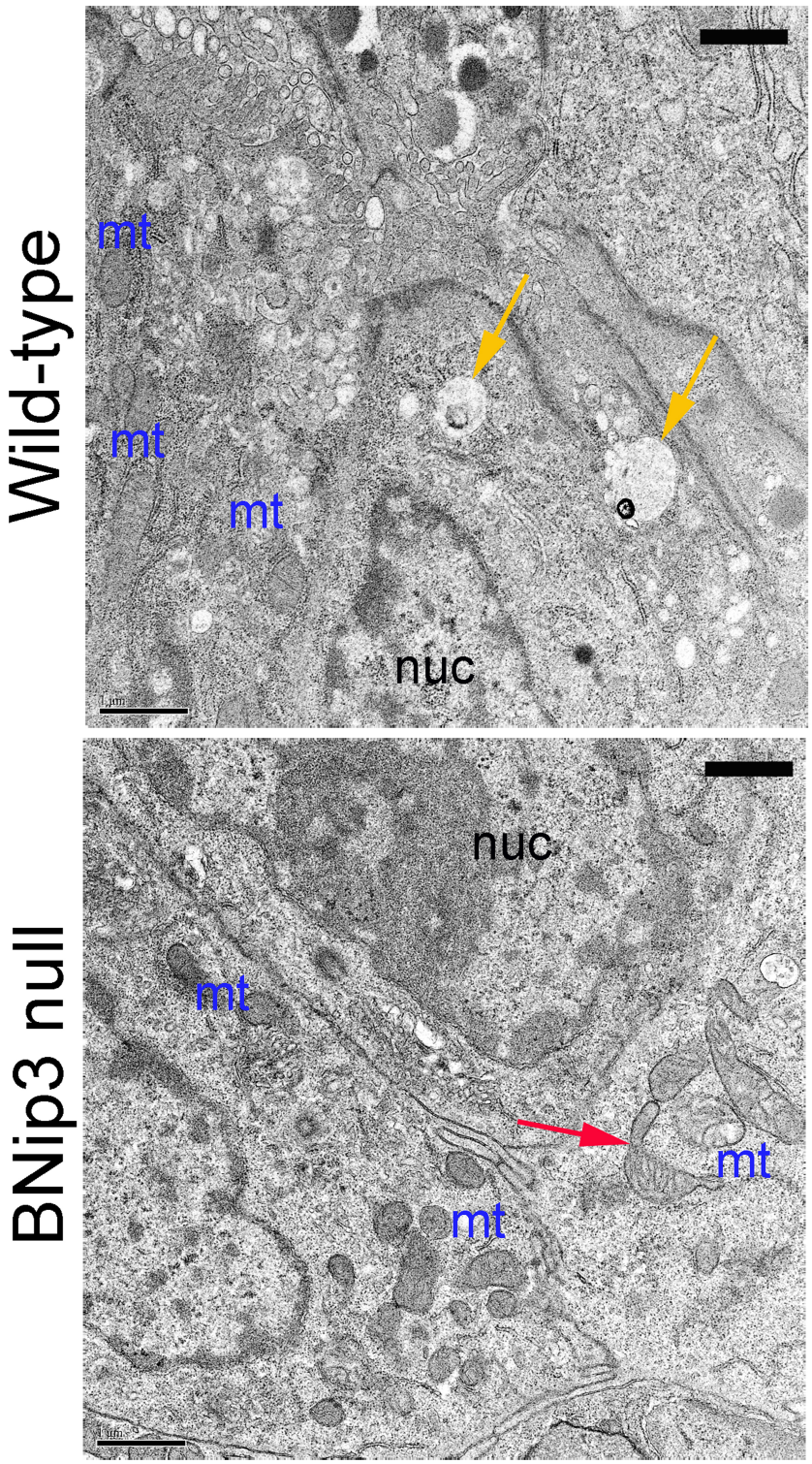


**Figure 19. Transmission electron micrographs of wild-type and BNip3 null primary tumors.** Micrographs at d35 illustrate increased mitochondrial density (mt) in BNip3 null tumors compared to wild-type, altered structure (red arrow) and the presence of vesicles in wild-type tumors (yellow arrows). Scale bar is 1 um.

### 4.4. BNip3 null tumor cells exhibit reduced mitochondrial function

Mitophagy functions to eliminate dysfunctional mitochondria by increasing their turnover at the autophagosome. Given that our data showed that loss of BNip3 reduced mitophagy in mammary tumor cells, we examined the effect of BNip3 loss on mitochondrial function in these cells.

Healthy mitochondria with optimally functioning respiratory chain at the IMM, generate a mitochondrial membrane potential that can serve as an indicator of mitochondrial function. Thus, we determined the effect of BNip3 loss on mitochondrial function by measuring the mitochondrial membrane potential using a cell permeant, potentiometric dye, TMRE, that is taken up by active mitochondria due to their relative negative charge. We observed a significant decrease in TMRE uptake by BNip3 null MECs as compared to wild-type mammary tumor cells at atmospheric oxygen (Figure 20A) indicating that loss of BNip3 is associated with increased depolarized mitochondria in tumor cells. While BNip3 null MECs also showed reduced TMRE uptake under hypoxic conditions as compared to wild-type cells, the difference was not statistically significant.

As a measure of mitochondrial function, we also measured mitochondrial uptake of substrates such as $^{14}$C-labeled pyruvate and $^{14}$C-labeled glutamine. Upon mitochondrial uptake, while pyruvate is converted to acetyl coA which enters the TCA cycle, glutamine is converted to a-ketoglutarate as a part of glutaminolysis. We observed that BNip3 null tumor cells had a significantly reduced uptake of both these substrates as compared to wild-type MECs (Figure 20B). We also detected a significant decrease in citrate synthase activity in BNip3 null MECs compared to wild-type MECs

(Figure 20C). However, in order to ensure that the reduced enzymatic activity was not a due to reduced levels of the protein in the mitochondria, we measure the levels of citrate synthase in tumor cells by immunoblot and did not detect any significant differences between wild-type and BNip3 null MECs at atmospheric oxygen or hypoxia (Figure 18). Together, these results suggest that loss of BNip3 reduces overall mitochondrial function, thus adversely affecting integrity of the mitochondrial pool in mammary tumor cells.

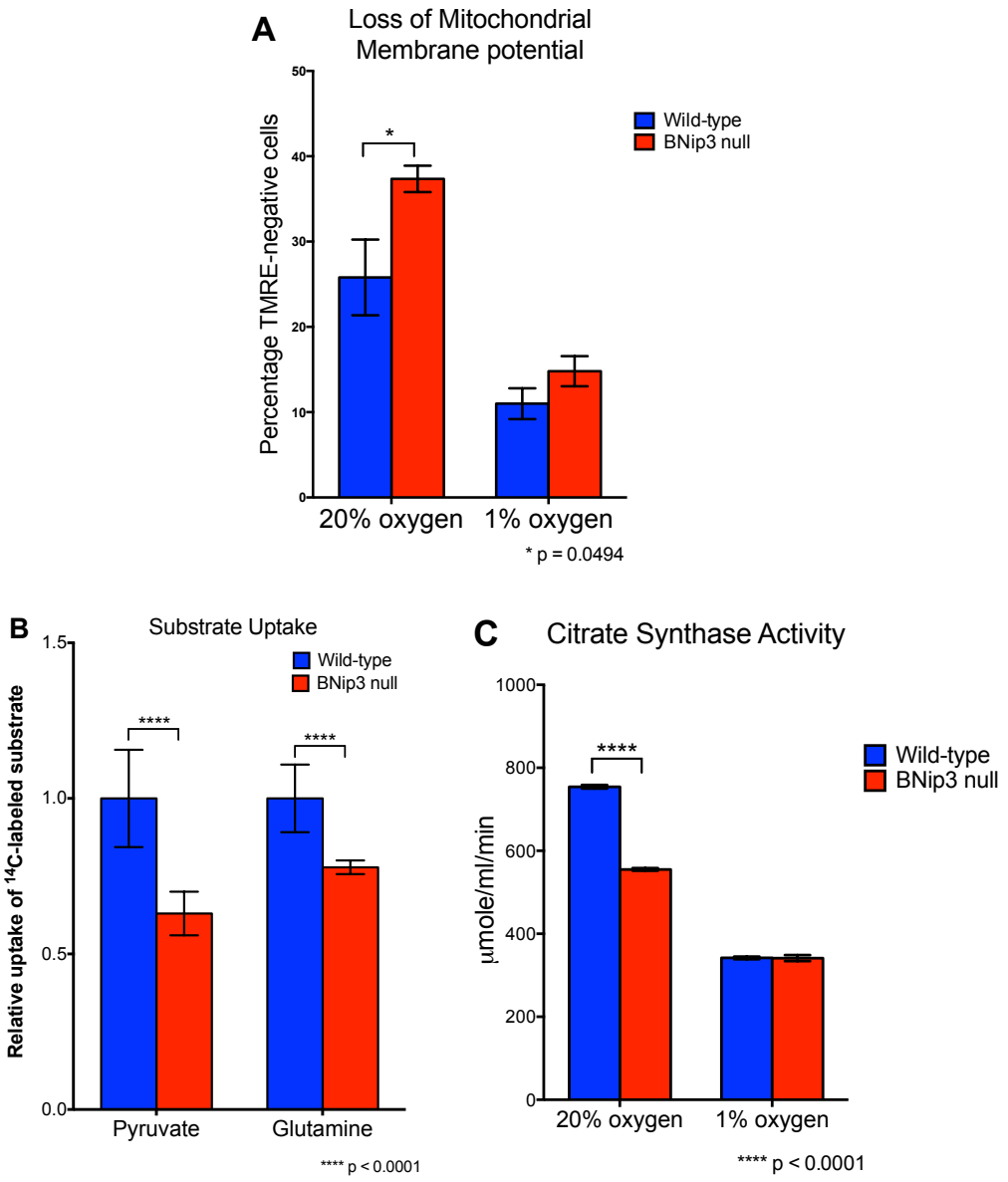


**Figure 20. BNip3 null mammary tumor cells exhibit reduced mitochondrial function.** (A) Flow cytometric analysis of TMRE staining as a measure of mitochondrial membrane potential in wild-type and BNip3 null MECs grown at 20% and 1% oxygen, measured in triplicate experiments. (B) Measurement of uptake of 14C-labeled pyruvate or glutamine by wild-type and BNip3 null MECs, measured in triplicate experiments. (C) Citrate synthase activity assay as a measure of mitochondrial function on wild-type and BNip3 null MECs grown at 20% and 1% oxygen, measured in triplicate experiments.

### 4.5. Loss of BNip3 is associated with increased glucose uptake and aerobic glycolysis *in vitro* and *in vivo*

Cellular metabolism is one of the key functions of mitochondria in cells (1,2). However, cancer cells often have highly altered metabolism as a result of mutations in mitochondrial genome or nuclear-encoded mitochondrial proteins, changes in mitochondrial dynamics or mass, oncogenic regulation of mitochondrial function as well as retrograde signaling from mitochondria to the nucleus (22). Thus, given that our data indicated that loss of BNip3 increased mitochondrial mass but reduced mitochondrial function, we examined the effect of BNip3 on tumor cell metabolism.

We performed Micro-PET/CT imaging of 2-deoxy-2-[fluorine-18]fluoro-D-glucose ($^{18}$F-FDG) on age-matched wild-type and BNip3 null mice at day50 in order to assess for glucose uptake by their respective tumors (160). Positron emission tomography (PET) with $^{18}$F-FDG integrated with computed tomography (CT) is a strong tool for detection of tumors owing to their property of high glucose uptake. Fluorine-18 is a positron emitting radioisotope which substitutes for the normal hydroxyl group at the 2' position in glucose such that it can be detected by PET/CT. We chose day50 as our time-point for assessment since, tumors at this stage were similar in size and thus any changes in $^{18}$F-FDG uptake would not be skewed due to differences in tumor volume. We observed significantly higher $^{18}$F-FDG uptake by BNip3 null tumors as compared to tumors in wild-type mice (Figure 21A). In order to determine whether BNip3 null tumor cells exhibited similar phenotype *in vitro*, we performed glucose uptake assay using 2-[N-(7-nitrobenz-2-oxa-1,3-diazol-4-yl) amino]-2-deoxy-D-glucose or 2-NBDG which is a fluorescently labeled deoxyglucose analog that is easily taken up by cells in culture

(161). We observed that consistent with their behavior *in vivo*, BNip3 null MECs showed an increase in glucose uptake compared to wild-type MECs at atmospheric oxygen as well as under hypoxic conditions (Figure 21B). These results suggested that BNip3 null tumors were more glycolytic than wild-type tumors.

A common characteristic of glycolytic tumors is increased conversion of pyruvate to lactate by lactate dehydrogenase. We measured the conversion of $^{13}$C-2-glucose to lactate in wild-type and BNip3 null MECs by NMR and observed that BNip3 null MECs had significantly increased lactate output at atmospheric oxygen and hypoxia as compared to wild-type cells (Figure 21C).

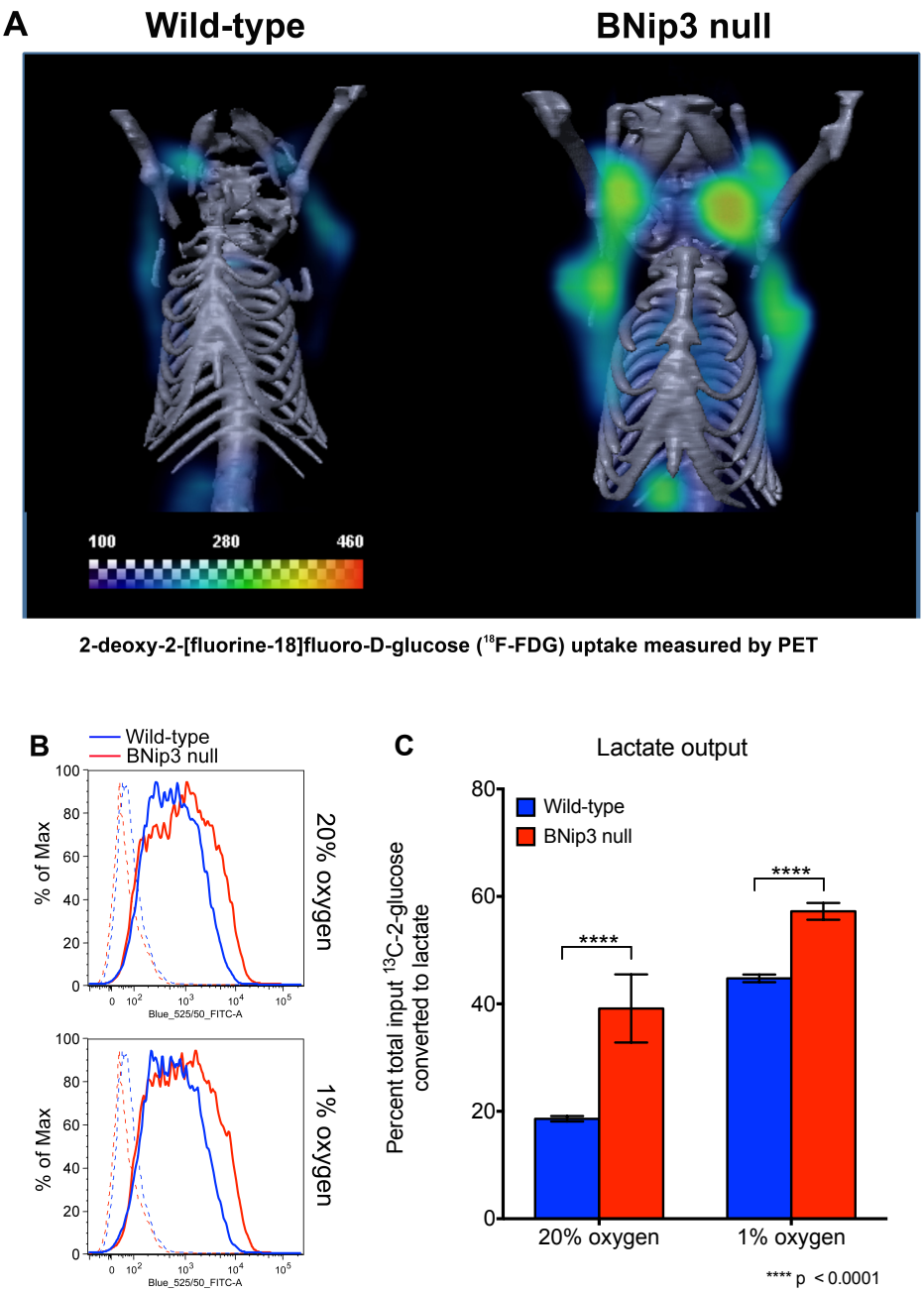


**Figure 21. BNip3 loss increases glucose uptake and lactate output.**
(A) μPET/CT imaging of wild-type and BNip3 null mice at d50 following injection of mice with $^{18}$F-FDG to examine glucose uptake by tumors. (B) Flow cytometric measurement of fluorescent glucose uptake by wild-type and BNip3 null MECs grown in vitro at 20% and 1% oxygen. (C) Lactate output by wild-type and BNip3 null MECs grown at 20% and 1% oxygen was measured by NMR.

Given that the above-mentioned results were consistent with BNip3 null MECs being more glycolytic, we performed a comprehensive metabolite profiling by culturing wild-type and BNip3 null MECs in [U-$^{13}$C]-glucose or [U-$^{13}$C]-glutamine for 6 hours and measuring levels of $^{13}$C-labeled metabolites by LC-MS. We detected significantly higher levels of glycolytic intermediates such as glucose-6-phosphate (Glu-6-P), fructose-1,6-bisphosphate(fru-1,6-BisP), glyceraldehyde-3-phosphate (G3P), dihydroxyacetone phosphate (DHAP), phosphoenol pyruvate (PEP) and pyruvate in BNip3 null MECs compared to wild-type cells (Figure 22A). However, levels of 2,3-bisphosphoglycerate (2,3-BisPG) and 3-phosphoglycerate (3PG) were not increased in BNip3 null MECs possibly due to an increased use of DHAP for G3P synthesis (Figure 22B).

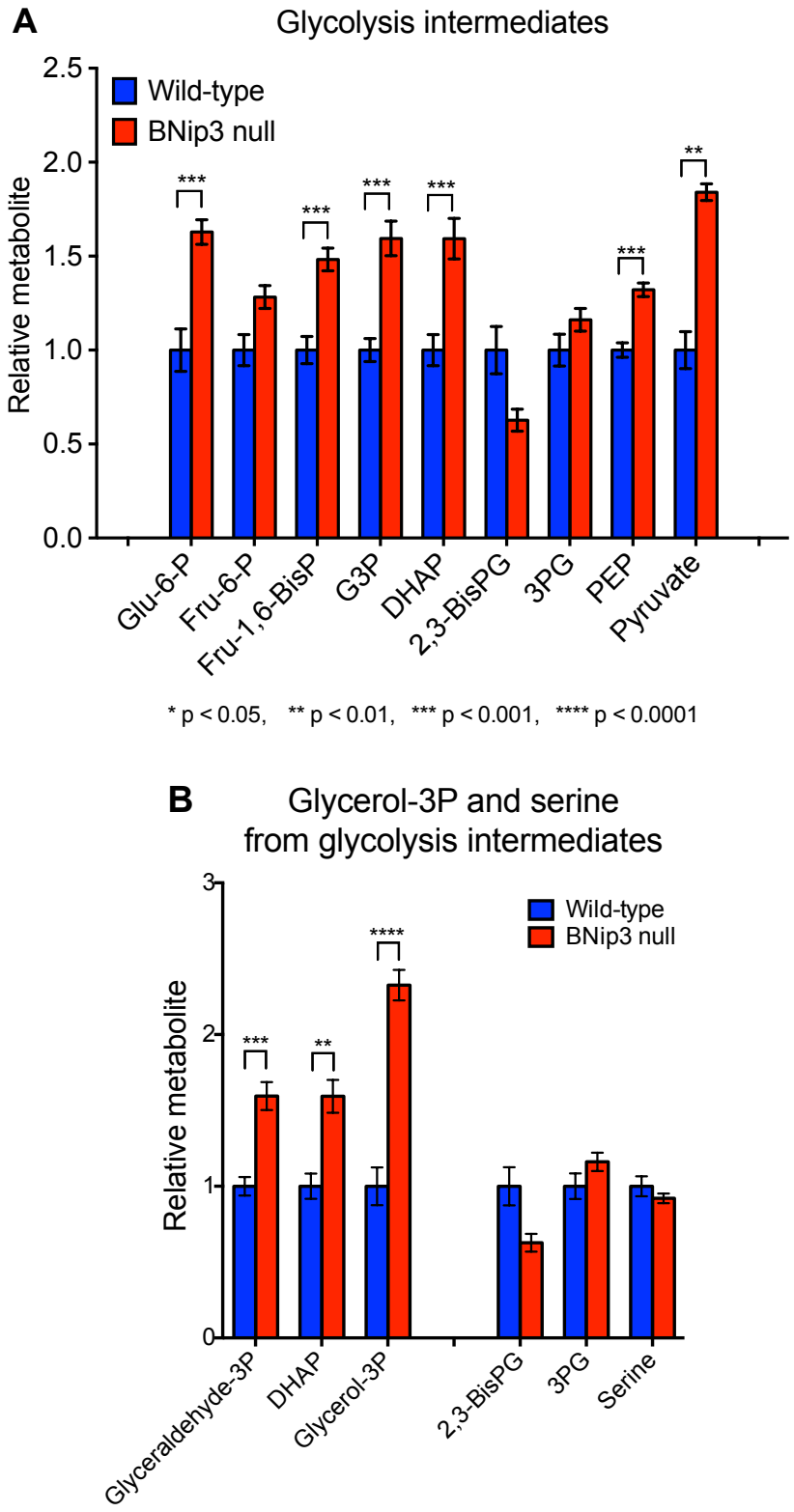


**Figure 22. Loss of BNip3 induces aerobic glycolysis in MECs.** (A) Mass spectrometric measurement of total levels of glycolytic intermediates. (B) Mass spectrometric measurement of total levels of glycerol-3P and serine from glycolysis intermediates.

Interestingly, analysis of TCA cycle intermediates from glucose revealed significantly reduced total metabolite levels of intermediates such as citrate, isocitrate, succinate and oxaloacetate (OAA) (Figure 23A) in BNip3 null MECs which was consistent with our earlier results of reduced substrate uptake by mitochondria (Figure 20B). However, upon evaluation of $^{13}$C-glucose derived metabolite levels, it was evident that BNip3 null MECs had a significantly higher proportion of glucose derived carbon contribution towards all of the TCA cycle intermediates when compared to wild-type MECs (Figure 23A). These results suggested that BNip3 null cells had either greater consumption and/or reduced generation of TCA intermediates such as citrate and oxaloacetate. Given that tumor cells utilize citrate for fatty acid synthesis and convert oxaloacetate to aspartate for purine and pyrimidine biosynthesis, it is likely that reduced total levels of citrate and oxaloacetate in BNip3 null MECs is due to their diversion into these biosynthetic pathways. This is consistent with our results for nucleic acid (DNA and RNA) synthesis from $^{14}$C-glucose and lipid synthesis from $^{14}$C-glucose and $^{14}$C-glutamine, which show a significantly increased rate of nucleic acid and lipid production in BNip3 null MECs compared to wild-type cells (Figure 23B and Figure 23C). However, given that nucleic acid production in BNip3 null MECs was primarily via the oxidative arm of the pentose phosphate pathway, oxaloacetate may be serving as only a partial source for nucleotide synthesis. On the other hand, given that there was reduced conversion of $^{14}$C-glutamine into lipids in BNip3 null MECs, it is more likely that glucose derived glycerol-3-phosphate and citrate contribute towards lipid synthesis and not reductive carboxylation from glutamine.

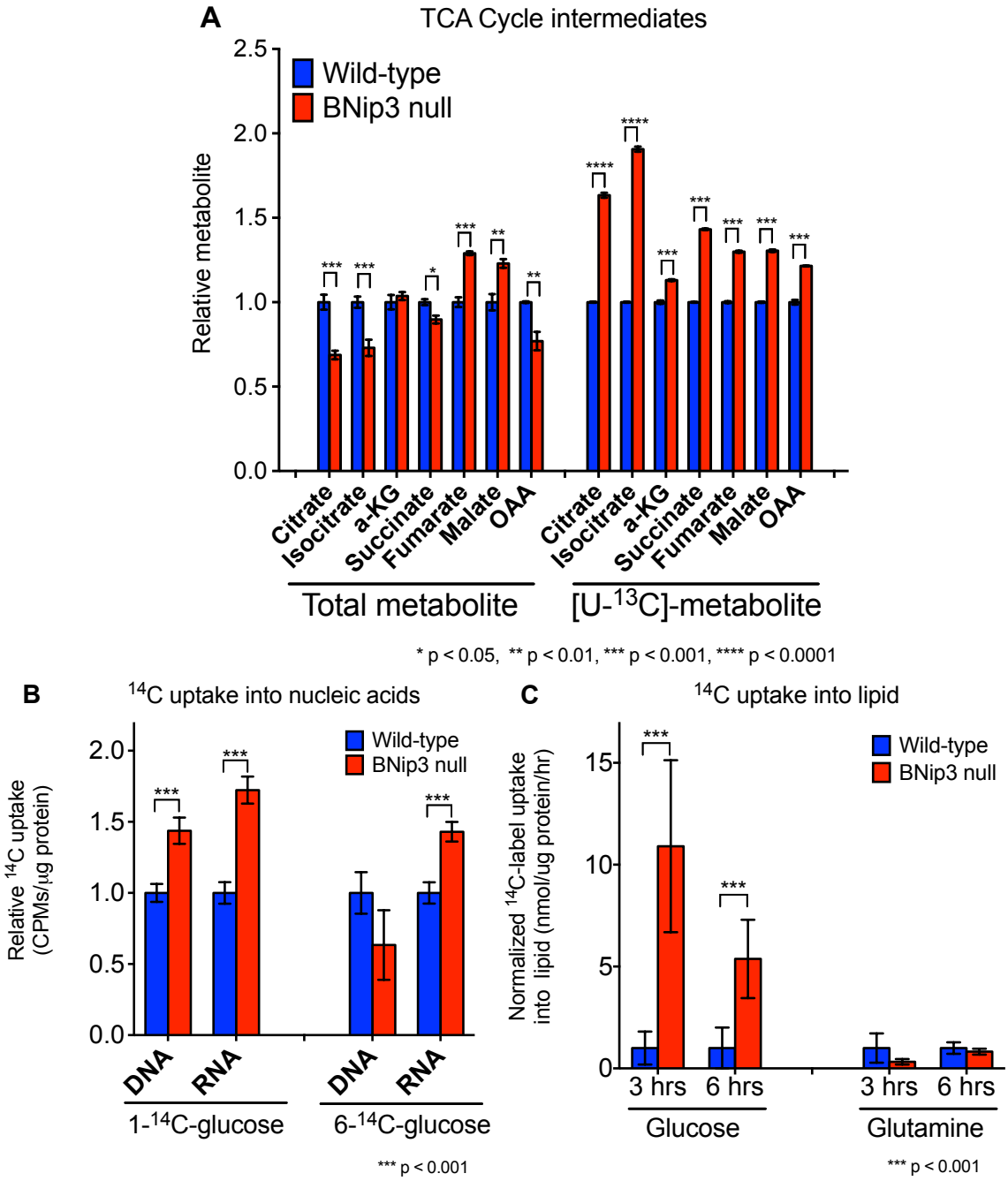


**Figure 23. Loss of BNip3 induces aerobic glycolysis in MECs.** (A) Mass spectrometric measurement of total levels of TCA cycle intermediates and of $^{13}$C-labeled intermediates after growth in [U$^{13}$C]-glucose for 6 hours. (B) Measurement of uptake of $^{14}$C-labeled glucose into nucleic acids in wild-type and BNip3 null MECs. (H) Measurement of uptake of $^{14}$C-labeled glucose or glutamine into lipid in wild-type and BNip3 null MECs. (Lipid uptake data from Michelle Boland)

### 4.6. BNip3 null tumor cells have markedly reduced oxidative metabolism

A key function of mitochondria is to generate ATP by maintaining oxidative metabolism. Our data suggested that loss of BNip3 reduced overall mitochondrial function as well as total levels of key TCA cycle intermediates such as citrate, isocitrate, succinate and oxaloacetate in mammary tumor cells, thus prompting us to investigate the effect of BNip3 loss on mitochondrial respiration. We examined changes in oxygen consumption rate (OCR) between wild-type and BNip3 null MECs using Seahorse XF96. OCR was measured using glucose, glutamine and glucose + glutamine as substrates in order to assess if OXPHOS in mammary tumor cells was driven by glycolysis or glutaminolysis or both. Cells were treated with oligomycin (inhibits ATP synthase), FCCP (uncoupler of the electron transport chain) and antimycin A (inhibitor of cytochrome c reductase) during the assay in order to detect effects on basal and maximal respiration (99,149). BNip3 null MECs exhibited significantly reduced basal respiration as well as FCCP stimulated spare respiratory capacity when compared to wild-type tumor cells in the presence of each of these substrates (Figure 24A, Figure 24B and Figure 24C). In order to confirm that the effect on mitochondrial respiration was indeed due to BNip3, we infected BNip3 null MECs with empty-vector and BNip3-wild-type expressing vector and observed that both, basal respiration and spare respiratory capacity were increased upon exogenous expression of BNip3 (Figure 24D). These results indicate that loss of BNip3 compromises mitochondrial function by reducing oxidative metabolism in mammary tumor cells regardless of the substrate source.

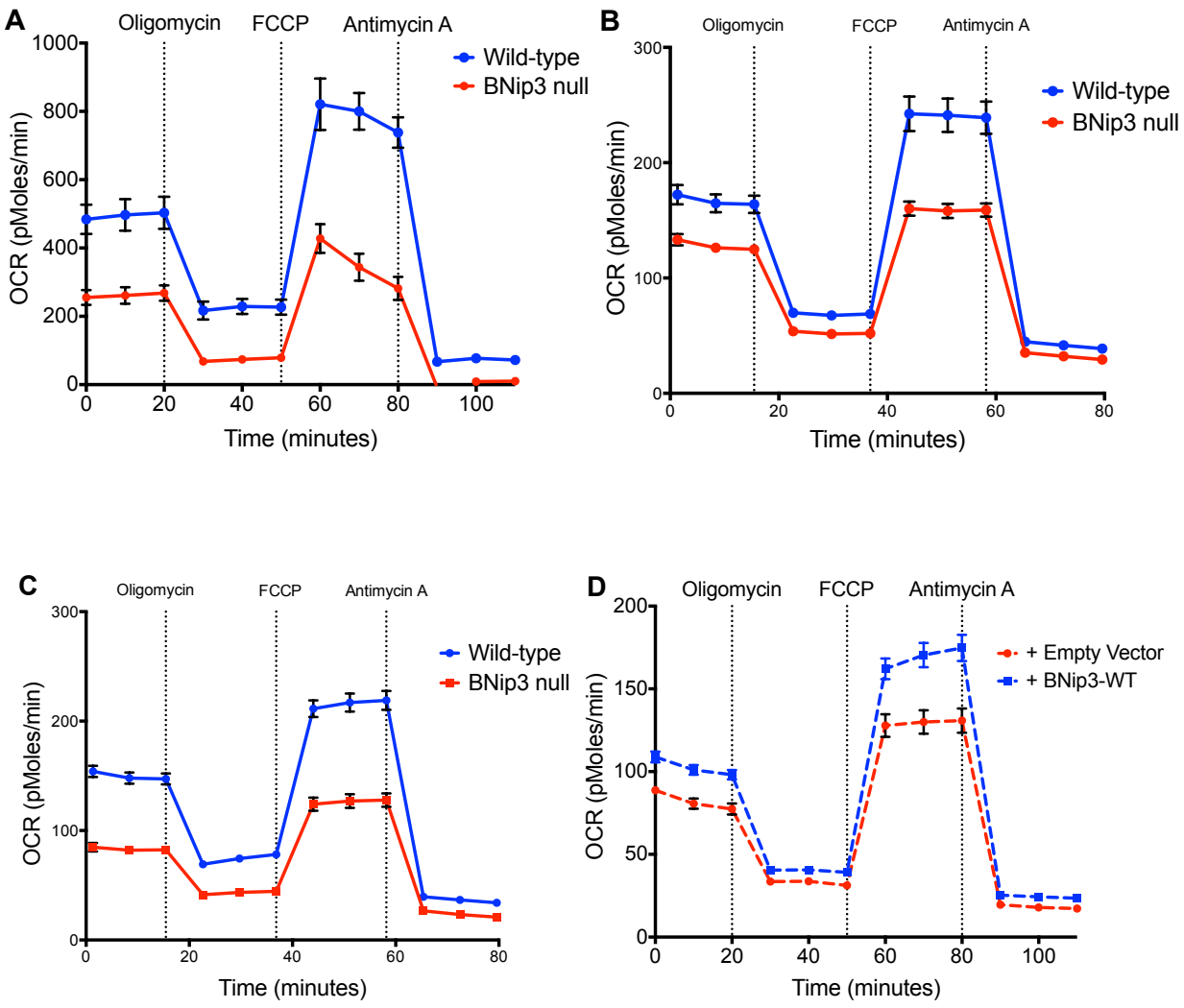


**Figure 24. Loss of BNip3 suppresses oxidative phosphorylation in MECs.** Oxygen consumption using Seahorse XF96 by wild-type and BNip3 null MECs in the presence of (A) Glucose, (B) Glutamine and (C) Glucose + Glutamine. (D) Oxygen consumption in BNip3 null MECs with empty-vector control and exogenous BNip3 wild-type in the presence of glucose + glutamine + sodium pyruvate.

## 4.7. Conclusion

In this chapter, we have shown that loss of BNip3 significantly impairs mitophagy in mammary tumor cells. Other mitophagy proteins such as Nix and Parkin are unable to completely rescue the defect in mitophagy, even though we observed increased levels of Nix in BNip3 null tumor cells, probably owing to increased mitochondrial accumulation. We have also shown that while mitochondrial mass is significantly increased in BNip3 null tumors and cells, the mitochondria are functionally compromised as observed by reduced substrate uptake and mitochondrial membrane potential. However, BNip3 null tumor cells have significantly increased levels of aerobic glycolysis as observed by increased levels of glucose uptake, glycolysis intermediates and lactate output. Glucose in BNip3 null cells is utilized for nucleic acid and fatty acid synthesis supporting growth. Lastly, we have shown that while BNip3 null tumor cells have significantly reduced levels of mitochondrial respiration, which is independent of the type of substrate availability, all of which are features of the Warburg effect. Overall, we have shown that loss of BNip3 in mammary tumor cells severely impairs mitophagy resulting in accumulation of dysfunctional mitochondria and reliance on the Warburg effect.

# CHAPTER 5

# INCREASED ROS PRODUCTION IN BNIP3 NULL TUMORS CONTRIBUTES TO HIF STABILIZATION

## 5.1. Introduction

Mitochondrial electron transport chain is the dominant source of ROS in cells (23,24). During the transfer of electrons to complex IV, which finally reduces molecular oxygen to water, electrons in complex I, II and III can prematurely reduce oxygen to form superoxide anions. However, ROS can also be generated by other systems including NADPH oxidase complex, lipoxygenase, cycloxygnase and peroxisomes and can exist in other forms including hydrogen peroxide, hydroxyl radicals and hypochlorus acid in cells. While some amounts of ROS exist in cells under normal physiological conditions, there is a propensity for their levels to increase in rapidly proliferating cells owing to the dramatic increase in oxygen demand and ATP (25). However, tumor cells adapt to these high levels of ROS of by reprograming their metabolism and a key way in which they do so is by increase in levels of HIF-1 (26-28). Under conditions of low oxygen, HIF-1$\alpha$ gets stabilized as it escapes hydroxylation by prolyl hydroxylases and its subsequent proteasomal degradation by pVHL. Stabilized HIF-1$\alpha$ can then translocate to the nucleus where together with HIF-1$\beta$, it modulates gene expression for several targets involved in processes including cellular metabolism, invasion and metastasis and epithelial to mesenchymal transition. Apart from BNIP3, other common metabolic targets of HIF-1$\alpha$ are the glucose transporter, hexokinase, pyruvate

dehydrogenase kinase, phosphofructokinase and lactate dehydrogenase all of which are involved in glycolysis (29,30). Thus elevated levels of HIF-1α often result in increased aerobic glycolysis, which supports tumor cells in meeting their energy demand under conditions of oxygen stress. HIF-1α also induces expression of angiopoietins and vascular endothelial growth factor, which promote angiogenesis in order to overcome the oxygen depletion (32).

Both, ROS and HIF-1α are known to promote tumor growth and metastasis (24,154,155). Given that Hif-1α drives the Warburg effect as well as invasion and metastasis in tumors, all of which were characteristics of loss of BNip3 in the MMTV-PyMT model, we investigated the effect of BNip3 loss on Hif-1α in wild-type and BNip3 null tumor and cells. In this chapter, we also investigate the mechanism by which BNip3 affects stabilization of Hif-1α in mammary tumors.

## 5.2. Loss of BNip3 is associated with increased Hif-1α levels and activity *in vitro* and *in vivo*

Our data showed that loss of BNip3 in MMTV-PyMT driven mammary tumors results in increased glucose uptake, aerobic glycolysis, glucose derived fatty acid and nucleic acid synthesis, but reduced oxidative metabolism which are key characteristics of the Warburg effect (29,162,163). HIF-1α and Myc are some of the key oncogenic drivers of the Warburg effect in tumor cells that can act independently or in concert to modulate tumor cell metabolism and proliferation. Given that BNip3 is a direct target of HIF, we investigated the effect of BNip3 loss on Hif-1α in the MMTV-PyMT mammary tumors.

IHC staining for HIF-1α on wild-type and BNip3 null tumors at day50 showed significantly increased Hif-1α levels in BNip3 null tumors (Figure 25A). Given that wild-type and BNip3 null tumors are similar in size at day50, we chose this time-point in order to rule out differences in protein levels due to changes in tumor volume. The increased level of Hif-1α in BNip3 null tumors was consistent *in vitro* as well. We cultured wild-type and BNip3 null MECs at 20% oxygen and 1% oxygen for 24 hours and determined Hif-1α levels in nuclear lysates by immunoblot. Interestingly, we observed elevated levels of Hif-1α in BNip3 null MECs under both these growth conditions suggesting that elevation of Hif-1α in the absence of BNip3 may be driven by factors such as oxidative stress (Figure 25B). This finding prompted us to investigate levels of Nrf2 in tumor cells by immunoblot. NRF2 is a transcription factor that drives cellular response to oxidative stress by inducing antioxidants including superoxide dismutase and glutathione peroxidase. However, while we observed elevated levels of Nrf2 in BNip3 null MECs in hypoxia, we did not observe a significant change in Nrf2 levels at atmospheric oxygen (Figure 25B). In order to confirm that elevated levels of Hif-1α were due to loss of BNip3 in mammary tumor cells, we infected BNip3 null MECs with an empty-vector and BNip3-wild-type vector and determined Hif-1α levels by immunoblot after culturing cells in hypoxia for 24 hours. Exogenous expression of wild-type BNip3 into BNip3 null MECs reduced levels of Hif-1α to the levels in wild-type MECs, whereas levels of Hif-1α remained elevated with the empty-vector indicating that changes in Hif-1α protein levels were indeed due to alteration in BNip3 expression (Figure 25C).

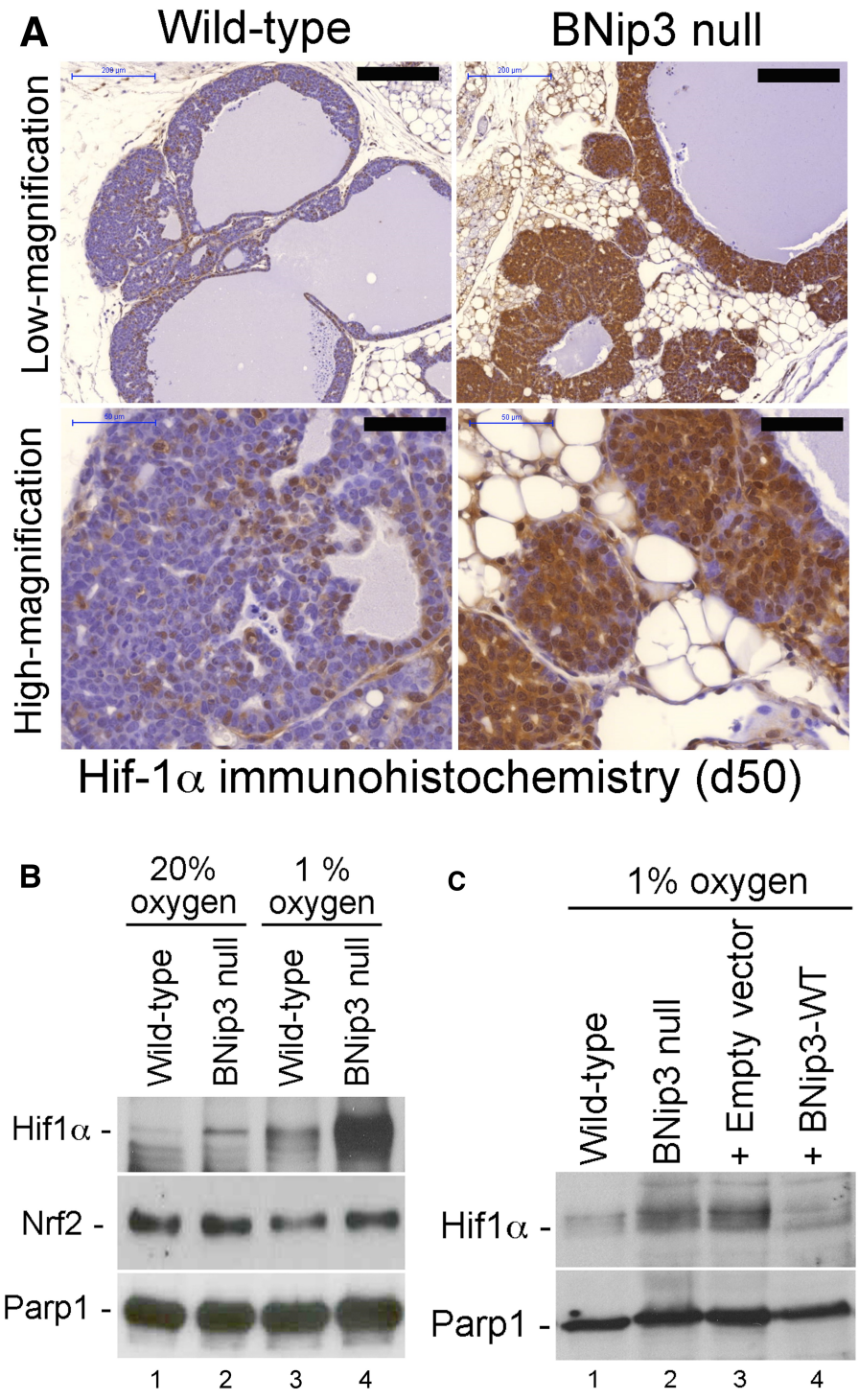


**Figure 25. Loss of BNip3 increases Hif-1α levels.** (A) Immunohistochemical staining for Hif-1α in wild-type and BNip3 null tumors at d50. (B) Immunoblot for Hif-1α, Nrf2 and Parp-1 on nuclear extracts from wild-type andBnip3 null MECs in 20% oxygen and 1% oxygen. (C) Immunoblot for Hif-1α and Parp1 in wild-type and BNip3 null MECs with empty-vector control and BNip3 wild-type expressing vector at 1% oxygen.

Given that we observed elevated Hif-1$\alpha$ levels in BNip3 null tumors, we examined if this elevation also translated to increased Hif-1$\alpha$ activity in these tumors. HIF-1 is a transcription factor that induces genes involved in glycolysis including hexokinase 2 (Hk2), pyruvate dehydrogenase kinase isoenzyme 1 (Pdk1), phosphoglycerate kinase 1 (Pgk1) and solute carrier family 2 member 1 (Slc2a1) and those involved in angiogenesis including vascular endothelial growth factor A (Vegfa), angiopoietin 2 (Angpt2) and FMS-like tyrosine kinase 1 (Flt1) (164). We determined changes in the above-mentioned genes in wild-type and BNip3 null tumors by qRT-PCR and observed significantly increased levels of HIF target gene expression in BNip3 null tumors compared to wild-type (Figure 26). An increase in expression levels of glycolysis genes in BNip3 null tumors was consistent with the phenotype of increased glucose uptake and aerobic glycolysis in BNip3 null tumors (in Chapter 4). Interestingly, previous studies in the lab had also shown increased vessel count, but reduced pericyte coverage for BNip3 null tumors as compared to wild-type tumors by performing CD31 and $\alpha$-SMA immunostaining of frozen tumor sections at day 80 (Figure 27A-C). This phenotype is highly consistent with increased expression levels of angiogenesis genes in BNip3 null tumors.

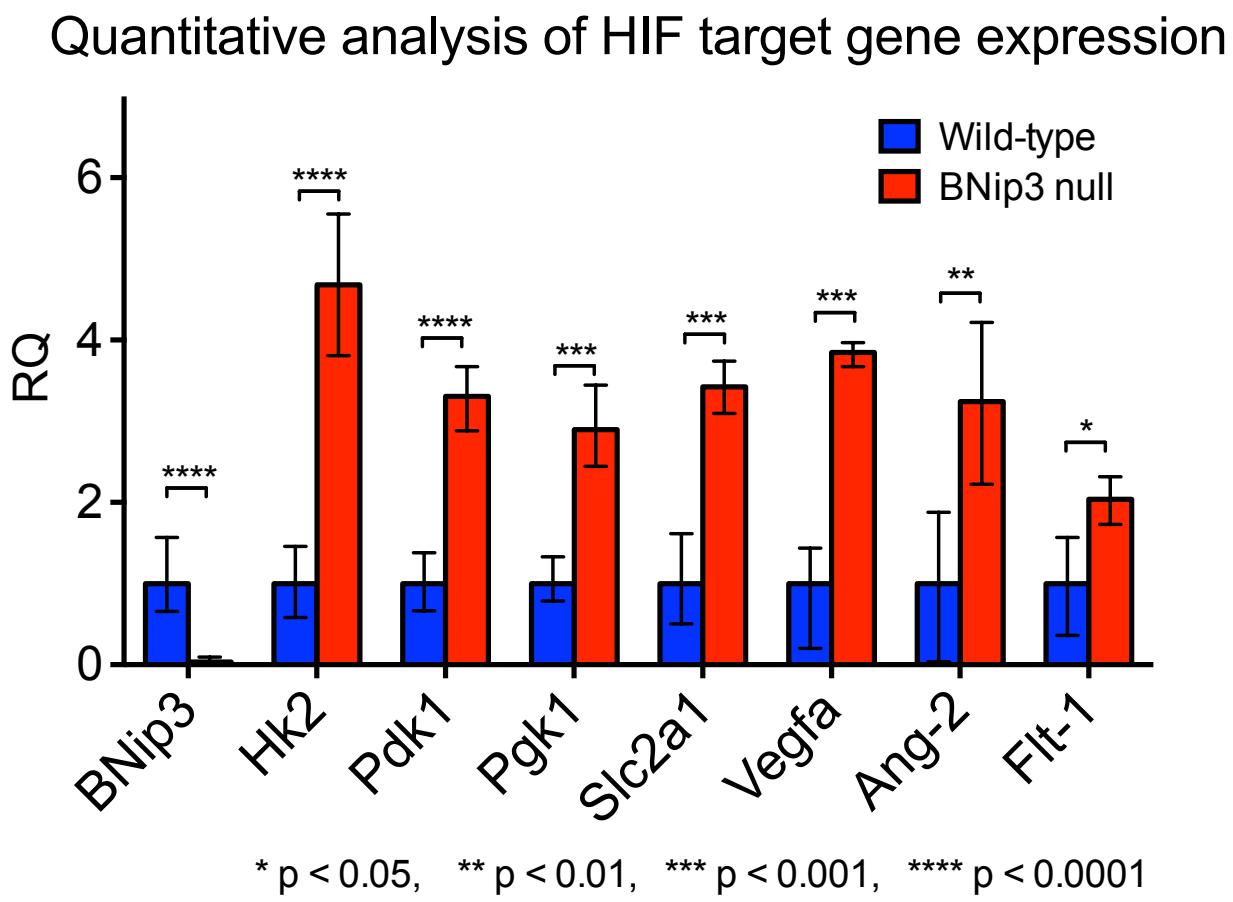


**Figure 26. Loss of BNip3 promotes Hif-1α activity.** qPCR for expression of key Hif target genes and other growth related genes in tumors from wild-type and BNip3 null mice at d80.

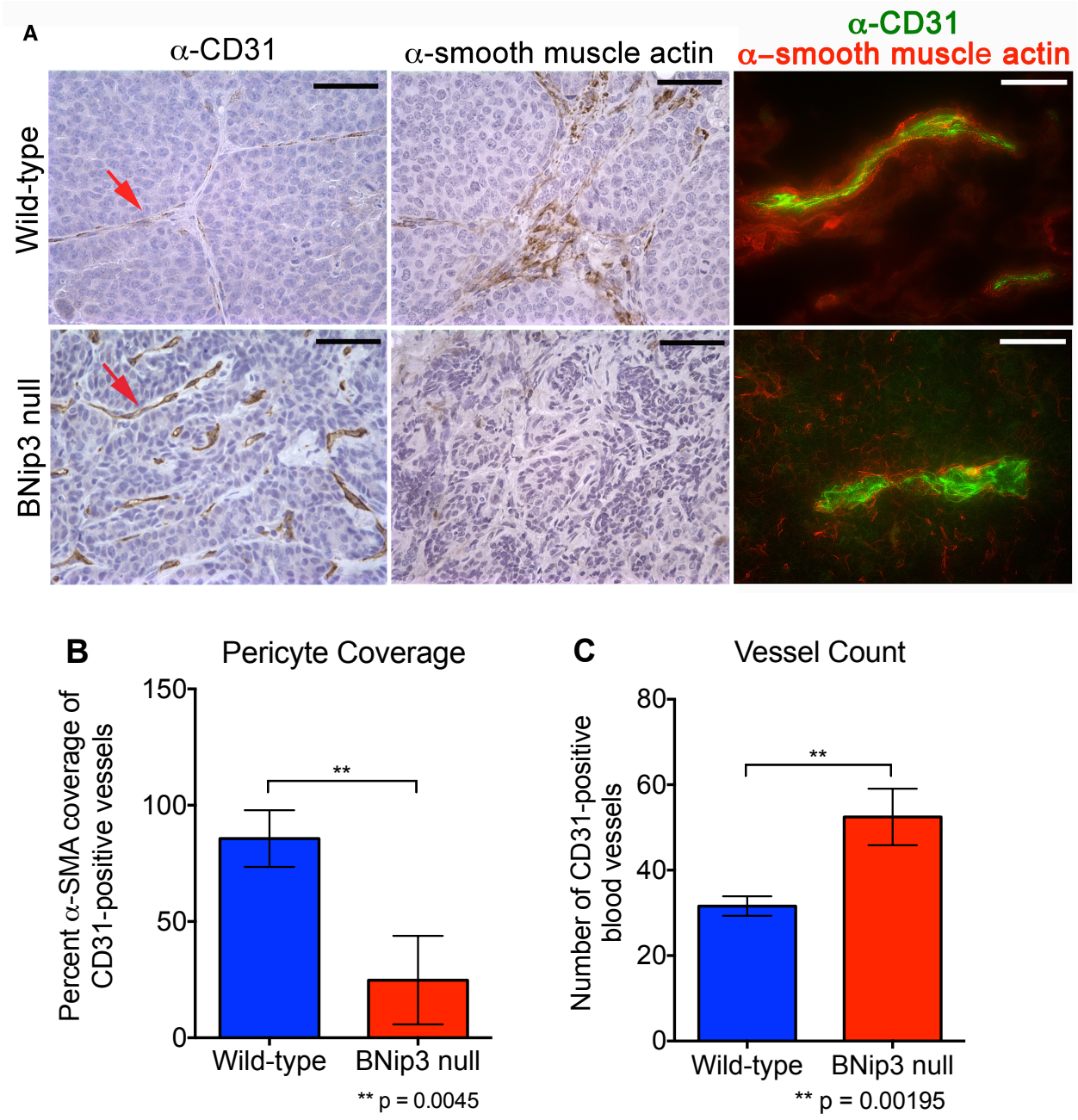


**Figure 27. BNip3 loss promotes angiogenesis.** (A) Co-staining for CD31 and α-SMA on frozen sections of wild-type (n = 8) and BNip3 null (n = 8) tumors at d80. Quantification of pericyte coverage (B) and vessel count (C).

In order to determine the extent to which elevated Hif-1α levels drive cellular proliferation in BNip3 null MECs, we treated wild-type and BNip3 null tumor cells with 10ng/ml of Echinomycin and measured the changes in growth rate. Echinomycin is small molecule inhibitor that binds DNA at the hypoxia response element (HRE) sequences, thus inhibiting the DNA binding activity of Hif-1α (165). Treatment with Echinomycin significantly decreased the growth rate in BNip3 null MECs and brought it down to the level of untreated wild-type MECs (Figure 28A). We also examined the change in Hif-1α activity by measuring HIF target gene expression by qRT-PCR and observed significant reduction in Hk2, Slc2a1 and Pdk1 expression levels in BNip3 null MECs upon treatment with Echinomycin (Figure 28B). Together these results indicate that loss of BNip3 leads to increased levels of Hif-1α and its target genes, which promote tumor growth and progression.

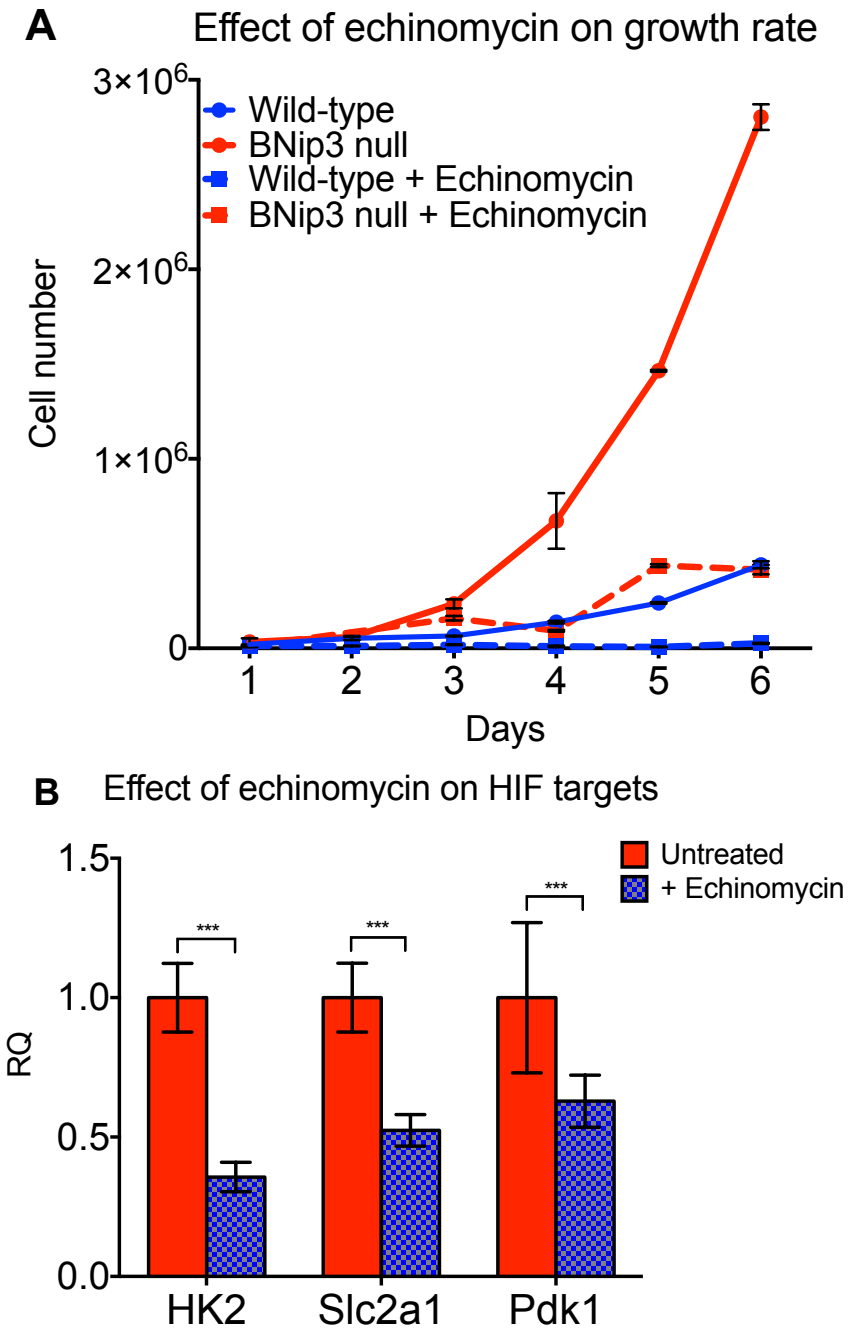


**Figure 28. Echinomycin treatment reduces cellular growth rate and Hif-1α activity in BNip3 null MECs.** (A) Growth rate of primary wild-type (blue) and BNip3 null MECs (red) treated with 10 ng/ml Echinomycin, measured in triplicate. (B) qPCR for key Hif target genes in BNip3 null MECs upon treatment with Echinomycin. (Growth rate data from Lauren Drake)

Given that overexpression of HIF-1α is associated with poor prognosis in human breast cancer, our results indicating stabilization of Hif-1α in the absence of BNip3 in MMTV-PyMT driven mammary tumors prompted us to investigate the significance of increased copy number loss of BNIP3 in TNBC with respect to HIF-1α. Our analysis of the TCGA data for TNBC patients revealed that low BNIP3 levels stratified metastasis free survival (MFS) with HIF1A levels such that high HIF1A levels were indicative of a significantly reduced MFS as compared to low HIF1A levels (Figure 29). However, this stratification in HIF1A levels was lost in the case of high BNIP3 levels. These results indicate that a combination of low BNIP3 with high HIF1A levels can be used as a strong prognostic indicator for MFS in TNBC patients as compared to HIF1A levels alone.

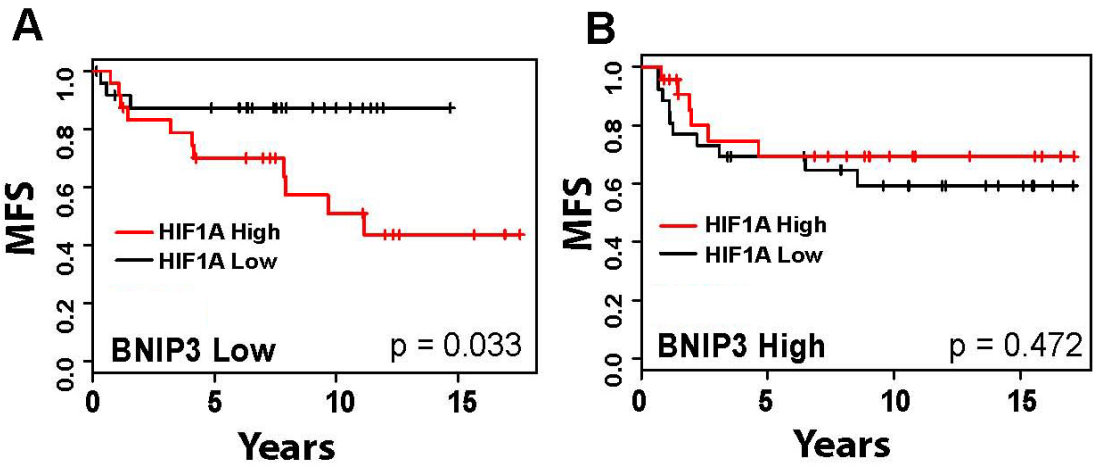


**Figure 29. BNIP3 loss predicts reduced metastasis free survival in TNBC.**
(A) TNBC patient metastasis-free survival in low BNip3 expressing patients (below median, n = 51) stratified by high (above median) and low (below median) expressing Hif-1α. (B) TNBC patient metastasis-free survival in high BNip3 expressing patients (above median, n = 50) stratified by high (above median) and low (below median) expressing Hif-1α. (Data from Casey Frankenberger)

### 5.3. Loss of BNip3 is associated with increased levels of ROS *in vitro* and *in vivo*

Generation of ROS is a common characteristic of mitochondrial dysfunction (23,24). ROS can be generated by complexes I, II and III of the respiratory chain due to reduction of molecular oxygen to superoxide anion during oxidative metabolism. Once in the cytosol, ROS is known to inhibit the activity of prolyl hydroxylases and preventing hydroxylation and subsequent proteasomal degradation of Hif-1$\alpha$, thus stabilizing the protein (25,27). Our data with the MMTV-PyMT mammary tumor model had shown that loss of BNip3 affects oxidative metabolism and reduces mitochondrial function along with stabilization of Hif-1$\alpha$. These results prompted us to determine the effect of BNip3 loss on ROS levels in mammary tumors.

We performed staining for dihydroethidine (DHE) on frozen sections of wild-type and BNip3 null tumors at day35. DHE is fluorescent indicator that intercalates into the DNA and fluoresces bright red upon oxidation by superoxide (166). We observed significantly increased DHE staining for BNip3 null tumors as compared to wild-type tumors at day35 suggesting that even at that early time point, BNip3 null tumor cells had elevated levels of ROS (Figure 30A-B). We further examined levels of 8-hydroxy-2'-deoxyguanosine (8-OHdG) by IHC in wild-type and BNip3 null tumors at day 80. 8-OHdG is a widely accepted biomarker for oxidative stress as it is commonly found in free radical-induced oxidative lesions in mitochondrial and nuclear DNA. Similar to DHE staining, we observed significantly increased levels of 8-OHdG in BNip3 null tumors compared to wild-type (Figure 30A-B).

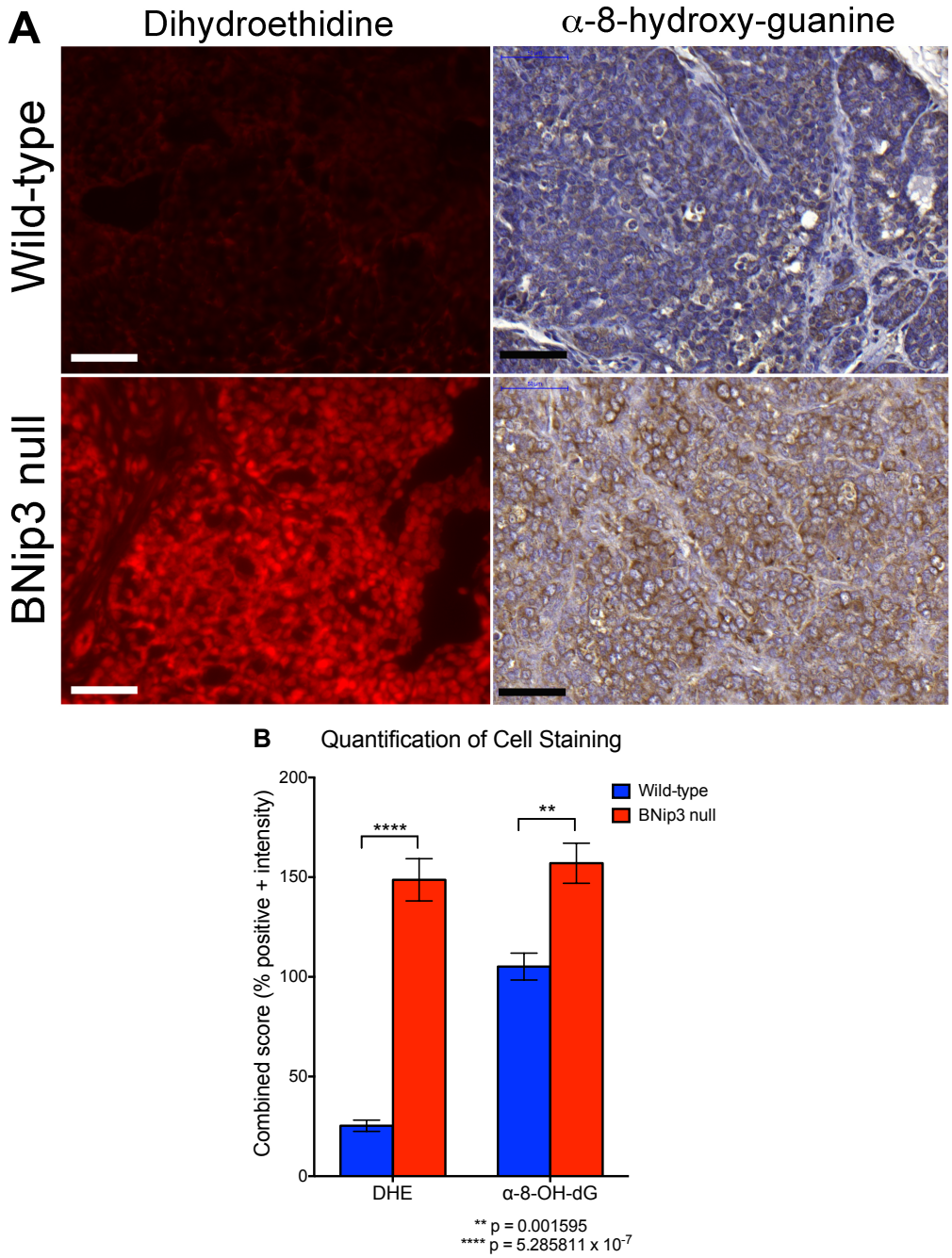


**Figure 30. Loss of BNip3 increases levels of ROS in mammary tumors.** (A) Staining of frozen sections of wild-type and BNip3 null tumors at d35 for dihydroethidine (left panel) and immunohistochemical analysis of FFPE sections of wild-type and BNip3 null tumors for 8-hydroxyguanine at d80 (right panel). (B) Quantification of above staining (n=4 for each genotype).

Interestingly, BNip3 null tumor cells maintained this phenotype *in vitro* as well. We cultured wild-type and BNip3 null MECs at 20% oxygen and 1% oxygen prior to treating with MitoSOX dye for 20 mins. MitoSOX is a live cell permeant fluorogenic dye that targets mitochondria and fluoresces red upon oxidation by superoxide only. We observed a significant increase in MitoSOX positivity in BNip3 null MECs as compared to wild-type tumor cells (Figure 31A). The increased percentage of MitoSOX positive BNip3 null MECs was found in at atmospheric oxygen as well as hypoxia. The presence of increased ROS warrants increased antioxidant activity in tumor cells. The above-mentioned results were consistent with our metabolomics analysis that showed increased levels of antioxidant, glutathione, in BNip3 null tumor cells. Glutathione is an antioxidant that exists in the reduced state as GSH and in the oxidized state as GSSG. Reduced glutathione or GSH stabilizes free radicals by donating a reducing equivalent to them and in the process gets oxidized to glutathione disulfide or GSSG. Thus, an obvious way to determine antioxidant activity is to analyze GSSG:GSH ratio in cells. Metabolomics analysis performed on wild-type and BNip3 null MECs revealed significantly reduced levels of GSH, but significantly increased GSSG:GSH ratio in BNip3 null MECs as compared to wild-type tumor cells (Figure 31B) indicating increased antioxidant activity in BNip3 null tumor cells. We also detected significantly reduced levels of amino acids, glycine and cysteine, in BNip3 null MECs (Figure 31B). Both these amino acids are required for glutathione synthesis. Given that these two amino acids were found selectively depleted in BNip3 null MECs, further supports our data that increased glutathione activity is required to counter increased levels of ROS in BNip3 null MECs as compared to wild-type tumor cells.

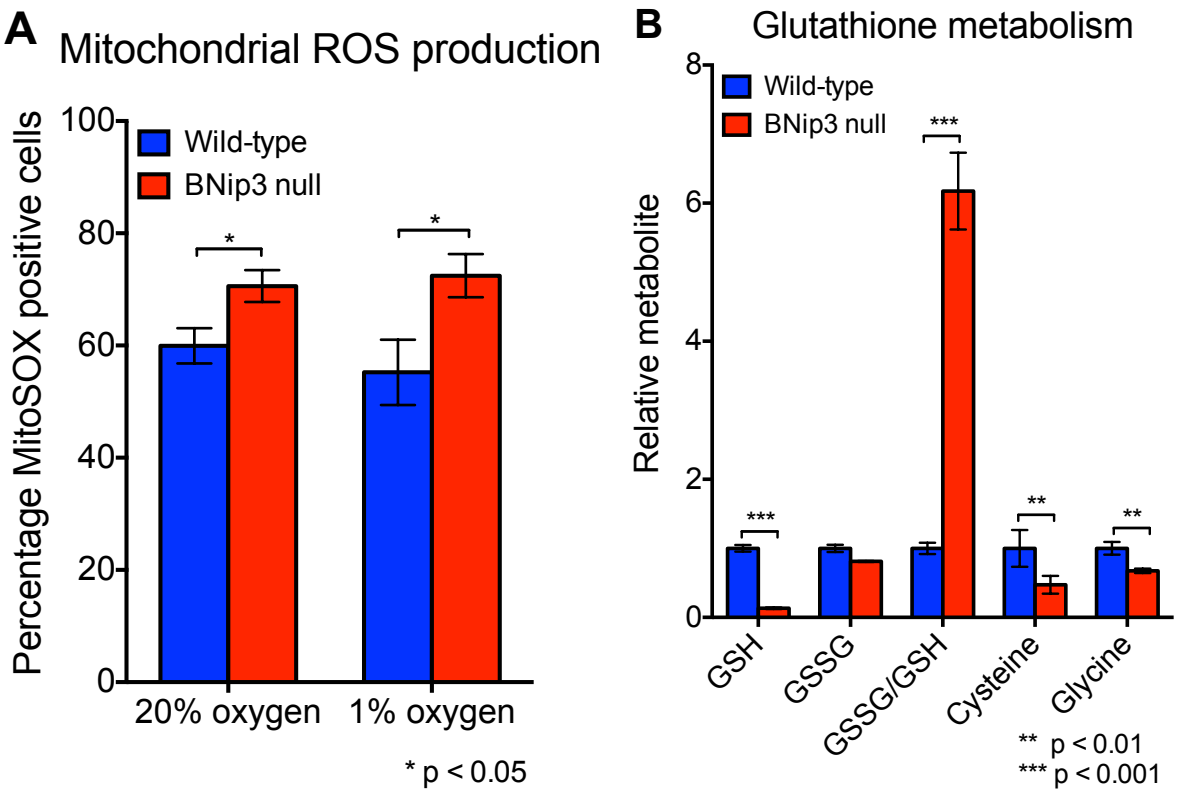


**Figure 31. BNip3 loss increases levels of ROS *in vitro.*** (A) Flow cytometric analysis of mitochondrial ROS using MitoSOX fluorescent probe. (B) Quantification of total levels of reduced and oxidized glutathione, glycine and cysteine in wild-type and BNip3 null tumor cells.

### 5.4. Treatment of BNip3 null mice with BHA reduces ROS associated levels of Hif-1α, tumor growth and metastasis

Our results showing increased levels of ROS in BNip3 null tumors at as early as day35 along with increased antioxidant activity indicated that increased ROS levels might play a crucial role in stabilizing Hif-1α in the absence of BNip3. In order to test this hypothesis, we fed wild-type and BNip3 mice a diet supplemented with butylated hydroxyanisole (BHA) from day65 till day80. This time point was chosen for the MMTV-PyMT mice as by day65, visible tumors are formed but have not metastasized, thus allowing adequate time to study the effect of BHA on tumor growth and metastasis. BHA is a commonly used antioxidant, which induces phase II metabolic enzymes including glutathione transferase, UDP-glucoronyl transferase, quinone reductase, and epoxide hydrolase that facilitate detoxification of xenobiotics (167). Tumors from wild-type and BNip3 null mice were harvested at day80 and analyzed for tumor volume. While BHA treatment had no effect on tumor volume in wild-type mice, we observed a significant reduction in tumor volume for BHA-treated BNip3 null mice when compared to untreated BNip3 null mice (Figure 32A). IHC analysis for Ki67 of wild-type and BNip3 null tumors treated with BHA also showed a significant reduction in tumor cell proliferation in BHA-treated BNip3 null tumors compared to untreated BNip3 null tumors (Figure 32B, Figure 33). We also observed a significant decrease in lung metastases in BHA-treated BNip3 null mice as compared to untreated BNip3 null mice at day80 (Figure 32C). Together these results indicate that increased levels of ROS in BNip3 null mice were promoting tumor growth and metastasis.

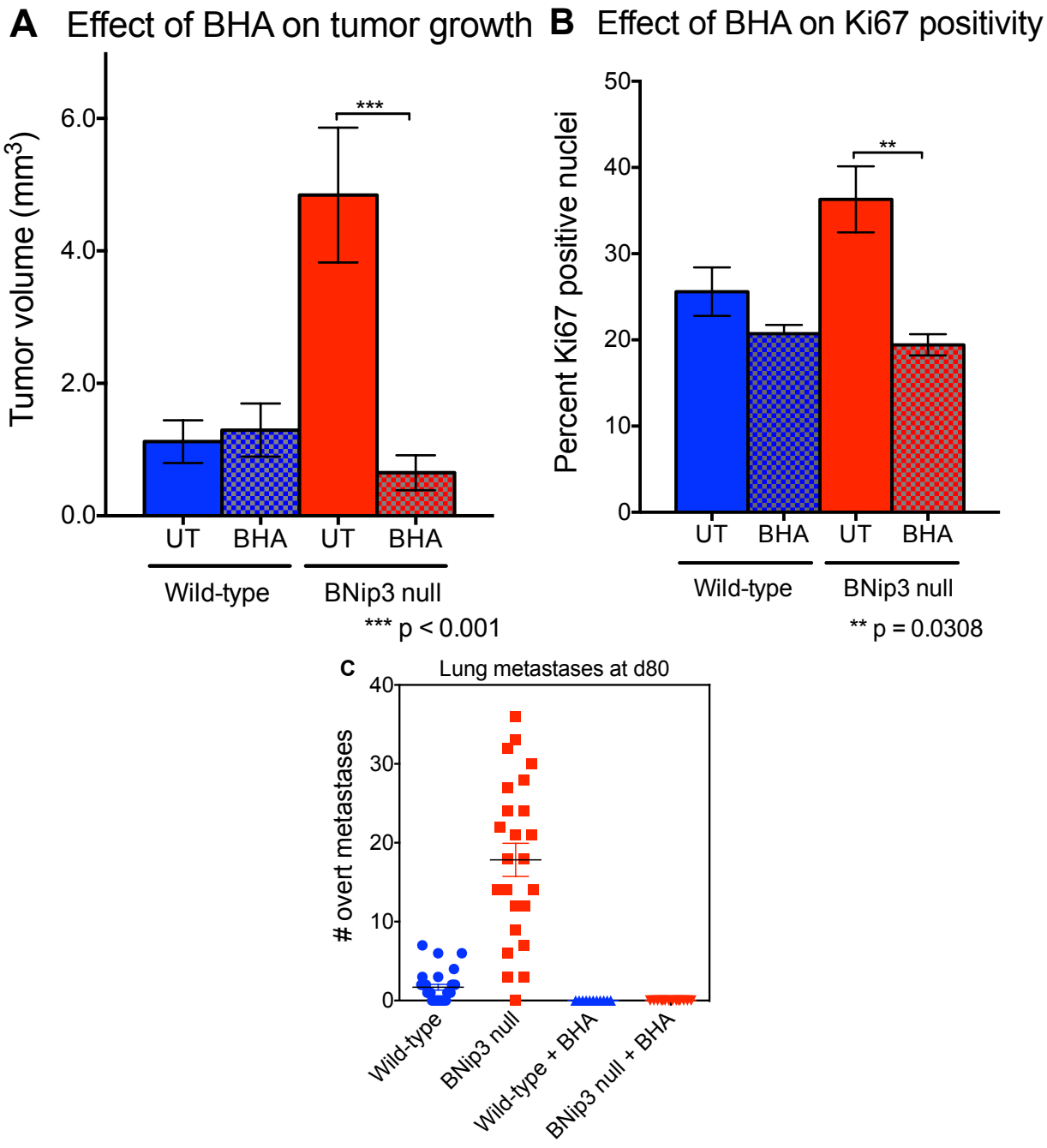


**Figure 32. Effect of BHA diet on BNip3 null tumor growth and metastasis. (A)** Effect of BHA diet supplementation on MMTV-PyMT tumor volume in wild-type and BNip3 null mice stating d65 (n=4 for each genotype and treatment). (B) Quantification of IHC staining for Ki67 on wild-type and BNip3 null tumors at d80. (C) Effect of BHA diet supplementation on MMTV-PyMT lung metastases in wild-type and BNip3 null mice stating d65 (n=4 for each genotype and treatment).

Given that we observed differences in tumor growth only in case of untreated and BHA-treated BNip3 null mice, we analyzed their tumors for levels of ROS by DHE staining and observed a significant reduction in DHE staining in the BHA-treated group of mice (Figure 33). We also observed a reduction in IHC for 8-OHdG in BHA-treated BNip3 null mice as compared to untreated mice. Importantly, we did not observe any difference in TOM20 IHC for untreated and BHA-treated BNip3 null tumors. Together, these results showed that BHA did indeed reduce the levels of free radicals and subsequent oxidative damage in BNip3 null mice without affecting mitochondrial mass in tumors.

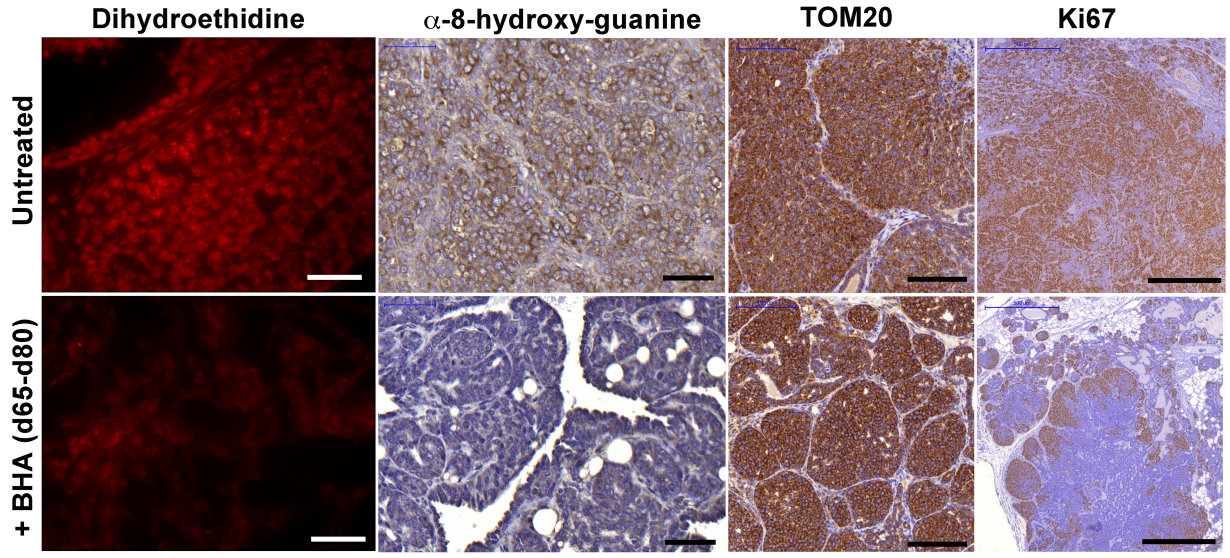


**Figure 33. Effect of BHA diet on BNip3 null tumors.** Effect of BHA diet supplementation on BNip3 null tumors as seen by dihydroethidine staining of frozen sections and 8-hydroxyguanine, TOM20 and Ki67 staining of FFPE sections at d80 (n=4 for each genotype and treatment). (Top panel: untreated BNip3 null tumors, Bottom panel: BHA treated BNip3 null tumors)

Since, elevated ROS levels are known to stabilize Hif-1α levels, we investigated the effect of BHA on Hif-1α in untreated and BHA-treated BNip3 null tumors at day80. We observed a marked reduction in Hif-1α levels by IHC in BHA-treated BNip3 null tumors as compared to untreated tumors (Figure 34A). In order to confirm if changes in Hif-1α levels translated to altered activity as well, we examined the effect of BHA treatment on HIF target gene expression by qRT-PCR. Indeed, we observed a significant reduction in HIF target genes including Hk2, Pdk1, Pgk1, Slc2a1, Vegfa and Flt-1 in BHA-treated BNip3 null tumors as compared to untreated BNip3 null tumors (Figure 34B). Consistent with the tumor growth data from BHA treatment in wild-type mice, we did not see an effect of BHA treatment on HIF target gene expression in wild-type tumors. These results indicate that elevated levels of ROS in BNip3 null mice result in increased Hif-1α levels and activity.

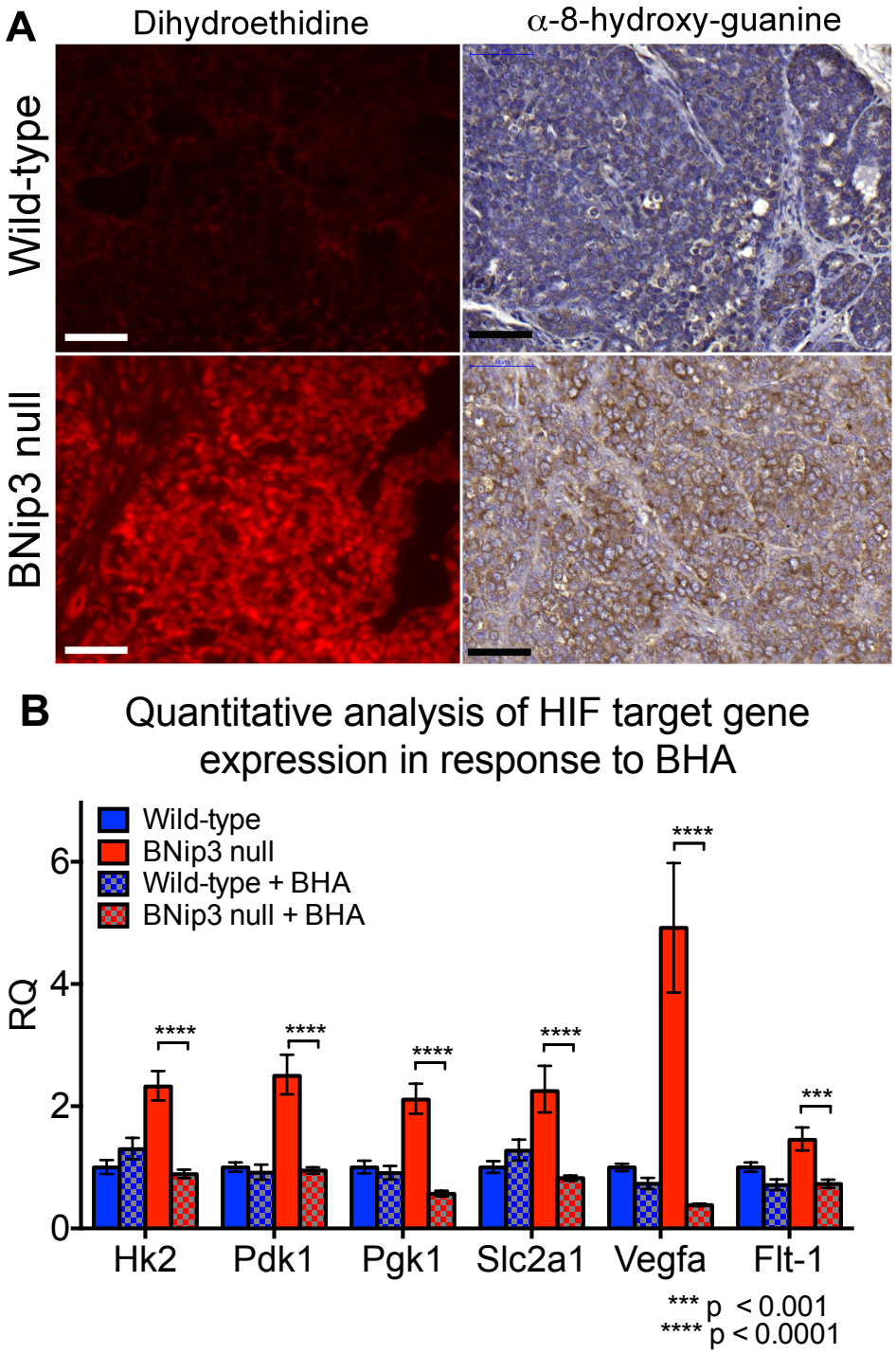


**Figure 34. BHA diet supplementation reduces Hif-1α activity in BNip3 null tumors.** (A) Immunohistochemical staining for Hif-1α on wild-type and BNip3 null tumors at d80 having been fed regular chow or BHA supplemented chow from d65. (B) qPCR for expression of key Hif target genes and other growth related genes in tumors from wild-type and BNip3 null mice at d80 having been fed regular chow or BHA supplemented chow from d65.

## 5.6. Conclusion

We have shown in this chapter that loss of BNip3 stabilizes Hif-1$\alpha$ in mammary tumors and cultured cells and that the activity of Hif-1$\alpha$ drives aerobic glycolysis and angiogenesis. Accumulation of ROS generated by dysfunctional mitochondria in mitophagy deficient BNip3 null tumor cells promotes the stabilization of Hif-1$\alpha$. Thus, we have shown a novel negative feedback loop in which BNip3, a HIF target, functions via mitophagy to inhibit Hif-1$\alpha$ stabilization in tumor cells by lowering levels of ROS.

# CHAPTER 6

# BNIP3 NULL TUMOR CELLS RELY ON AUTOPHAGY FOR SURVIVAL

## 6.1. Introduction

Autophagy is the classic way in which cells cope with nutrient stress conditions (33-35). While baseline autophagy is a continuous process by which cells eliminate excessive and damaged cargo to maintain cellular homeostasis, autophagy is markedly up-regulated in cells in response to starvation, oxidative and genomic instability, and proteotoxic and pathogenic insults. Studies have shown autophagy to have both, tumor suppressive as well as tumor promoting roles (168-170). However, the broader consensus in the field is that autophagy is context dependent, with it being inhibitory during the earlier events of malignant transformation but supportive of tumor progression.

Our data showed that there were no significant differences in cell survival between wild-type and BNip3 null tumor cells. Given that BNip3 null cells have reduced oxidative metabolism but increased aerobic glycolysis, it suggested that BNip3 null tumor cells might depend on elevated glycolysis for survival. In this chapter, we have investigated if mitophagy deficient BNip3 null tumor cells rely on glycolysis for survival or if there are other mechanisms in play. Recent studies have shown that autophagy suppresses tumor cell proliferation but promotes tumor progression by preserving the mitochondrial function under nutrient starvation (169). Thus, we have also investigated the reliance of BNip3 null cells on autophagy in the absence of glycolysis.

## 6.2. Inhibition of glycolysis with 2DG treatment reduces cell growth in BNip3 null tumor cells

Our data revealed that BNip3 null tumors and MECs exhibited elevated aerobic glycolysis but defective oxidative metabolism indicating that these cells were reliant on glycolysis as their key source of energy. This prompted us to investigate the effect of inhibition of glycolysis on the growth rate of mammary tumor cells. We measured the growth rate of wild-type and BNip3 null MECs at atmospheric oxygen for 6 days where cells were treated with 5mM 2-deoxyglucose (2DG) for the last three days. 2DG is a glucose analog that does not undergo glycolysis due to the presence of hydrogen in place of 2-hydroxyl group (171). 2DG is phosphorylated by hexokinase to form 2-deoxyglucose-6-phosphate which cannot be further metabolized in the cell, thus resulting in its cellular accumulation. We observed a significant decrease in the growth rate of 2DG-treated BNip3 null MECs as compared to untreated cells (Figure 35A). However, when we performed PI staining in order to determine the effect of 2DG on tumor cell viability, we did not observe a highly significant increase in cell death for 2DG-treated BNip3 null MECs compared to untreated BNip3 null MECs or 2DG-treated wild-type tumor cells (Figure 35B). These results indicated that BNip3 null MECs rely on glycolysis for cell growth, but not for cell survival.

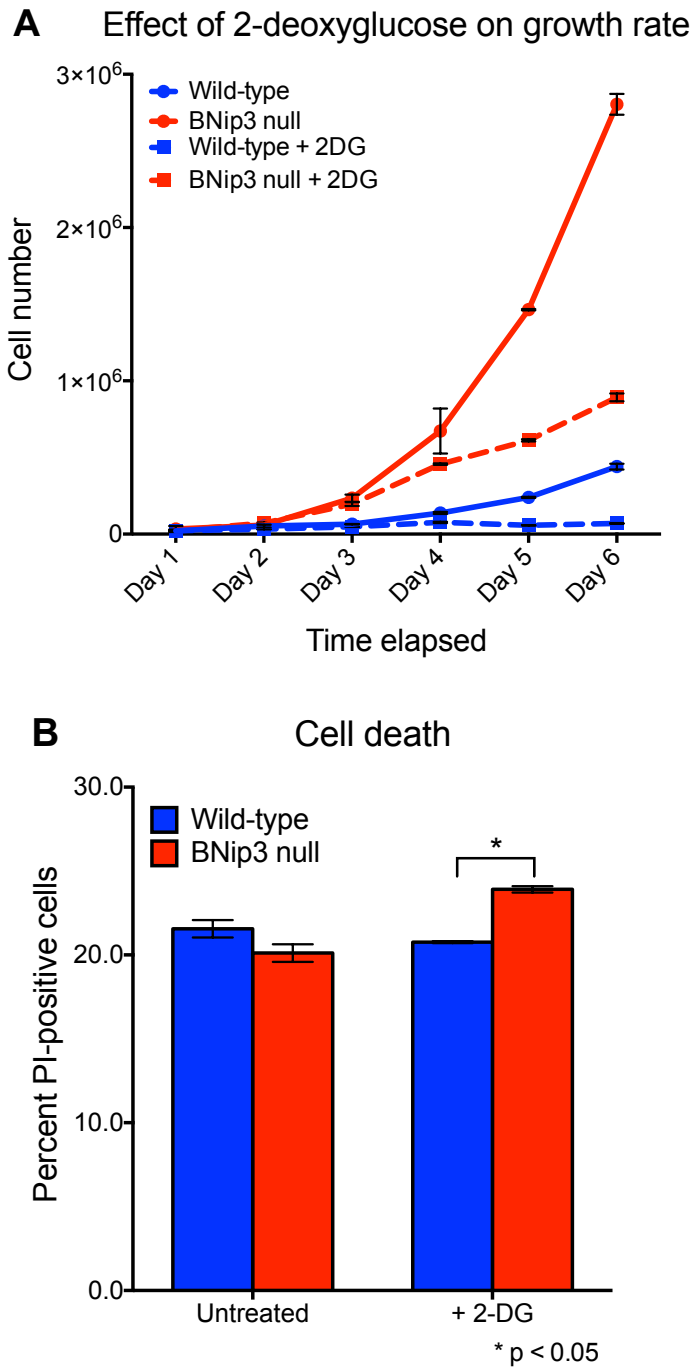


**Figure 35. BNip3 null MECs do not rely on glycolysis for survival.** (A) Effect of inhibiting glycolysis with 2-deoxyglucose on growth rate of wild-type and BNip3 null MECs grown. (B) Effect of inhibiting glycolysis with 2-deoxyglucose on cell viability of wild-type and BNip3 null MECs. (Growth rate data from Lauren Drake)

### 6.3. Inhibition of glycolysis and autophagy with 2DG and bafilomycin increases cell death in BNip3 null tumor cells

Given that inhibition of glycolysis by treatment with 2DG generates a condition of nutrient deprivation and autophagy gets induced under nutrient deprivation for tumor cell survival, we investigated the extent to which BNip3 null mammary tumors relied on autophagy for survival under nutrient stress.

First, we tested the levels of autophagy markers, LC3B and p62, in wild-type and BNip3 null mammary tumors at day80. LC3B, which functions to select cargo for autophagic degradation, is expressed in most cell types (33,172). It gets processed and stably integrated into the outer and inner membrane of growing autophagosomes and serves as an excellent marker of autophagy since it is the only autophagy protein that is retained by mature autophagosomes, unlike other autophagy proteins such as ATG12, ATG5 and ATG16L1. p62 is an autophagy receptor with LC3 interacting region that binds poly-ubiquitinated proteins and targets them for autophagic degradation. Since, p62 levels are modulated by autophagic flux, accumulation of p62 in cells is considered as a marker for inhibition of autophagy. We chose day80 tumors for evaluation of autophagy levels since both wild-type and BNip3 null tumors by this time point would experience nutrient stress. Interestingly, both wild-type and BNip3 null tumors at day80 showed similar levels of punctate LC3B and p62 staining, indicating that loss of BNip3 did not affect levels of macro-autophagy in tumors (Figure 36).

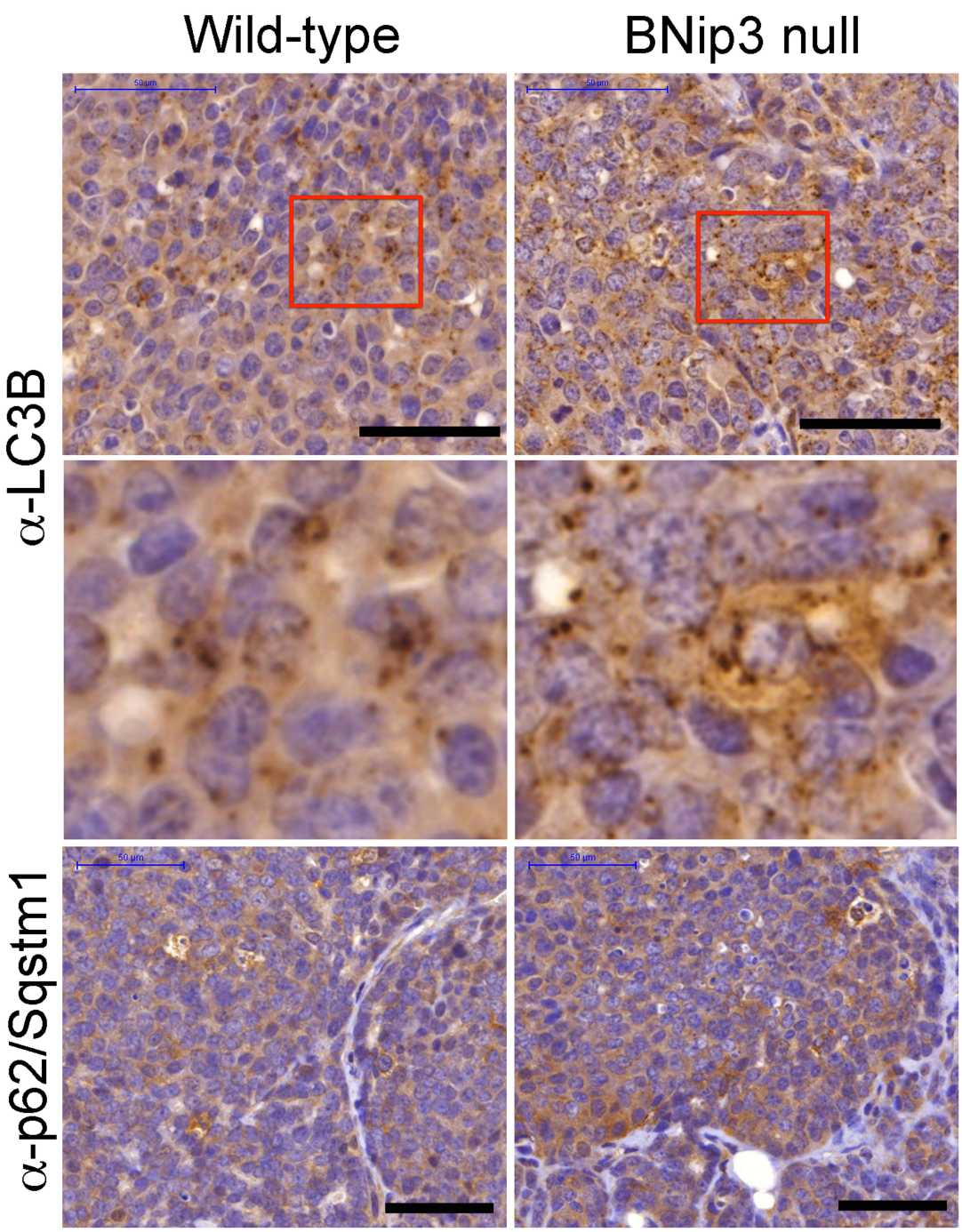


**Figure 36. Analysis of autophagy in wild-type and BNip3 null mammary tumors.** Immunohistochemical staining for LC3B and p62/sqstm1 on sections of wildtype and BNip3 null tumors at d80 (n=4 for each genotype) (LC3B staining done by Lauren Drake)

We also examined levels of autophagic flux in wild-type and BNip3 null MECs by immunoblot and observed effective autophagy in MECs of both genotypes (Figure 37A). While LC3B and p62 protein levels were low under untreated condition, their protein levels increased significantly upon treatment with bafilomycin A1, validating inhibition of autophagy. Bafilomycin A1 also increased levels of BNip3 in wild-type MECs indicating accumulation of mitochondria due to inhibition of mitophagy. Interestingly, we observed an increase in BNip3 levels in wild-type MECs under 2DG treatment as well. However, while we did observe an increase in LC3B levels under 2DG treatment, the increase was not to the same extent as that of BNip3, suggesting that while 2DG did not affect the autophagic flux in cells as much, levels of BNip3 may have increased due to induction by nutrient stress. Lastly, both wild-type and BNip3 null MECs showed elevated levels of LC3B and p62 when treated with a combination of 2DG and bafilomycin A1.

In order to examine the extent to which mammary tumor cells relied on autophagy, we performed PI exclusion assay for cell survival. While both wild-type and BNip3 null MECs had similar percent of PI-positive cells, BNip3 null MECs had increased number of PI-positive cells with 2DG treatment (Figure 37B). However, the percent of PI-positive cells for BNip3 null MECS increased significantly when autophagy was inhibited by treatment with bafilomycin or hydroxychloroquine (HCQ). The level of cell death in BNip3 null MECs also increased significantly with a combination of 2DG and bafilomycin or 2DG and hydroxychloroquine, but this increase was not more than what we had observed with autophagy inhibition alone. Together, these results indicated that BNip3 null MECs relied greatly on autophagy for cell survival.

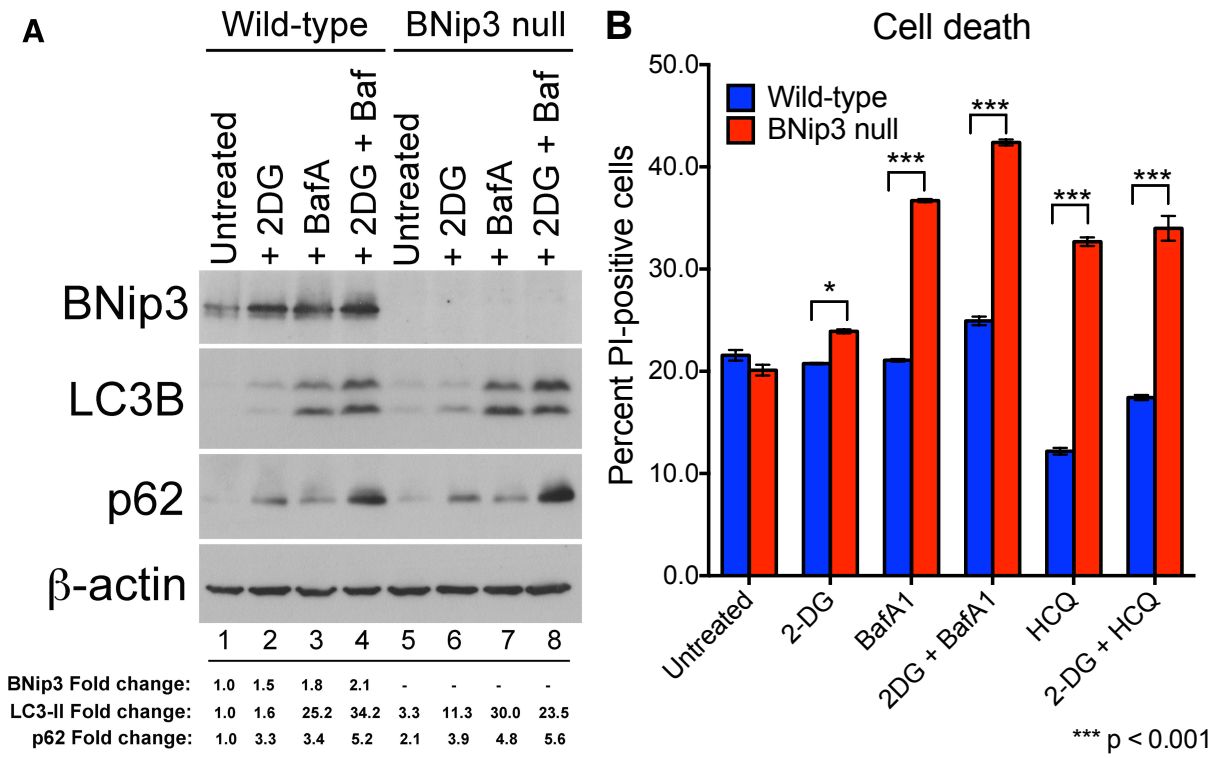


**Figure 37. BNip3 null MECs exhibit increased dependency on autophagy for survival.** (A) Immunoblot analysis of levels of processed LC3B and p62/Sqstm1 in the presence or absence of bafilomycin A1, as a measure of autophagic flux. (B) Measurement of cell death measured by flow cytometric quantification of propidium iodide uptake in the presence or absence of bafilomycin A1, hydroxychloroquine and/or 2-deoxyglucose.

## Conclusion

In this chapter we have shown that mitophagy deficient BNip3 null tumor cells rely on glycolysis for growth. BNip3 null tumors and cells exhibit similar autophagic flux as wild-type cells and rely on autophagy for survival under conditions of nutrient stress. In contrast to recent studies suggesting that autophagy is required to maintain functional mitochondria that can drive tumor progression, we have shown that dysfunctional mitochondria arising from defective mitophagy promote tumor growth and progression.

# CHAPTER 7

# BNIP3 LOSS INCREASES PRIMARY TUMOR GROWTH AND REDUCES LATENCY OF LIVER AND LUNG METASTASIS IN PDX-1-CRE;LSL-KRAS$^{G12D}$ MOUSE MODEL OF PDAC

## 7.1. Introduction

PDAC is a highly aggressive malignancy with KRAS being one of the earliest and most frequently (more than 90% of PDAC cases) mutated oncogenes in the disease (126,132-134). BNIP3 is transcriptionally up-regulated by RAS in a variety of cell types including fibroblasts, macrophages and human cancer cell lines (109-111). BNIP3 expression is induced in response to activated RAS via the RAS-MEK/ERK-HIF pathway. Studies have shown that BNIP3 is induced by increased promoter activity in the presence of constitutively activated RAS, but not in the presence of a dominant-negative or S-nitrosylation mutant form of RAS in macrophages (109). Further, this induction is inhibited in the presence of MEK inhibitor, U0126, or mutation of the HIF binding site on the BNIP3 promoter.

However, while BNIP3 gets induced by oncogenic RAS, it is epigenetically silenced by promoter hypermethylation in human PDAC (121-124). BNIP3 expression is approximately 6-fold lower in pancreatic cancer tissue as compared to normal pancreas and BNIP3-negative pancreatic cancer patients have significantly lower overall survival as compared to BNIP3-positive pancreatic cancer patients (121). Moreover, down-regulation of BNIP3 increases chemoresistance of human pancreatic

cancer cell lines to 5-fluoro-uracil and gemcitabine (122). On the other hand, decitabine (5-aza-2'-deoxycitidine) treatment of human pancreatic cancer cell lines where BNIP3 is silenced by promoter hypermethylation results in restoration of BNIP3 expression and reduced cellular viability (124). Our own preliminary data from 9 and 10 month old PDX-1-Cre;LSL-KRAS$^{G12D}$ mice shows that while BNip3 expression is high in early stage PanIN lesions, it is reduced in late stage PanIN lesions. These studies suggest that up-regulation of BNIP3 in early stages of pancreatic tumorigenesis may be a result of early activation of oncogenic KRAS and may serve to limit tumor growth, underscoring the need to examine the function of BNIP3 in PDAC, a cancer driven by physiologically relevant oncogenic KRAS.

In this chapter, we will describe the generation of BNip3 null mice on PDX-1-Cre;LSL-KRAS$^{G12D}$ mouse model. We have investigated the effect of BNip3 loss on on overall survival of PDX-1-Cre;LSL-KRAS$^{G12D}$ mice and on tumor growth and metastasis.

## 7.2. Generation of BNip3 null mice in PDX-1-Cre;LSL-KRAS$^{G12D}$ mouse model

The PDX-1-Cre;LSL-KRAS$^{G12D}$ mouse model is a well characterized and highly established model of mPanINs used in the field of pancreatic cancer (141-143). While mice can develop PDAC and metastasis by approximately 12 months of age, the progression of early PanIN lesions to late PanIN lesions to PDAC recapitulates the disease as it occurs in humans (142,143). Moreover, the slow progression of the disease in this model makes it ideal to study potential tumor suppressors such as BNip3.

In order to examine the effect of loss of BNip3 Given the potent nature of activated KRAS and the fact that PDX-1-Cre;LSL-KRAS$^{G12D}$ mice develop early stage PanIN lesions by as early as 2.5 months of age, it was imperative that we activate KRAS$^{G12D}$ by introducing Cre in the final step of mouse crosses. Thus, we performed two generations of crossing PDX-1-Cre and LSL-KRAS$^{G12D}$ mice separately with mice carrying a targeted deletion of BNip3 (BNip3$^{-/-}$) in order to obtain PDX-1Cre;BNip3$^{-/-}$ and LSL-KRAS$^{G12D}$;BNip3$^{-/-}$ mice, which were then bred together to generate PDX-1-Cre;LSL-KRAS$^{G12D}$;BNip3$^{-/-}$ mice (146). All the mice were on C57BL/6 background.

### 7.3. Loss of BNip3 increases tumor growth and reduces overall survival *in vivo*

In order to examine the effect of BNip3 loss on tumor growth and latency in PDAC, we compared PDX-1-Cre;LSL-KRAS$^{G12D}$ (wild-type) with PDX-1-Cre;LSL-KRAS$^{G12D}$;BNip3$^{-/-}$ (BNip3 null) mice at 3 and 4.5 month when PanIN lesions are starting to form. We harvested pancreas and investigated formalin fixed paraffin embedded (FFPE) sections by IHC for Ki67 (proliferation marker), c-Myc, TOM20 (mitochondrial marker), alcian blue (marker for mucin secretion), CK19 (epithelial marker for tumor growth), amylase (acinar cell marker), a-SMA (pericyte marker), CD31 (endothelial cell marker), CD45 (leukocyte marker) and TUNEL (cell death marker). We observed similar early stage PanIN-1A/B lesions in both wild-type and BNip3 null pancreas at 3 months by analysis of H&E staining. We also did not observe any significant differences in IHC analysis conducted for the above-mentioned markers (Figure 38).

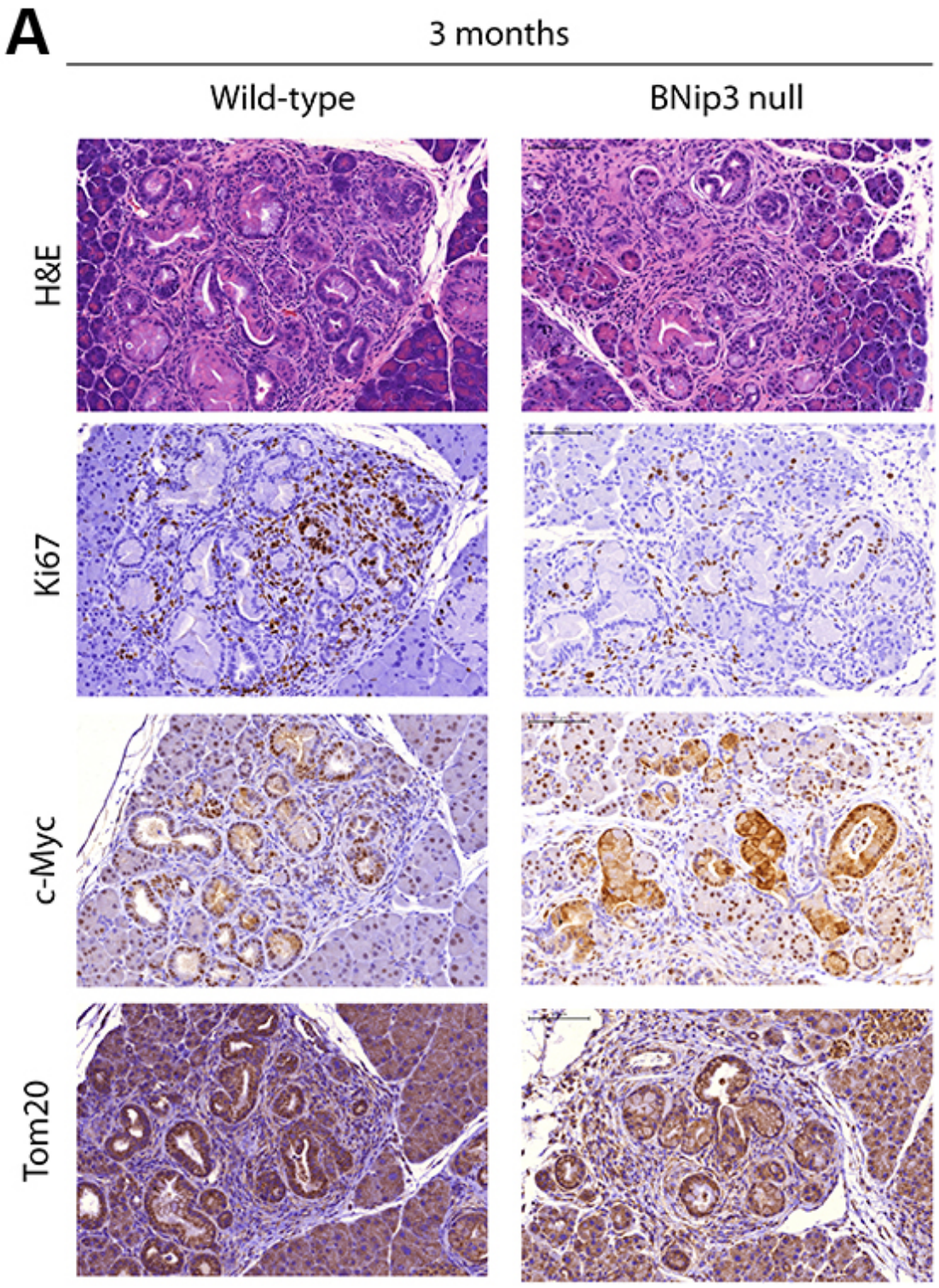


**Figure 38. Immunohistochemical analysis of 3 months old wild-type and BNip3 null pancreas.**

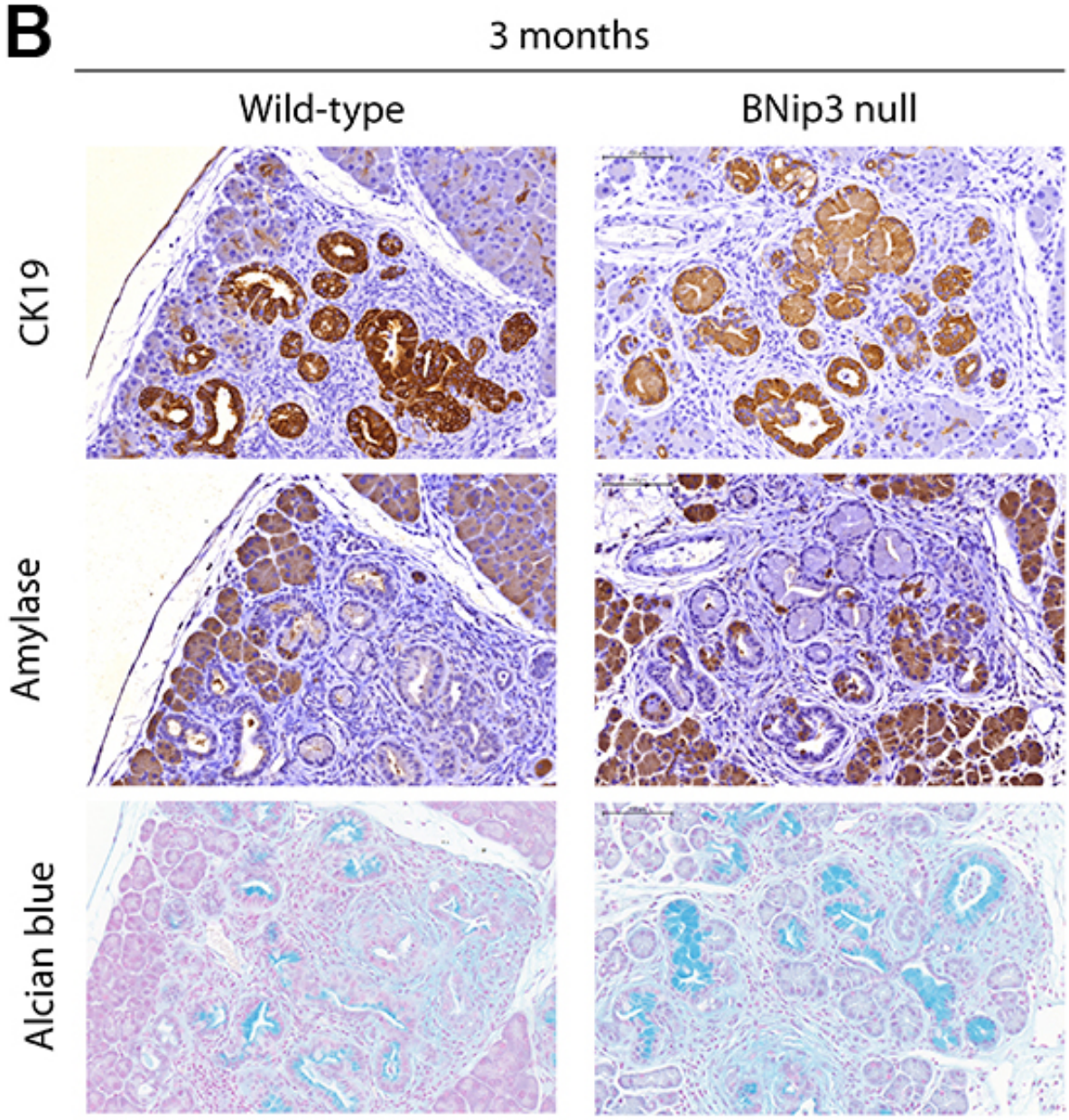


**Figure 38. Immunohistochemical analysis of 3 months old wild-type and BNip3 null pancreas.**

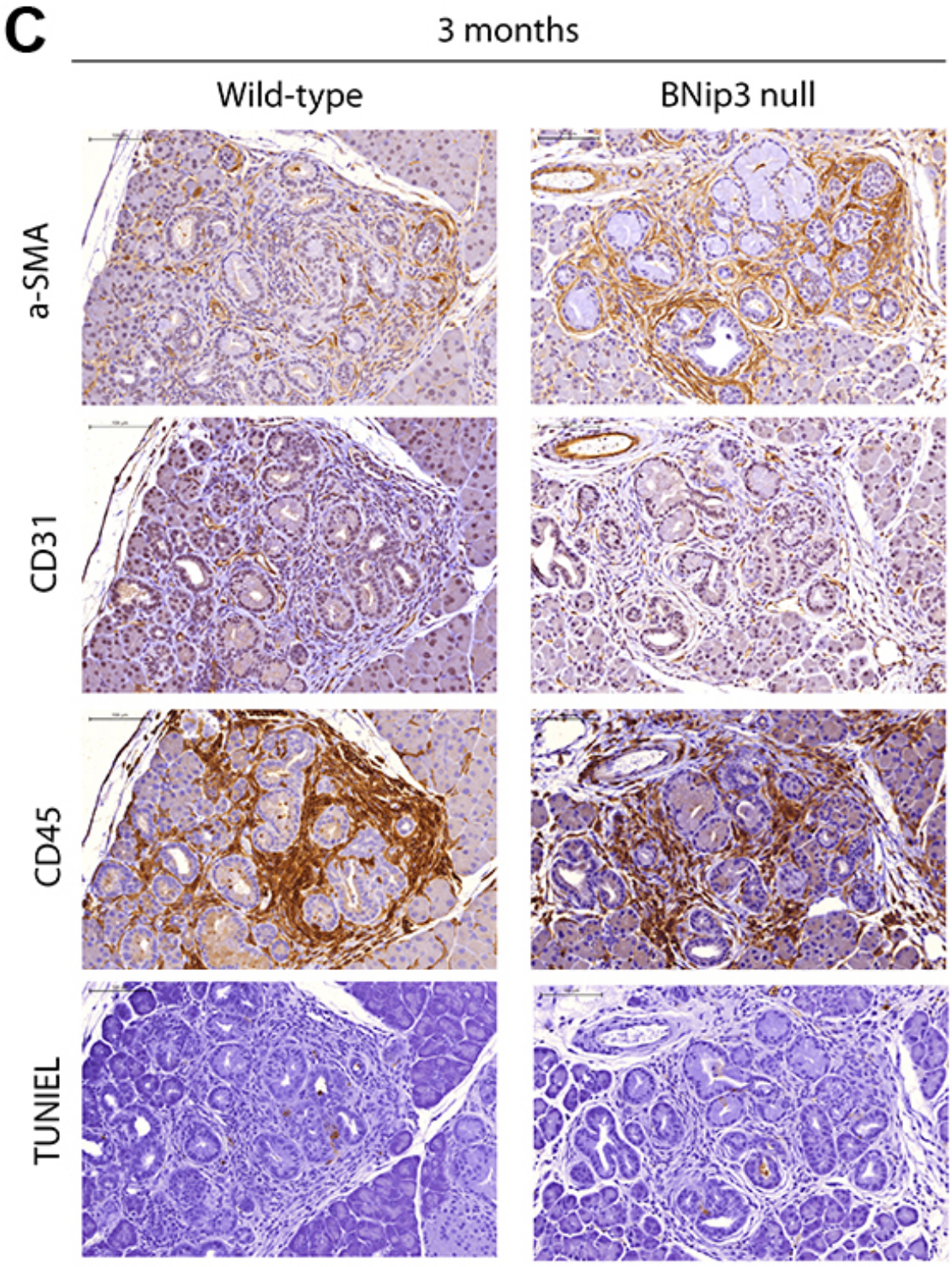


**Figure 38. Immunohistochemical analysis of 3 months old wild-type and BNip3 null pancreas.** Immunohistochemical staining of 3 months old wild-type and BNip3 null pancreas. (n=3 per genotype)

However, at 4.5 months, we observed increased number of PanIN lesions in BNip3 null pancreas by H&E. Interestingly, we also observed higher grade PanIN2 and PanIN3 lesions in BNip3 null pancreas compared to wild-type by H&E staining, suggesting that PanINs were progressing more rapidly in this genotype. However, given the complexity of these lesions, these will be examined by a pathologist in order for us to confirm this observation. In order to confirm tumor growth, we analyzed CK19 staining at 4.5 months using Aperio's ImageScope analysis and observed a significant increase in percent positive cells for CK19 in BNip3 null pancreas compared to wild-type (Figure 39B,D). We also observed increased staining for alcian blue which is indicative of increased mucin content, a precursor for adenocarcinomas in humans and mice (Figure 39B). However, an Aperio based analysis of alcian blue was not successful owing to similar coloration of eosin and alcian blue and will need to be scored by a pathologist. Also, we observed reduced levels of amylase in BNip3 null pancreas, suggesting that more of the pancreas had PanIN lesions and thus, reduced number of acinar cells (Figure 39B). We examined nuclear c-Myc levels and remainder markers in wild-type and BNip3 null pancreas at 4.5 months, but did not observe significant differences between PanIN lesions in the two genotypes (Figure 39A). We have also harvested pancreas from wild-type and BNip3 null mice between 6-8 months and 9-11 months time points that are currently under analysis. Strikingly, as the mice aged, we observed significantly reduced overall survival for BNip3 null mice as compared to wild-type mice (Figure 40). This data is consistent with the study on human PDAC patients that shows reduced overall survival in patients with lower levels of BNIP3 (121).

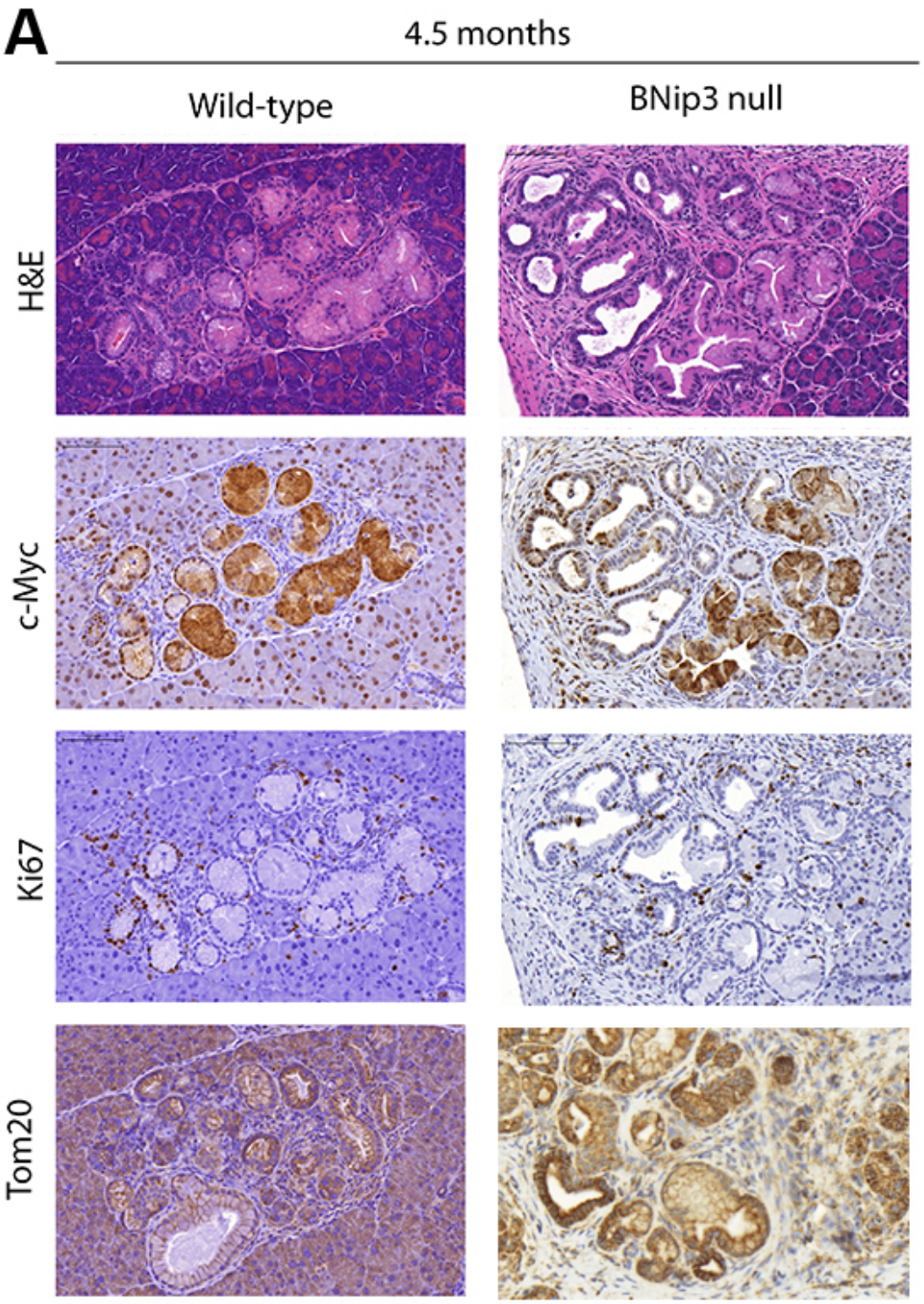


**Figure 39. Immunohistochemical analysis of 4.5 months old wild-type and BNip3 null pancreas.**

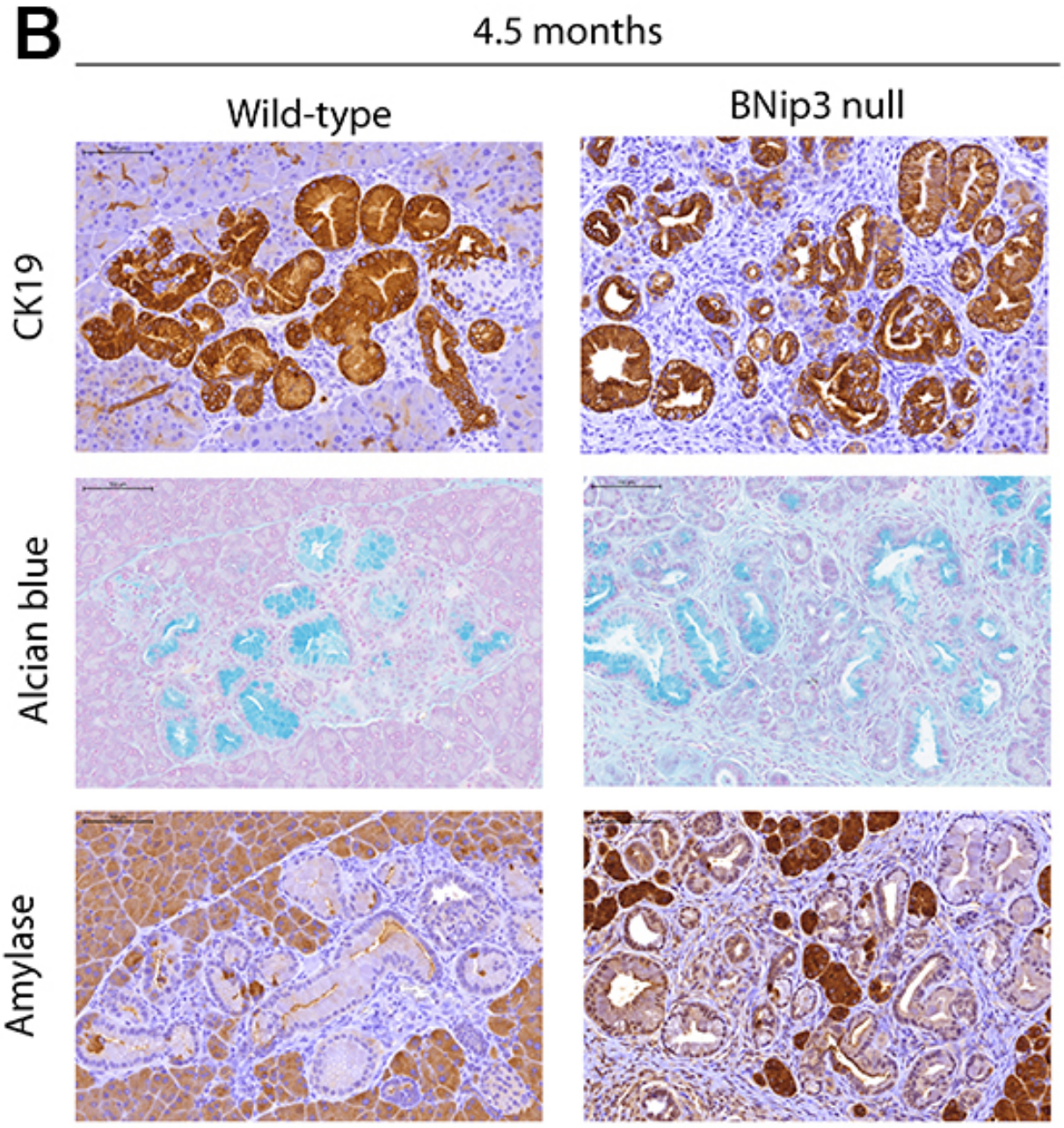


**Figure 39. Immunohistochemical analysis of 4.5 months old wild-type and BNip3 null pancreas.**

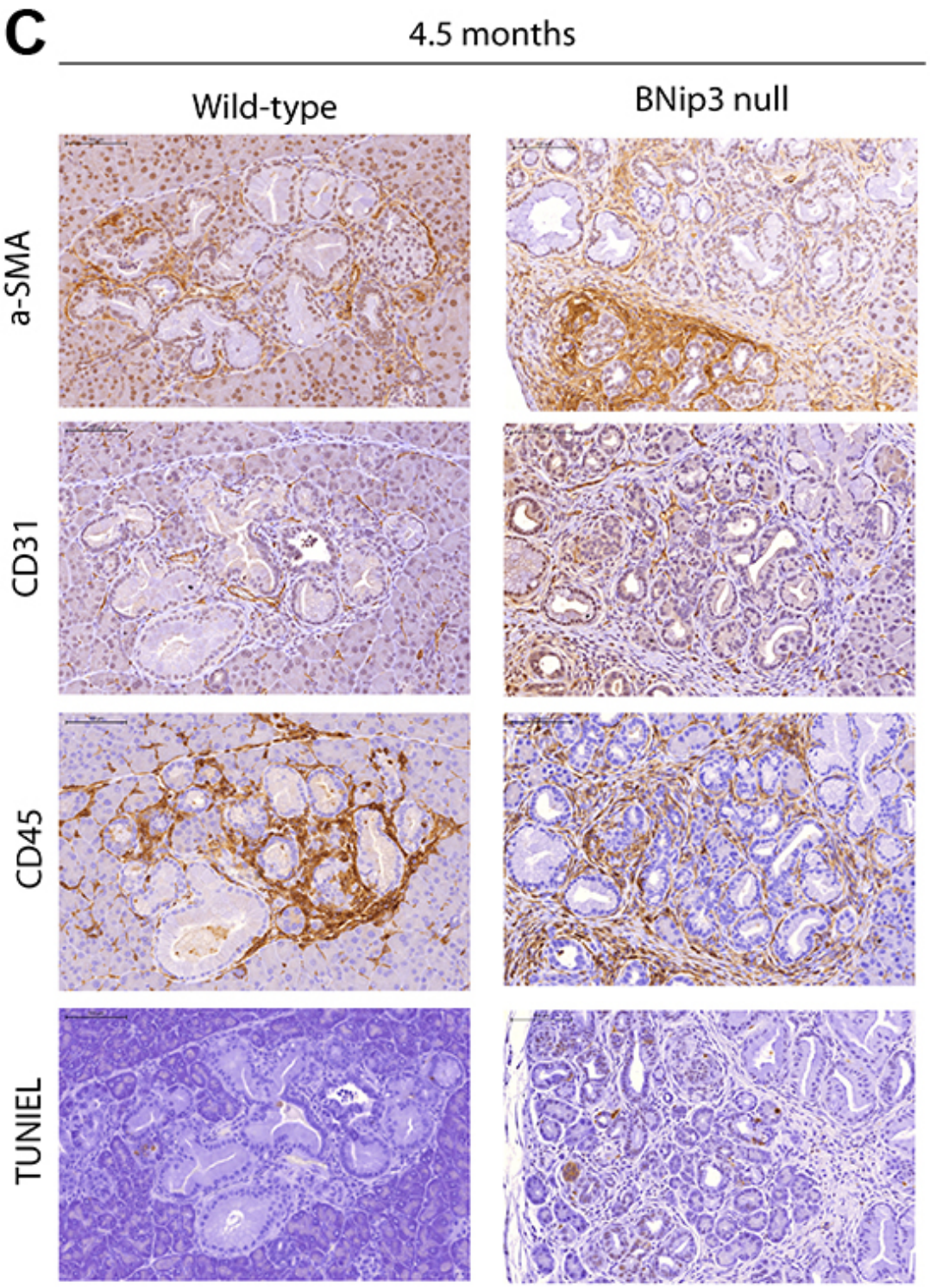


**Figure 39. Immunohistochemical analysis of 4.5 months old wild-type and BNip3 null pancreas.**

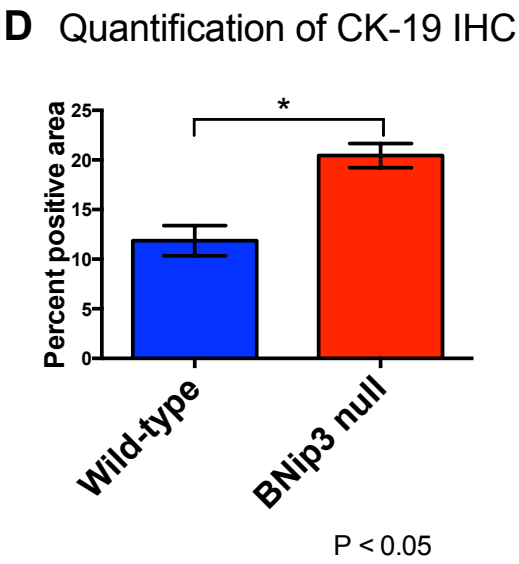


**Figure 39. Immunohistochemical analysis of 4.5 months old wild-type and BNip3 null pancreas.** (A-C) Immunohistochemical staining of 4.5 months old wild-type and BNip3 null pancreas. (D) Quantification of IHC for CK-19 in wild-type and BNip3 null pancreas using Aperio (n=3 per genotype)

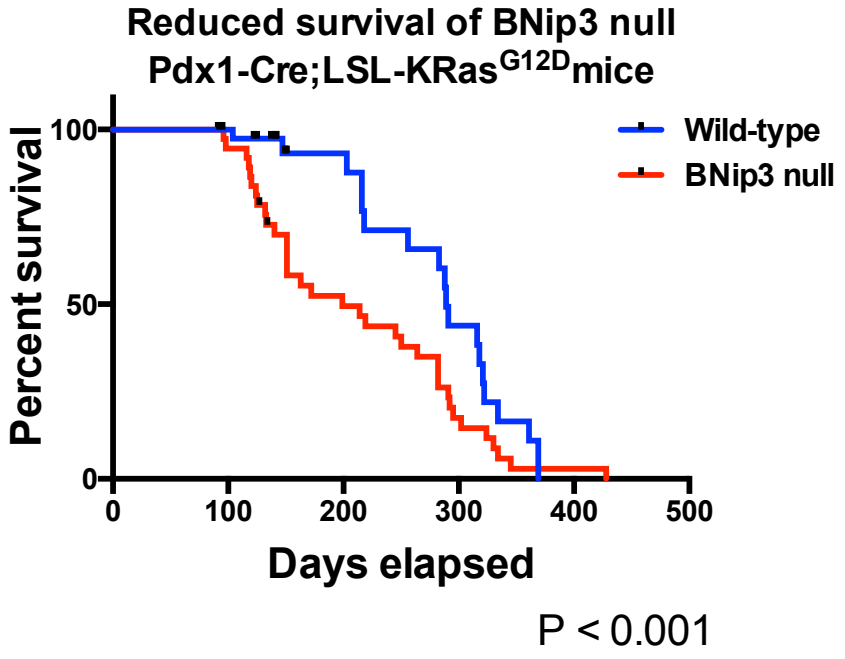


**Figure 40. BNip3 loss reduces survival in PDX1-Cre;LSL-KRAS$^{G12D}$ mice.** Kaplan-Meier survival curve of wild-type (n=44) and BNip3 null mice (n=41).

### 7.4. BNip3 loss reduces latency of lung metastasis

Given that we observed increased PanIN lesions in BNip3 null mice at 4.5 months and reduced over all survival, we investigated lungs, liver, spleen, intestines and diaphragm of wild-type and BNip3 null mice between age 6-8 months and 9-11 months for metastasis. We observed overt lung metastasis at 9 months in BNip3 null mice, nut not in wild-type mice (Figure 41). This suggests that BNip3 null mice have reduced latency of lung metastasis compared to wild-type mice.

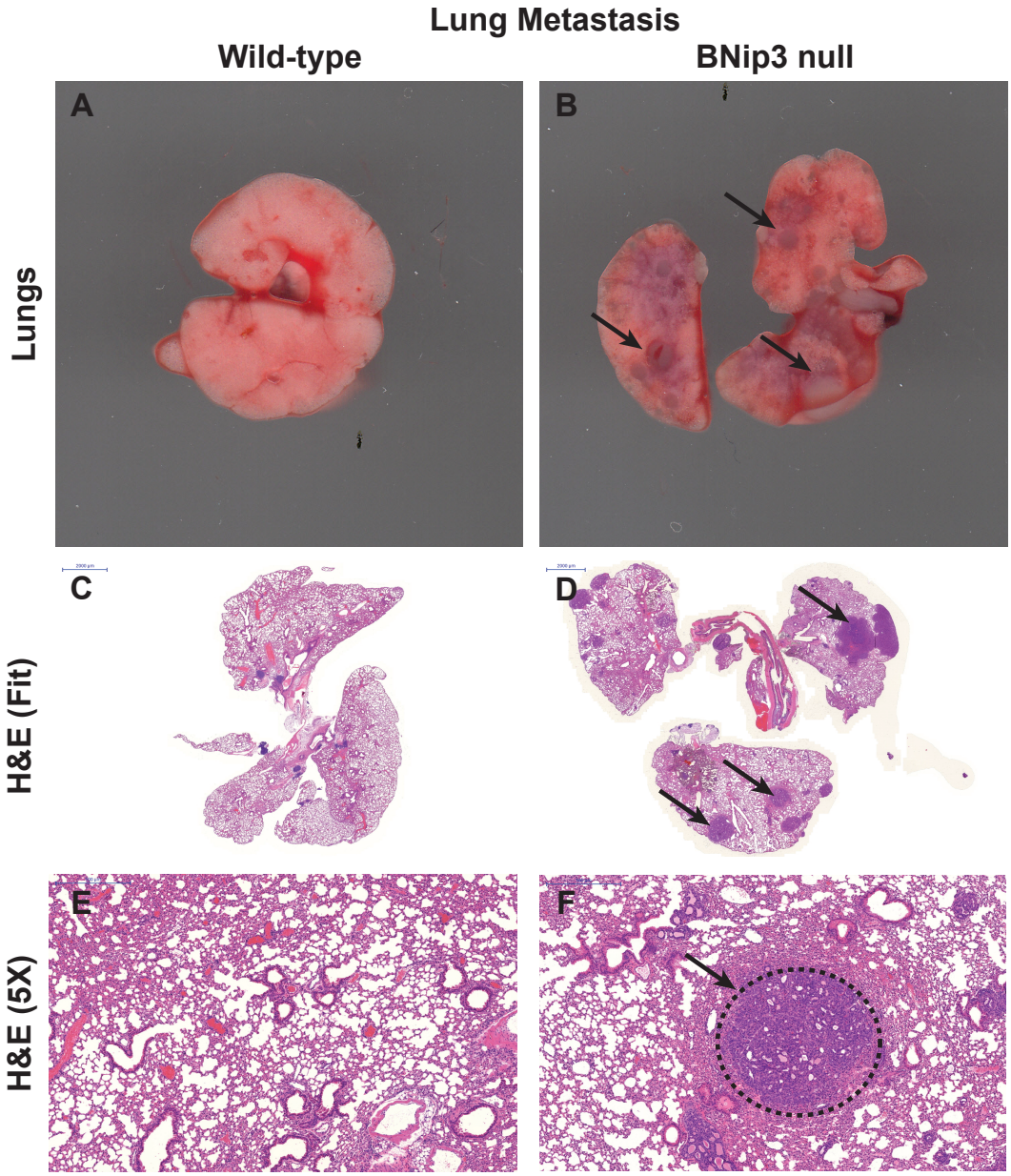


**Figure 41. BNip3 loss reduces latency of lung metastasis in PDX1-Cre;LSL-KRAS$^{G12D}$ mice.** (A-B) Overt lung metastases seen in BNip3 null mice (n=6) at 9 months, but not in age-matched wild-type mice (n=4). (C-F) H&E staining showing overt lung metastases (black arrows) in BNip3 null mice (n=6), but not in age-matched wild-type mice (n=4).

## 7.5. Conclusion

Overall, we have shown that loss of BNip3 promotes tumor growth and significantly reduces overall survival in PDX-1-Cre;LSL-KRAS$^{G12D}$ mice. However, in order to confirm whether loss of BNip3 affects tumor latency, we will need to examine even earlier time points of 1 and 2 months of age. We have also shown that BNip3 null mice have reduced latency of overt lung metastasis, but will require a complete analysis of pancreas from wild-type and BNip3 null mice at later time points (as mentioned in Chapter 7.3) to follow disease progression in the two genotypes. Overall, our results suggest that BNip3 functions as tumor suppressor in PDAC.

# CHAPTER 8

# LOSS OF BNIP3 INCREASES CELL GROWTH AND IS ASSOCIATED WITH INCREASED C-MYC PROTEIN LEVELS IN HUMAN PANCREATIC CANCER CELL LINES

## 8.1. Introduction

Myc is one of the most common oncogenic transcription factors detected in about 70% of all malignancies (79-81). Increased levels of c-Myc in tumors can be a result of gene translocation, gene amplification, overexpression and increased protein stability. While gene translocation is more common in hematological malignancies, the latter three are usually seen in solid tumors. It is now well established that c-Myc deregulation due to overexpression and protein stability can occur by activation of growth factors and their receptors, Ras/MAPK pathway, PI3K/Akt pathway, Wnt/β-catenin signaling and Notch pathway (81). c-Myc protein stabilization is increased by Ras-dependent phosphorylation pathway where activated MAPK phosphorylates c-Myc at Serine62 (Ser62) at the N-terminal site in response to Ras (173). c-Myc is also stabilized by acetylation at its N-terminal by p300/CBP complex (173,174). Up-regulation of c-Myc results in not only increased cellular proliferation, but also in disruption of epithelial apical/basolateral polarity. On the other hand, c-Myc degradation mainly occurs by phosphorylation of Threonine-58 by GSK-3β which results in recruitment of Skp, Cullin, F-box containing complex (SCF) that directs its ubiquitination and subsequent proteasomal degradation (175).

While c-Myc is deregulated in several cancers, it was shown that c-Myc inhibition in KRas driven lung cancer in mice leads to not only rapid and long-term tumor regression, but also extends their overall survival, thus projecting c-Myc as a promising clinical target (176). In case of PDAC that is also essentially KRas driven, c-Myc overexpression was reported in about 70% of human PDAC cases examined in one study, while another study reported that the increased c-Myc expression in human PDAC cell lines was a result of increased protein stability (177-179). Preliminary data in the lab from early mouse PanIN lesions showed increased BNip3 expression with reduced c-Myc expression. In addition, our work with mouse mammary tumor cell lines suggested that BNip3 suppressed c-Myc by increasing its degradation at the proteasome. The above-mentioned evidence suggests that BNip3 regulates c-Myc expression via GSK-3β in pancreatic cancer.

In this chapter, we will assess the effect of BNIP3 on cellular growth in human pancreatic cancer cell lines. We will also examine if BNIP3 regulates cellular growth rate by suppressing c-Myc in these cell lines.

## 8.2. Exogenous expression and stable knockdown of BNIP3 in human pancreatic cancer cell lines

In order to examine the function of BNIP3 in pancreatic cancer, we studied a panel of human pancreatic cancer cell lines and their BNIP3 expression status. While BNIP3 is epigenetically silenced by promoter hypermethylation in MiaPaca-2 and HPAC cell lines, it is highly expressed in CFPAC-1, Panc-1 and Capan-2 cells. These cells have mutant KRAS and p53 (122).

In order to validate the expression status of BNIP3 by immunoblot for whole cell lysates, MiaPaca-2 and CFPAC-1 cells were grown under conditions of 20% oxygen and 1% oxygen for 24 hours. As expected, MiaPaca-2 cells did not express any BNIP3 protein under either of the conditions (Figure 42A) indicating that it was indeed silenced in these cells. On the other, CFPAC-1 cells expressed BNIP3 under 20% oxygen and the protein level was significantly increased under 1% oxygen, indicating that the promoter is not hypermethylated and responsive to hypoxic conditions (Figure 42B).

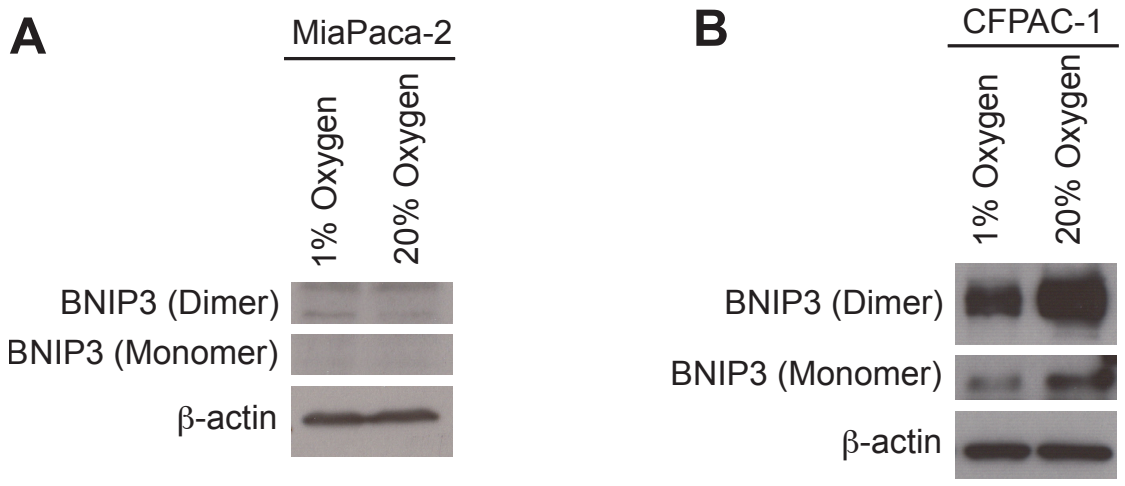


**Figure 42. BNIP3 expression in human pancreatic cancer cell lines.** (A) Immunoblot analysis for BNIP3 and b-actin for MiaPaca-2 cells at 20%oxygen and 1% oxygen. (B) Immunoblot analysis for BNIP3 and b-actin for CFPAC-1 cells at 20%oxygen and 1% oxygen.

Next, we generated stable cell lines for MiaPaca-2 cells expressing empty-vector and BNIP3 wild-type-HA using pcDNA3.1 plasmids under G418 selection. We examined BNIP3 expression by qRT-PCR and immunoblot for whole cell lysates (Figure 43A-B). We also generated stables cell lines for CFPAC-1 cells by knocking down BNIP3 using two shRNAs targeting the coding sequence and 3'-UTR sequence of BNIP3. We performed the knockdown using lentivirus containing control or BNIP3 shRNAs under puromycin selection and validated it by qRT-PCR and immunoblot for whole cell lysates (Figure 44A-B). Interestingly, while we observed BNIP3 expression in whole cell lysates, we also observed its expression in nuclear lysates, suggesting that BNIP3 might have functions other than mitophagy.

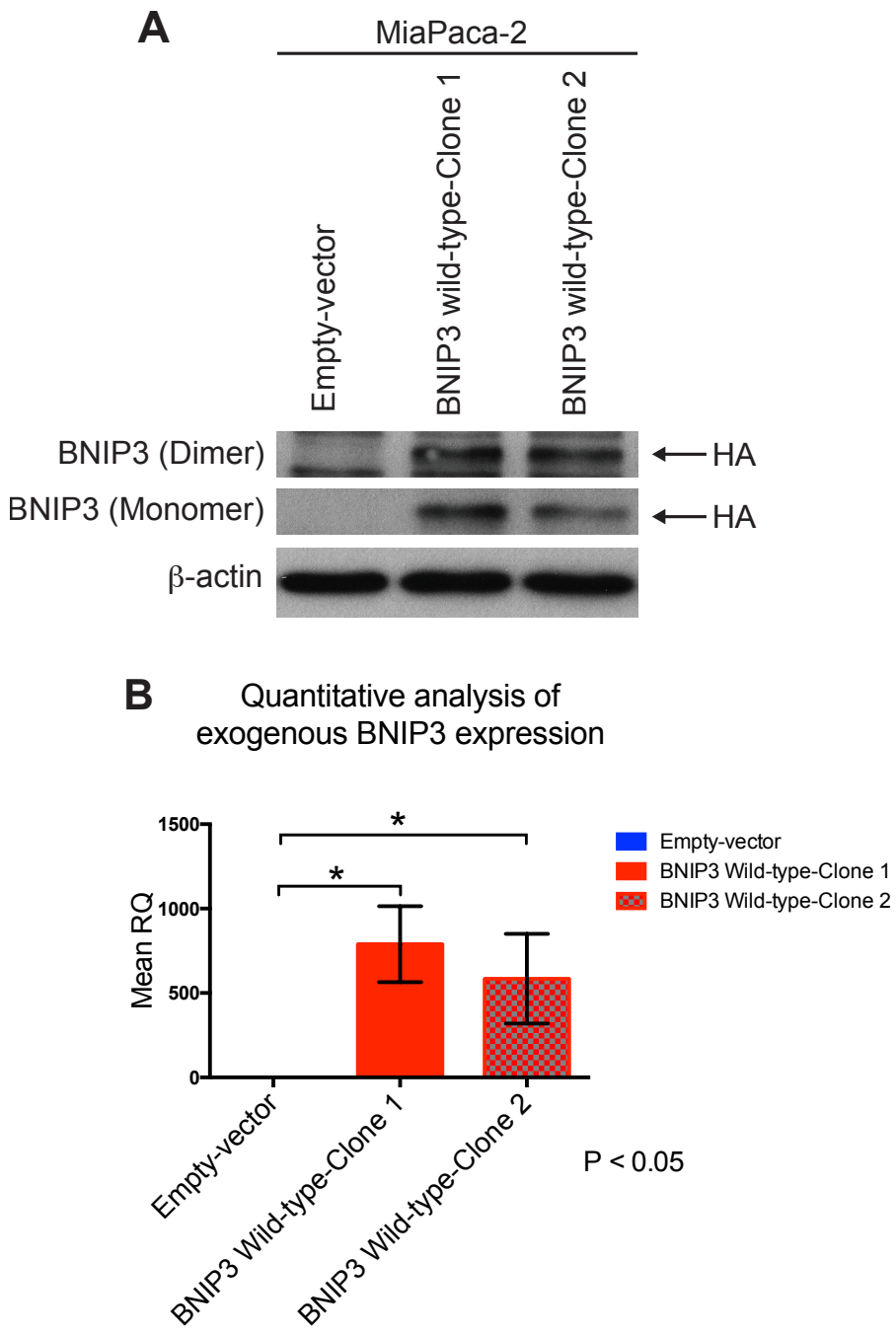


**Figure 43. Generation of MiaPaca-2 cell lines stably expressing empty-vector control and wild-type BNIP3.** (A) Immunoblot analysis for BNIP3 and β-actin for MiaPaca-2 cell lines stably expressing empty-vector control and BNIP3 wild-type. (B) qPCR analysis for BNIP3 in MiaPaca-2 cell lines stably expressing empty-vector control and BNIP3 wild-type performed in triplicate.

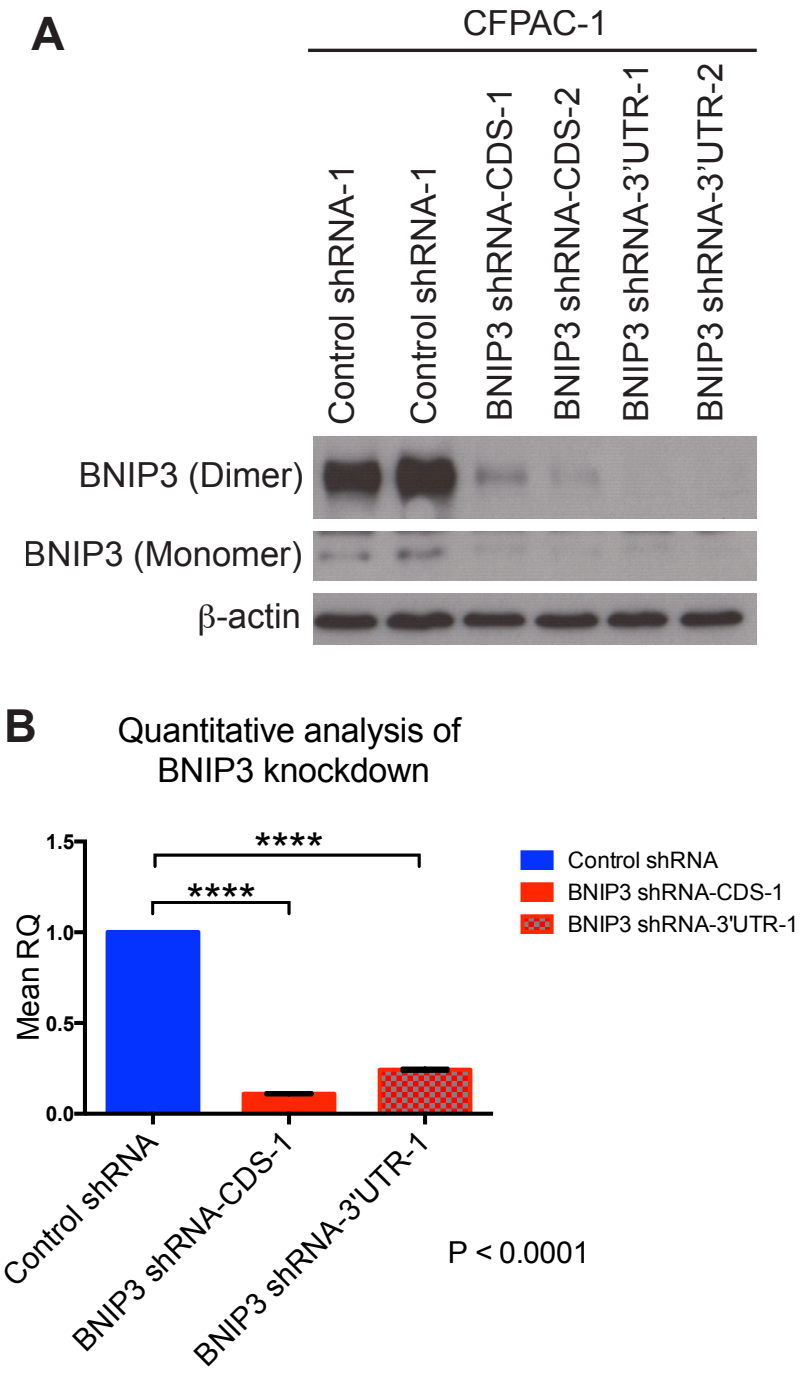


**Figure 44. Generation of CFPAC-1 cell lines with stable knockdown of BNIP3.** (A) Immunoblot analysis for BNIP3 and β-actin for CFPAC-1 cell lines showing knockdown with control shRNA or BNIP3 shRNA for the CDS and 3'UTR regions. (B) qPCR analysis for BNIP3 in CFPAC-1 cell lines with control shRNA or BNIP3 shRNA for CDS and 3'UTR regions performed in triplicate.

### 8.3. BNIP3 reduces cell growth and c-Myc levels in pancreatic cancer cell lines independent of its mitophagy function

In order to investigate the effect of BNIP3 on cell growth in MiaPaca-2 cell lines, we measured growth rate performed over a period of 8 days. Given that we had observed expression of BNIP3 in nuclear lysates, we also examined if the effect of BNIP3 was due to its function of mitophagy or independent of it. For this purpose, we generated a cell line containing a mitophagy mutant of BNIP3, BNIP3-W18A (Figure 45A). This is a critical mutation in the LIR of BNIP3, which is required for its interaction with LC3 (22,36,37, 180). We observed that MiaPaca-2 cell line expressing wild-type BNIP3 was growing significantly slower than the empty-vector cell line (Figure 45B). Moreover, this effect was not rescued by the W18A mutant, suggesting that BNIP3 was functioning to suppress growth independent of mitophagy. Similarly, we examined the effect of BNIP3 knockdown in CFPAC-1 cell lines and observed that cell lines with BNIP3 knockdown were growing significantly faster than the control (Figure 46A). We also measured growth rates with previously established osteosarcoma (Saos2) cell lines with BNIP3 overexpression and observed that BNIP3 overexpressing cell lines were growing slower than the controls (Figure 46B). The above data shows that BNIP3 suppresses cell growth in pancreatic cancer cell lines.

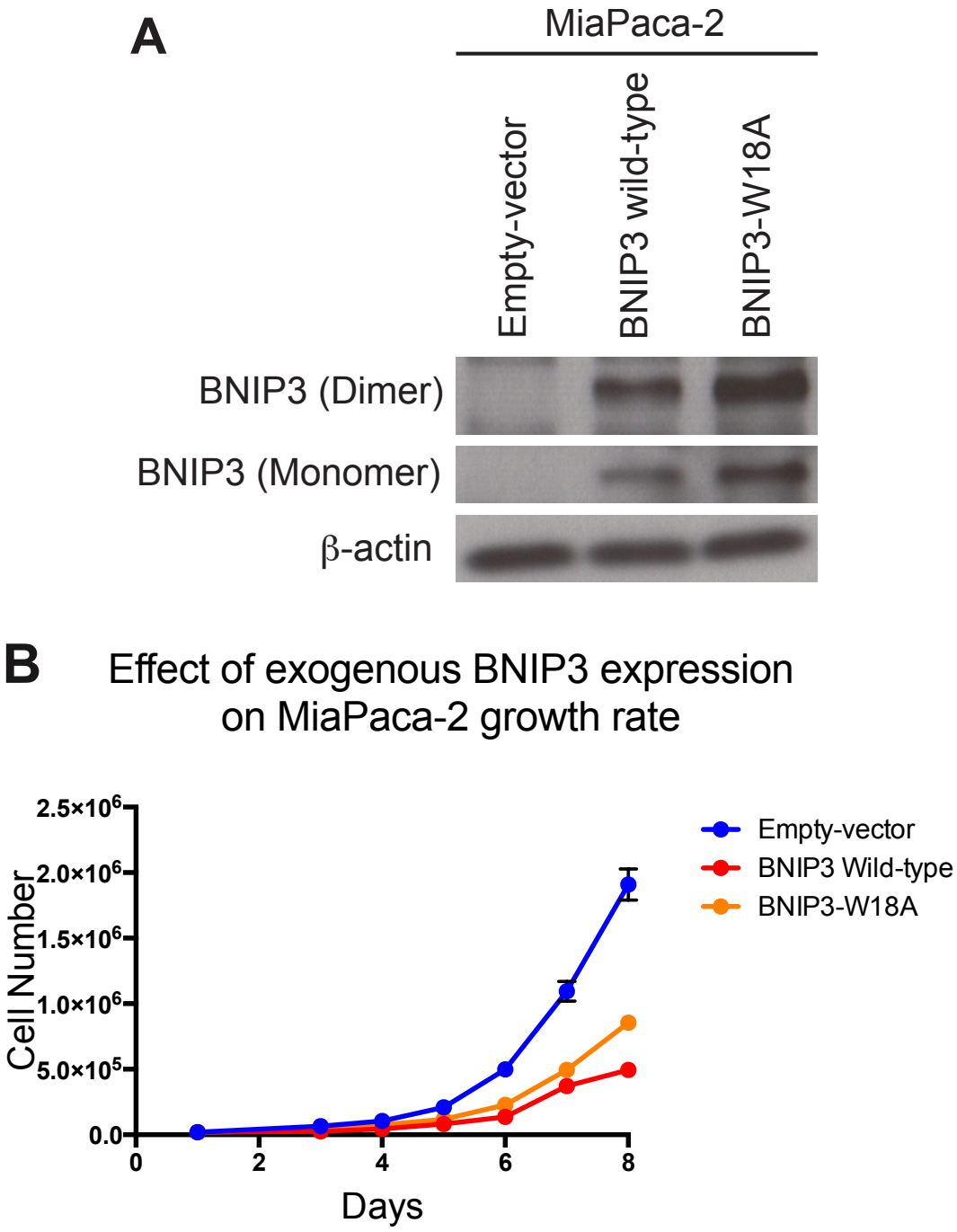


**Figure 45. BNIP3 reduces cellular growth rate, but not via mitophagy.** (A) Immunoblot analysis for BNIP3 and β-actin for MiaPaca-2 cell lines stably expressing empty-vector control, BNIP3 wild-type and BNIP3-W18A. (B) Growth rate of MiaPaca-2 cell lines expressing empty-vector control, BNIP3 wild-type and BNIP3-W18A performed in triplicate.

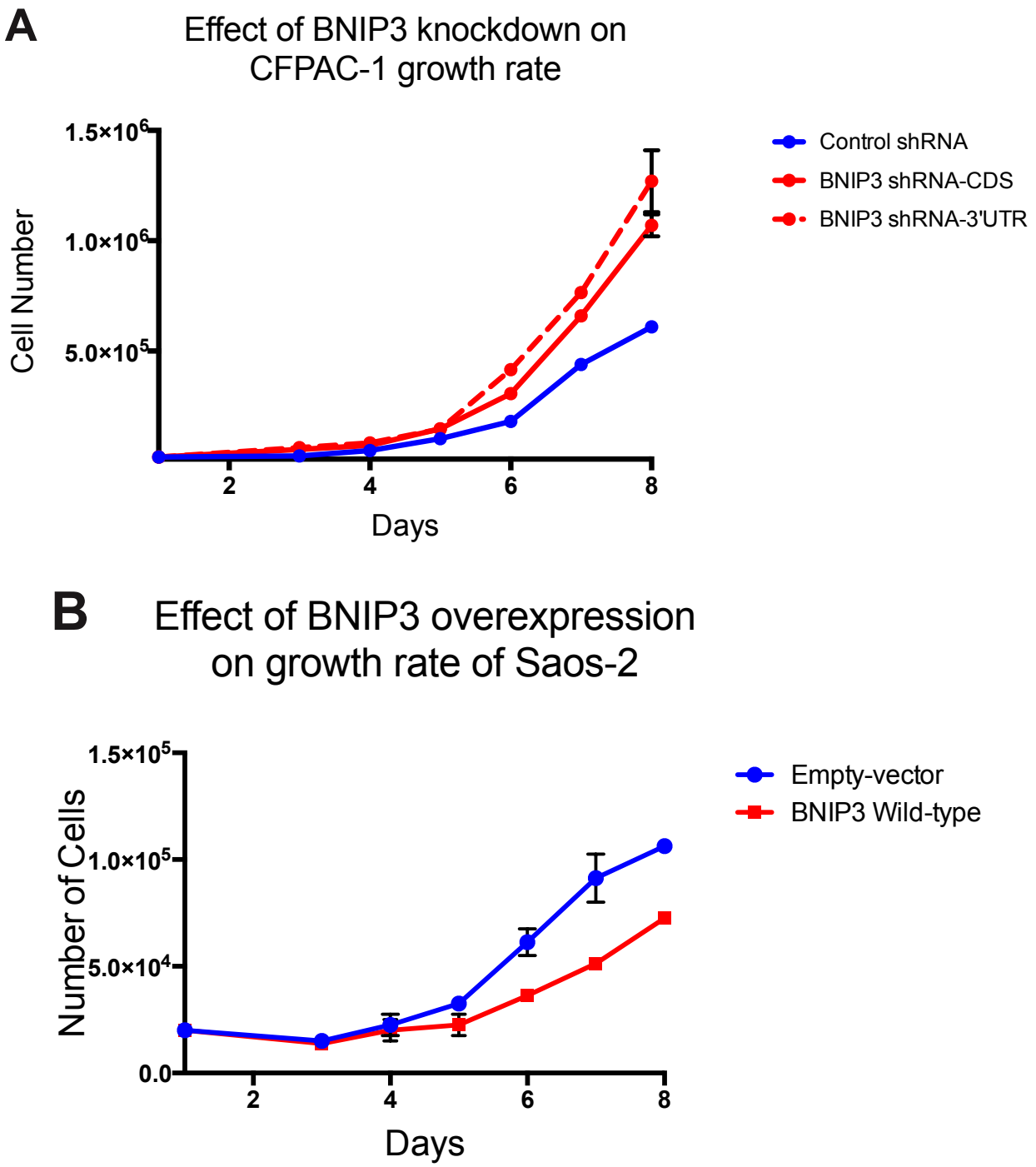


**Figure 46. BNIP3 reduces cellular growth rate.** (A) Growth rate of CFPAC-1 cell lines with control shRNA or BNIP3 shRNA for CDS and 3'UTR regions performed in triplicate. (B) Growth rate of Saos-2 cell lines stably expressing empty-vector control or BNIP3 wild-type performed in triplicate.

In order to examine the effect of BNIP3 on c-Myc levels in MiaPaca-2 cell lines, we performed immunoblot for nuclear lysates and observed that BNIP3 wild-type and BNIP3-W18A cell lines had reduced nuclear c-Myc levels (Figure 47A). This suggested that the effect of BNIP3 on c-Myc was independent of its function of mitophagy. Thus, we performed all further experiments without the mitophagy mutant. In order to test whether reduced levels of c-Myc also translated into decreased c-Myc activity in MiaPaca-2 cell lines, we performed qRT-PCR for c-Myc targets including carbamoyl-phosphate synthetase2, aspartate transcarbamylase, and dihydroorotase (CAD), PGC-1β (PPARGC1B), ornithine decarboxylase 1 (ODC1), cyclin D2 (CCND2) and p21 (CDKN1A). While CAD, PGC-1β and ODC1 are metabolic targets that are induced by c-Myc, cyclin D2 and p21 are cell cycle regulators of which cyclin D2 is induced whereas p21 is repressed by c-Myc (79,81). We observed decreased expression of all target genes except p21 in BNIP3 wild-type expressing cell line as compared to the control cell line indicating that c-Myc activity was reduced upon expression of BNIP3 (Figure 47B). In order to test if effect of BNIP3 on cell growth was mediated by c-Myc, we examined growth rate of MiaPaca-2 cell lines in the presence of specific c-Myc inhibitor, 10074-G5, that inhibits binding of c-Myc with its transcription partner, Max, thus specifically inhibiting c-Myc activity (181,182). We observed that treatment with c-Myc inhibitor significantly reduced cell growth of control cells suggesting that effect of BNIP3 on cell growth was mediated by c-Myc (Figure 47C).

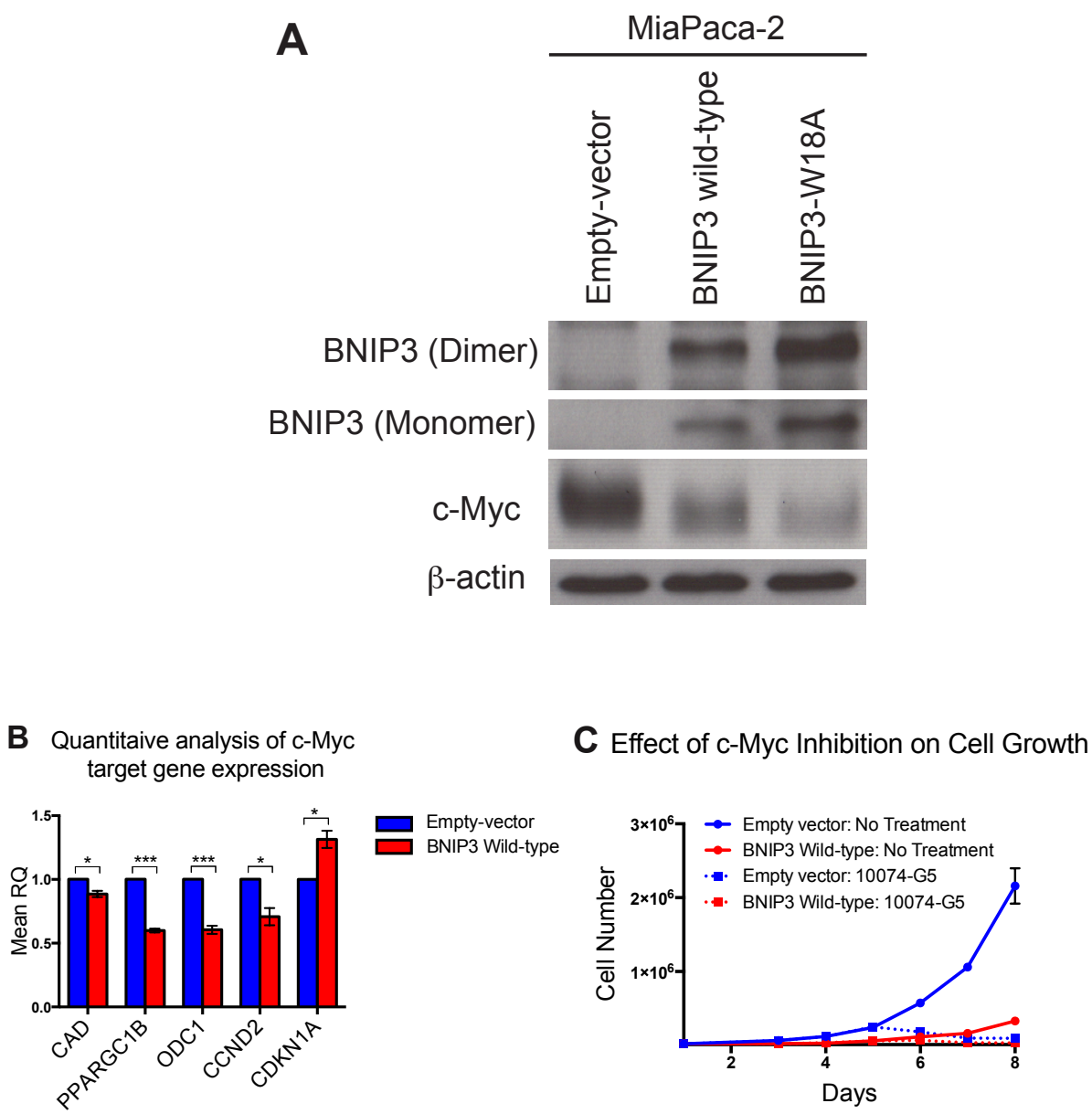


**Figure 47. Loss of BNIP3 promotes c-Myc activity.** (A) Immunoblot analysis for BNIP3, c-Myc and β-actin for MiaPaca-2 cell lines stably expressing empty-vector control, BNIP3 wild-type and BNIP3-W18A. (B) qPCR analysis for c-Myc target genes. (* $p<0.05$, ** $p<0.01$, *** $p<0.001$) (C) Growth rate of MiaPaca-2 cell lines expressing empty-vector control, BNIP3 wild-type treated with c-Myc inhibitor 10074-G5 performed in triplicate.

We also examined the effect of BNIP3 on c-Myc levels in CFPAC-1 and Saos-2 cell lines and observed that BNIP3 suppressed c-Myc levels (Figure 48A-B). Interestingly, in CFPAC-1 cell lines, not only did we observe an increase in c-Myc levels with BNIP3 knockdown, but we also observed nuclear BNIP3 expression.

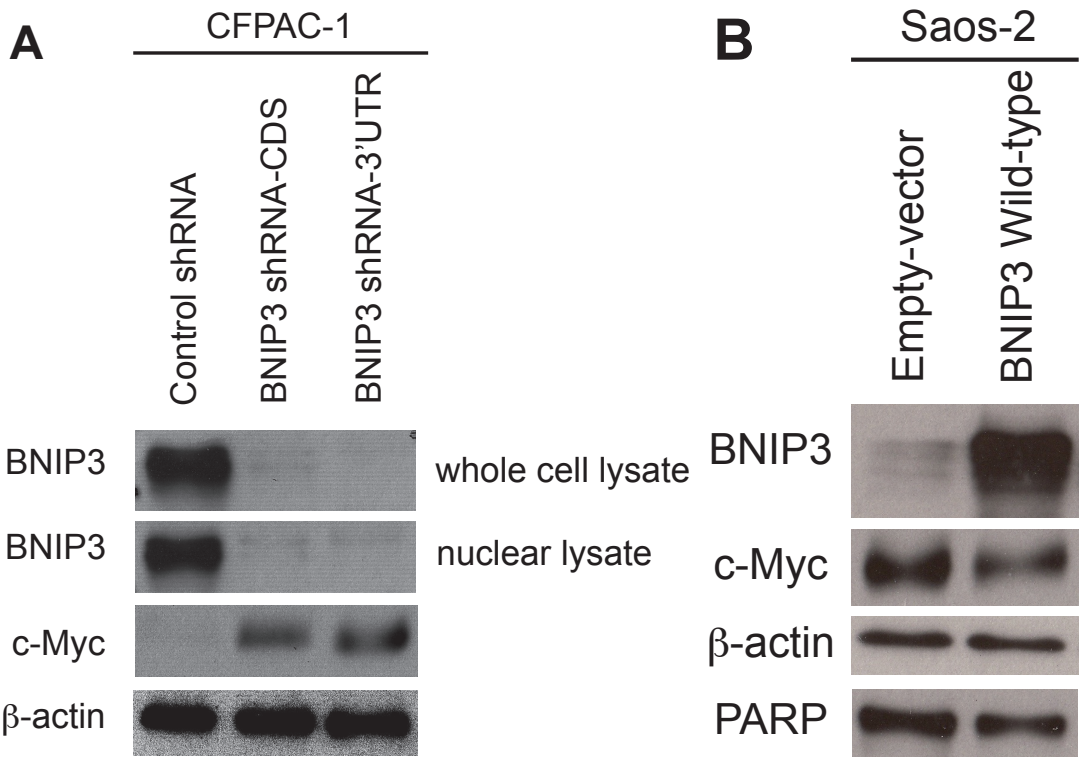


**Figure 48. Loss of BNIP3 promotes c-Myc protein levels.** (A) Immunoblot analysis for BNIP3, c-Myc and β-actin for CFPAC-1 cell lines with control shRNA or BNIP3 shRNA for CDS and 3'UTR region. (B) Immunoblot analysis for BNIP3, c-Myc and β-actin Saos-2 cell lines stably expressing empty-vector control or BNIP3 wild-type.

### 8.4. BNIP3 associated decrease in c-Myc protein level is not transcriptionally regulated.

In order to understand how BNIP3 was modulating protein level of c-Myc, we investigated whether BNIP3 associated decrease in c-Myc protein level was transcriptionally regulated. We performed qRT-PCR for c-Myc levels in MiaPaca-2 and CFPAC cell lines. We observed no significant difference in c-Myc mRNA levels in these cell lines (Figure 49A-B), indicating that BNIP3 associated change in c-Myc protein level was not transcriptional.

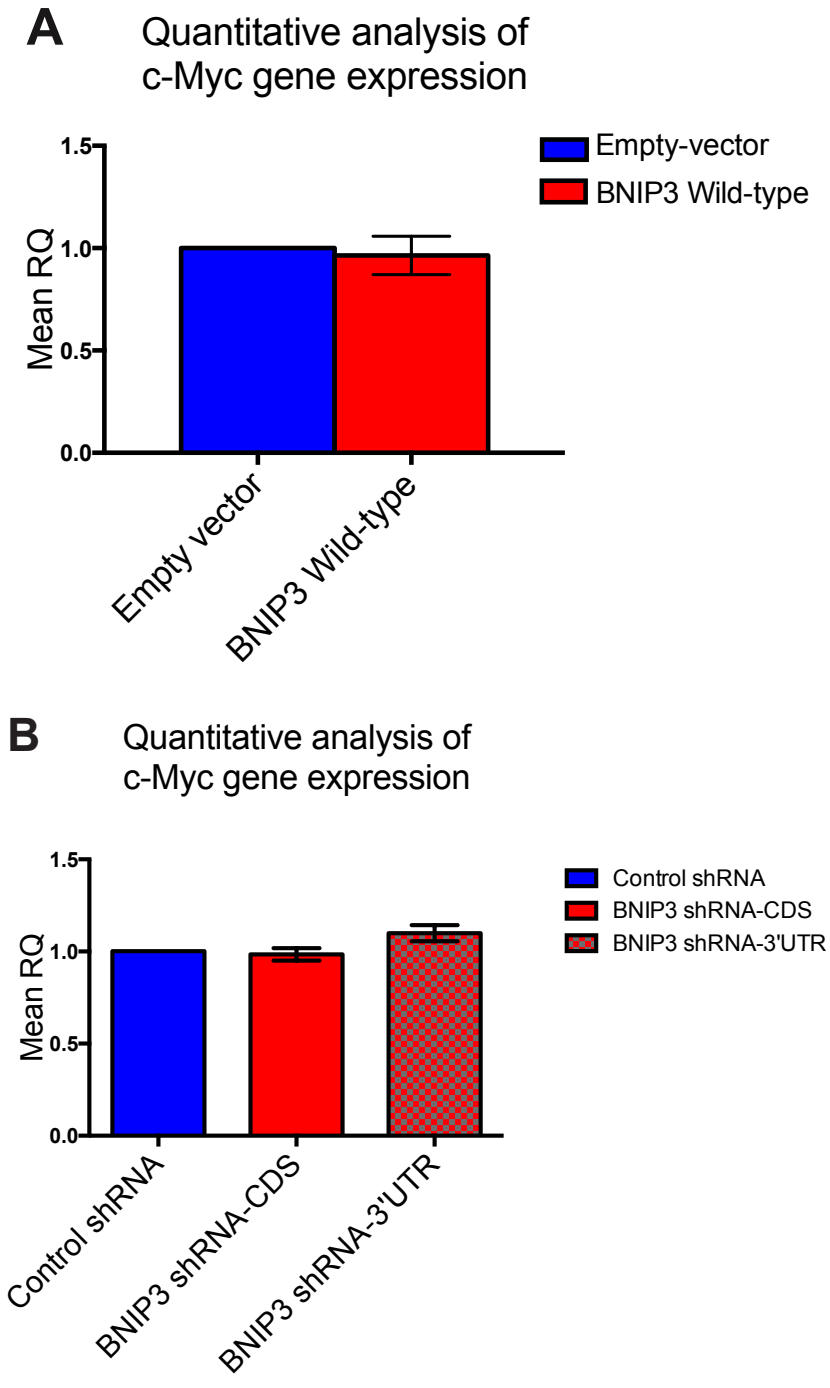


**Figure 49. c-Myc is not transcriptionally regulated by BNIP3.** (A) qPCR analysis for c-Myc in MiaPaca-2 cell lines stably expressing empty-vector control, BNIP3 wild-type performed in triplicate. (B) qPCR analysis for c-Myc in CFPAC-1 cell lines with control shRNA or BNIP3 shRNA for CDS and 3'UTR region.

Myc is post-translationally modified by phosphorylation at Threonine58 (Thr-58) by GSK3β, which results in its proteasomal degradation (173,175). We examined whether BNIP3 associated decrease in c-Myc protein level was due to increased phosphorylation of c-Myc at Thr-58 and subsequent proteasomal degradation. To test this, we treated MiaPaca-2 cell lines with MG132 for 4 hours. MG132 is a known proteasomal inhibitor and treatment with this compound would inhibit degradation of c-Myc and result in accumulation of the protein in BNIP3 expressing cell line. We measured levels of c-Myc by immunoblot of nuclear lysates and observed that upon treatment with MG132, c-Myc levels in BNIP3 expressing MiaPaca-2 cell line increased to levels observed in empty-vector cell line (Figure 50). These results suggested that BNIP3 associated modulation of c-Myc protein was likely due to a post-translational modification. To test whether c-Myc was indeed being regulated due to phosphorylation at Thr-58 site, we generated tamoxifen inducible Myc-wild-type and Myc-T58A mutant protein that does not get phosphorylated at Thr-58 resulting in its increased stabilization. We performed a time course experiment with 4 hours of tamoxifen treatment followed by release for 0, 2, 4, 8, 16 and 24 hours to follow changes in protein stability over time. However, we did not observe an increased stability in mutant Myc in BNIP3 expressing MiaPaca-2 cell lines (Figure 51), suggesting that modulation of c-Myc is not due to a post-translational modification at Thr-58.

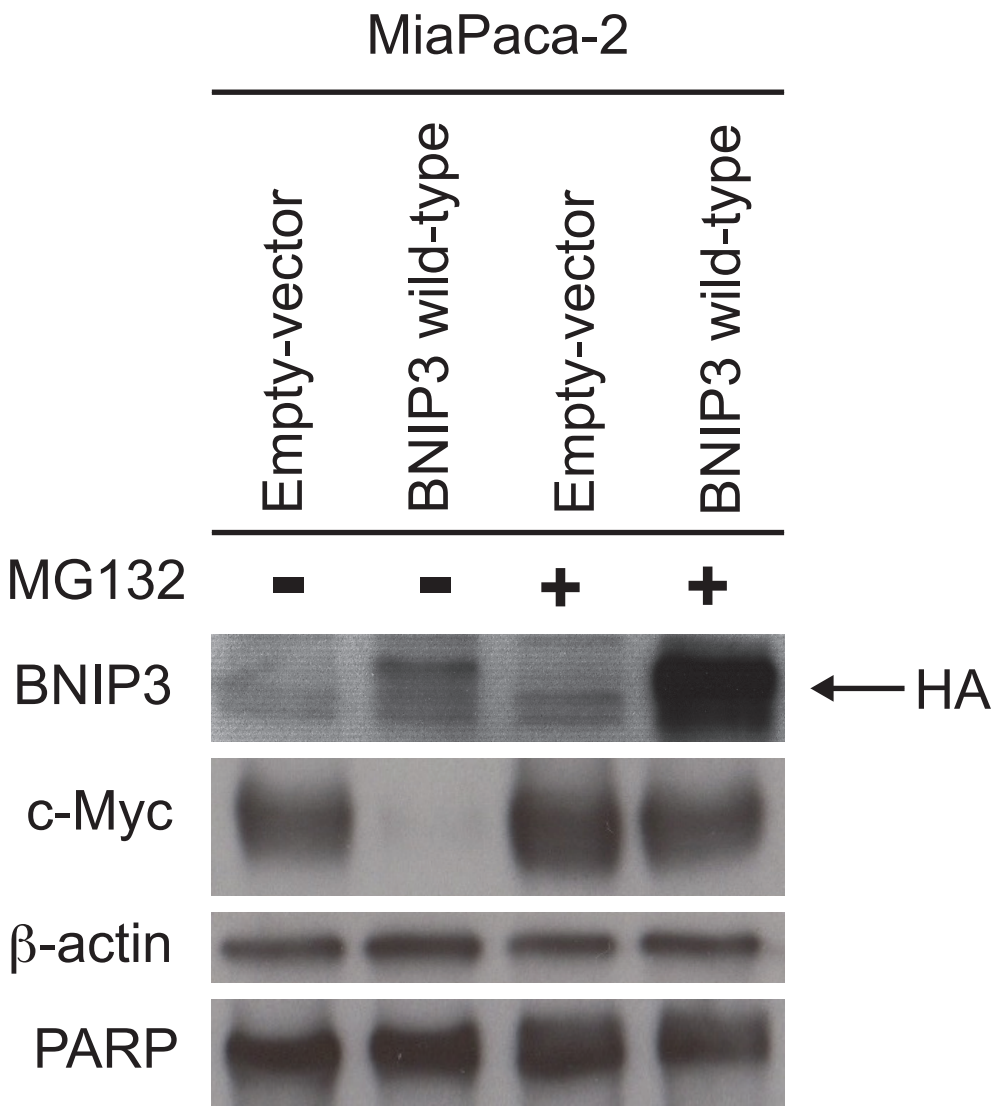


**Figure 50. BNIP3 promotes proteasomal degradation of c-Myc.** Immunoblot analysis for BNIP3, c-Myc, PARP and β-actin for MiaPaca-2 cell lines stably expressing empty-vector control and BNIP3 wild-type upon treatment with MG132 for 4 hours.

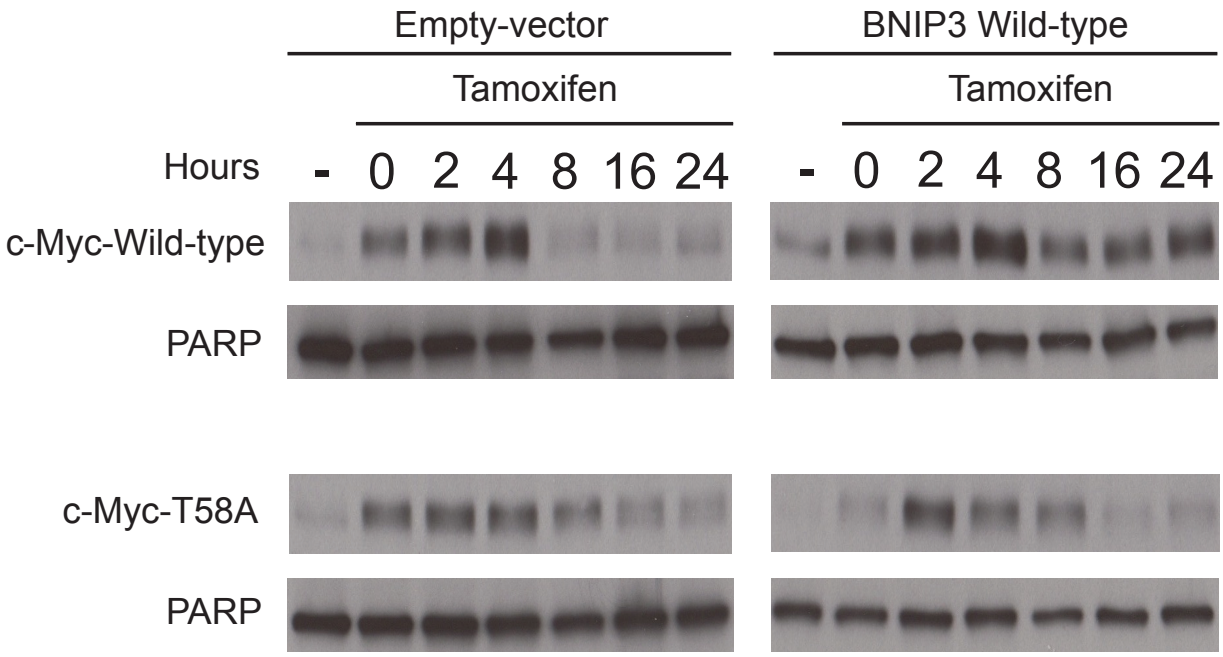


**Figure 51. BNIP3 does not promote proteasomal degradation of c-Myc via phosphorylation at Threonine58.** Immunoblot analysis for c-Myc and PARP in empty-vector and BNIP3-wild-type MiaPaca-2 cell lines expressing Tamoxifen inducible c-Myc wild-type and c-Myc-T58A.

## 8.5. Conclusion

In this chapter, we have shown that BNIP3 suppresses cellular growth rate in human pancreatic cancer cell lines, which is concomitant with reduced c-Myc protein levels. However, we have also shown that c-Myc is not transcriptionally regulated by BNIP3. While our results indicate the likelihood of a post-translational modification of c-Myc resulting in its decreased stabilization in the presence of BNIP3, we have shown that it is not due to regulation at Thr-58. These results indicate two possibilities. One, that c-Myc is getting modified by ways other than phosphorylation, for example., by acetylation of c-Myc results in increased stability or two, that changes in c-Myc levels is a readout of changes in cellular growth rate and not a direct consequence of BNIP3. These possibilities can be tested in future experiments.

# CHAPTER 9

# DISCUSSION

BNIP3 is a mitochondrial protein that is strongly induced by physiological stresses such as hypoxia and nutrient starvation (22,36). Not only is it a transcriptional target of HIF-1, but is also regulated by RAS, pRB/E2F, p53, NFκB and FoxO3 (100-111). It has a well-established function of targeting mitochondria for autophagic degradation by directly interacting with LC3 at the growing phagophore through its LC3 interacting region at the amino terminal domain (36). Thus, BNIP3 mediated mitophagy functions to eliminate damaged mitochondria and maintain the overall mitochondrial integrity of the cell. However, the function of BNIP3 in cancer is not well characterized. While it is up-regulated in early stages of tumor formation such as DCIS and PanIN, it is deleted or silenced by promoter hypermethylation in invasive breast cancer, PDAC, hematological malignancies, gastric and lung cancer (112-114,117-125). In order to address the function and mechanism of BNip3 in tumor growth and progression to metastasis, we employed two genetically engineered mouse models, the MMTV-PyMT mouse model of mammary tumorigenesis and the PDX1-Cre;LSL-$KRAS^{G12D}$ mouse model of pancreatic tumorigenesis (130,131,142,143). Overall, we have shown that BNip3 functions as tumor suppressor that inhibits progression to metastasis by mitophagy dependent and mitophagy independent pathways.

Our study of the effect of BNip3 loss in the MMTV-PyMT model of mammary tumorigenesis has shown that BNip3 exerts its effect as a tumor suppressor via its

function of mitophagy. BNip3 null tumors as well as cultured MECs had reduced levels of mitophagy as was confirmed by their elevated mitochondrial mass shown by increased mitochondrial proteins such as Vdac, CoxIV and Tom20 and increased mitochondrial:nuclear genome ratio. Moreover, we showed that BNip3 null MECs had significantly reduced LC3 (autophagosome) and cyclophilin D (mitochondrial) colocalization, establishing that mitophagy was compromised in BNip3 null MECs. The fact that BNip3 null MECs also exhibited significantly reduced mitochondrial substrate uptake (pyruvate and glutamine) and reduced mitochondrial membrane potential suggested that while there were more mitochondria, they were damaged or dysfunctional, an observation that is consistent with defective mitophagy. We examined the consequences of dysfunctional mitochondria arising from defective mitophagy on tumor growth and metastasis.

Interestingly, we observed that not only did BNip3 loss result in defective mitochondria, but it also increased aerobic glycolysis or the Warburg effect (Figure 52). BNip3 null tumors as well as cultured MECs exhibited elevated glucose uptake as was shown by $^{18}$F-FDG and fluorescence glucose uptake, respectively. BNip3 null MECs also showed significantly increased lactate output, glycolysis intermediates, and uptake of glucose for nucleic acid and lipid synthesis. However, loss of BNip3 resulted in significant reduction in oxidative metabolism as shown by reduced oxygen consumption levels in mammary tumor cells. All of the above-mentioned effects of BNip3 loss are key characteristics of the Warburg effect (29). Moreover, treatment of BNip3 null MECs with 2DG, an inhibitor of glycolysis, significantly reduced cell growth suggesting that BNip3 null MECs were heavily reliant on glycolysis for growth. Several studies have

shown increased aerobic glycolysis due to increased expression of glycolytic enzymes including HK2, PFK2, LDH-A and PDK1 in tumor cells (16,29). However, we show for the first time that tumor cells with defective mitochondria arising from defective mitophagy rely on aerobic glycolysis for growth.

A key point to remember here is that the Warburg effect in tumor cells does not occur due to defective oxidative metabolism, but rather from a deregulation of glycolysis itself (1,2). To understand how glycolysis was getting deregulated with loss of BNip3, we investigated the levels of Hif-1$\alpha$, which is a known regulator of expression of glycolytic enzymes in tumor cells and thus the Warburg effect (27,30,164). We observed increased level of Hif-1$\alpha$ in BNip3 null tumors as well as cultured MECs, an effect that was rescued by exogenous BNip3 expression in BNip3 null MECs. Consistently, we observed significantly increased expression of glycolysis enzymes, Hk2, Pdk1, Pgk1 and glucose transporter, Slca2a1, all of which are known HIF targets, thus explaining the increase in glycolysis (164). The fact that Hif-1$\alpha$ mediated glycolysis was driving cell growth in BNip3 null MECs was established by treatment of MECs with Echinomycin, an inhibitor of Hif-1$\alpha$ activity, which abrogated not only the expression of glycolysis genes but also cell growth in BNip3 null MECs. Hif-1$\alpha$ is an established positive regulator of tumor growth and metastasis in breast cancer as has been shown by deletion of Hif-1$\alpha$ in the MMTV-PyMT model in earlier studies. Given that no other HIF target has been shown to reduce its levels in tumor cells, our findings are significant in establishing a novel negative feedback loop where BNip3, which is induced by Hif-1$\alpha$, can significantly lower levels of Hif-1$\alpha$.

In order to understand how this negative feedback loop between Hif-1α and BNip3 is generated, we investigated the effect of BNip3 loss on reactive oxygen species in tumor tissue as well as cells. ROS can be generated in cells during oxidative metabolism due to defects in the mitochondrial electron transport chain or due to cellular oxygen tension as in conditions of hypoxia. In case of the former, complexes I, II, III can generate superoxide anions by incomplete reduction of molecular oxygen and leak them into the mitochondrial matrix or intermembrane space (23,24). Once leaked, excessive ROS can result in damaging effects such as oxidation of amino acids, lipid peroxidation and DNA damage. ROS is a major driver of tumor growth and metastasis (25,27). Studies have shown that mitochondrial DNA mutations resulting in deficiency in complex I of the electron transport chain can generate excessive ROS, which in turn enhances the metastatic potential of tumor, cells. ROS has also been shown to be essential for KRas driven lung tumors. But, most importantly, ROS generation can inhibit prolyl hydroxylases and result in stabilization of Hif-1α (27). We observed elevated levels of ROS in BNip3 null tumors and MECs as was shown by dihydroethidine staining of frozen tumor sections and MitoSOX staining of MECs. We also detected elevated DNA damage by staining for 8-OHdG consistent with increased ROS in BNip3 null tumors. Interestingly, we observed increased glutathione metabolism in BNip3 null MECs suggesting the increased demand to reduce ROS in cells. Importantly, not only did treatment of mice with BHA reduce tumor growth and metastasis in BNip3 null mice, but it also reduced levels of Hif-1α and its target genes. These results confirmed that Hif-1α stabilization resulting upon loss of BNip3 was due to

elevated levels of ROS. Thus, we established that BNip3 mediated mitophagy functions to limit mitochondrial ROS, lower Hif-1$\alpha$ levels and indeed limit aerobic glycolysis. `

High expression of Hif-1$\alpha$ is associated with significantly shorter disease free survival in lymph node positive and ER positive breast cancer (152,153). Hif-1$\alpha$ has been linked with invasiveness and metastatic potential in TNBC and was also found to be overexpressed in TNBC patients by gene set enrichment analysis (151,155,157). Our data showing negative regulation of Hif-1$\alpha$ by BNip3 in the mammary tumor model prompted us to investigate its clinical significance in breast cancer. Our data shows an increase in BNIP3 copy number loss in TNBC, but not in receptor positive breast cancer. Moreover, we also show that low BNIP3 levels with Hif-1$\alpha$ expression can be used to significantly stratify metastasis free survival in TNBC patient population, suggesting that together these two can be used as prognostic indicators for the disease. However, while the cause for selective loss of BNIP3 in TNBC is not yet known, a recent study that investigated the metabolic phenotypes in TNBC showed that “Warburg type” phenotype was most common in the disease with tumor cells exhibiting increased glycolysis as compared to the surrounding stroma (183). This highlights the need to study mitochondrial function or the lack of it due to defective mitophagy in TNBC.

Lastly, we also observed that BNip3 null tumors and MECs relied on autophagy for survival under low nutrient conditions. Wild-type and BNip3 null tumors and cells showed similar levels of autophagy under basal and low nutrient conditions. Upon inhibition of glycolysis, while cell growth in BNip3 null MECs reduced significantly, we did not see a concomitant increase in cell death. However, when we treated tumor cells with a combination of glycolysis and autophagy inhibitors, we saw a highly significant

increase in cell death in BNip3 null MECs, indicating that these cells were heavily reliant on autophagy for survival. This is in contrast with some recent studies, which suggest that dysfunctional mitochondria arising from defective mitochondrial autophagy by pan-autophagy inhibition suppress tumor progression (169,184). First, we show that dysfunctional mitochondria arising from selective targeting of mitophagy (and not autophagy) promote tumor progression. It is likely that in case of inhibition of autophagy, there are other pathways such as recycling of amino acids that get compromised, thus inhibiting tumor progression. Second, we show effective autophagic flux in mitophagy deficient BNip3 null tumor cells, thus elegantly highlighting that effects of mitophagy inhibition are not the same as effects of inhibition of global autophagy.

In summary, we have shown that BNIP3 dependent mitophagy promotes mitochondrial integrity by reducing mitochondrial mass, promoting oxidative metabolism, limiting aerobic glycolysis and limiting ROS, thus putting brakes on Hif-1$\alpha$ activity and tumor progression.

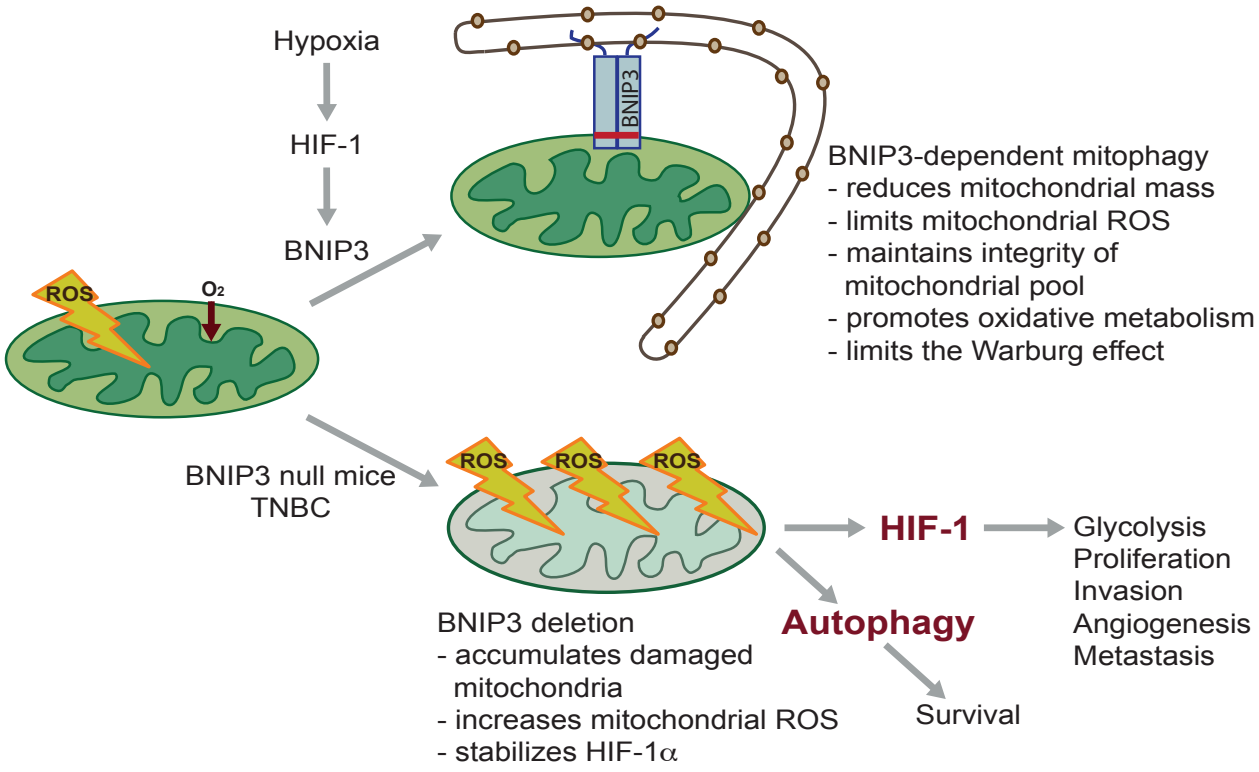


**Figure 52. Schematic summary of the role BNIP3 in suppressing tumor progression and metastasis in the MMTV-PyMT mouse model of mammary tumorigenesis.** (Adapted from Reference 150)

Our study of the effect of BNip3 loss in the PDX1-Cre;LSL-KRAS$^{G12D}$ mouse model of pancreatic tumorigenesis shows that BNip3 functions to suppress tumor growth and potentially, progression to metastasis. We have observed that loss of BNip3 increases the number of PanIN lesions by 4.5 months of age as shown by increased CK-19 staining of the pancreas of wild-type and BNip3 null mice. However, whether BNip3 also reduces latency of tumor initiation is currently being investigated in 1 and 2 month old mice in the lab. We have also observed that loss of BNip3 affects latency of tumor metastasis with overt lung metastasis seen in BNip3 null mice by 9 months of age. This data suggests that loss of BNip3 promotes tumor invasion and progression and is consistent with our observation of higher-grade PanIN lesions in BNip3 null mice at 4.5 months of age. However, in order to gain a definitive understanding of whether BNip3 does inhibit tumor progression, we will need to score pancreas sections from wild-type and BNip3 null mice at 4.5 and 6-8 months, a process that is currently under way in the lab. Given that PDAC is known to be highly desmoplastic, it will also be interesting to observe the effect of BNip3 on the tumor microenvironment (126, 132-134). Since, BNip3 null mice have a whole body deletion of BNip3 that affects not just the pancreatic epithelia but also the surrounding stromal and immune cell population, it would be worth investigating whether effect of loss of BNip3 on pancreatic tumor growth and progression is a cell intrinsic property or not. This can be achieved by culturing wild-type and BNip3 null pancreatic tumor cells *in vitro* and then orthotopically transplanting them into the pancreas of syngeneic wild-type mice. Lastly, we have observed that loss of BNip3 significantly reduces overall survival in BNip3 null mice. While this finding is consistent with the study in PDAC patients showing that loss of BNIP3 is indicative of

lower overall survival, it highlights the need to understand how BNIP3 functions to suppress pancreatic tumor growth and metastasis.

We have already shown that BNip3 functions to suppress mammary tumor growth and progression via its function of mitochondrial autophagy. However, given that BNIP3 is up-regulated by RAS, which is the primary driver of pancreatic cancer, we investigated the function of BNIP3 in PDAC (109-111). We examined the effect of exogenous expression of wild-type BNIP3 and mitophagy deficient BNIP3 in a human pancreatic cancer cell line in which BNIP3 is silenced by promoter hypermethylation. We observed that while BNIP3 inhibited cellular growth rate, this effect was not completely rescued by the mitophagy mutant BNIP3, thus indicating that BNIP3 is functions to suppress cellular growth independent of mitophagy. While this is an interesting finding, it is not entirely surprising since we have observed nuclear expression of BNIP3, which suggests of newer unexplored functions of the protein in tumor suppression. BNIP3 has a nuclear export signal (NES) in its sequence and has recently been shown to bind and activate acetyltransferase p300 and regulate cardiac gene expression (185). It would be worth investigating the effect of a double mutant (mutant for mitophagy and NES) BNIP3 protein that has impaired mitophagy and cannot be exported from the nucleus, thus restraining its activity to the nucleus alone. An unbiased investigation of BNIP3 transcriptome and proteome employing wild-type, mitophagy deficient and double mutant BNIP3 cell lines will be crucial in shedding light on the global effects of BNIP3 in tumorigenesis.

Lastly, we have observed that BNIP3 suppresses c-Myc protein levels in cancer cell lines. However, our data suggests that neither is this effect transcriptionally

regulated nor is it regulated by phosphorylation of c-Myc at Thr-58. Given that BNIP3 has been shown to be active in the nucleus via its binding of p300 and p300 is also known to bind and stabilize c-Myc, it will be interesting to explore if binding of BNIP3 with p300 has a direct implication on c-Myc stability or whether the change in c-Myc protein level is a mere readout of growth rate changes as observed with BNIP3 (173,174). However, an unbiased approach (as mentioned above) to understand the tumor suppressive function of BNIP3 will likely be the better choice moving ahead.

Overall, our work examining the tumor suppressive function of BNIP3 in mammary and pancreatic tumorigenesis through use of human cancer cell lines and genetically engineered mouse models has established that BNip3 mediated mitophagy functions to suppress tumor growth and progression by maintaining overall mitochondrial health and inhibiting Hif-1$\alpha$ activity, while also setting the stage to explore its mitophagy independent functions in cancer.

## REFERENCES


1. Koppenol, W.H., et al. 2011. Otto Warburg's contributions to current concepts of cancer metabolism. *Nat Rev Cancer* **11**, 325-337 (2011).

2. Wallace, D.C. Mitochondria and Cancer. *Nat Rev Cancer* **12**, 685-698 (2012).

3. Horton, T.M., et al. Novel mitochondrial DNA deletion found in a renal cell carcinoma. *Genes Chromosomes Cancer* **15**, 95-101 (1996).

4. Meierhofer, D., et al. Mitochondrial DNA mutations in renal cell carcinomas revealed no general impact on energy metabolism. *Br J Cancer* **94**, 268-274 (2006).

5. Petros, J.A., et al. mtDNA mutations increase tumorigenicity in prostate cancer. *Proc Natl Acad Sci U S A* **102**, 719-724 (2005).

6. Ishikawa, K., et al. ROS-generating mitochondrial DNA mutations can regulate tumor cell metastasis. *Science* **320**, 661-664 (2008).

7. Baysal, B.E., et al. Mutations in SDHD, a mitochondrial complex II gene, in hereditary paraganglioma. *Science* **287**, 848-851 (2000).

8. Niemann, S., et al. Mutations in SDHC cause autosomal dominant paraganglioma, type 3. *Nat Genet* **26**, 268-270 (2000).

9. Xiao, M., et al. Inhibition of α-KG-dependent histone and DNA demethylases by fumarate and succinate that are accumulated in mutations of FH and SDH tumor suppressors. *Genes Dev* **26**, 1326-1338 (2012).

10. Dang, L., et al. Cancer-associated IDH1 mutations produce 2-hydroxyglutarate. *Nature* **462**, 739-744 (2009).

11. Lu, C., et al. IDH mutation impairs histone demethylation and results in a block to cell differentiation. *Nature* **483**, 474-478 (2012).

12. Turcan, S., et al. IDH1 mutation is sufficient to establish the glioma hypermethylator phenotype. *Nature* **483**, 479-483 (2012).

13. Koivunen, P., et al. Transformation by the (R)-enantiomer of 2-hydroxyglutarate linked to EGLN activation. *Nature* **483**, 484-488 (2012).

14. Gupta, S.C., et al. Upsides and downsides of reactive oxygen species for cancer: the roles of reactive oxygen species in tumorigenesis, prevention, and therapy. *Antioxid Redox Signal* **16**, 1295-1322 (2012).

15. Jones, R.G., et al. Tumor suppressors and cell metabolism: a recipe for cancer growth. *Genes Dev* **23**, 537-548 (2009).

16. DeBerardinis, R.J., et al. The biology of cancer: metabolic reprogramming fuels cell growth and proliferation. *Cell Metab* **7**, 11-20 (2008).

17. Amuthan, G., et al. Mitochondria-to-nucleus stress signaling induces phenotypic changes, tumor progression and cell invasion. *EMBO J* **20**, 1910-1920 (2001).

18. Birsoy, K., et al. Metabolic determinants of cancer cell sensitivity to glucose limitation and biguanides. *Nature* **508**, 108-112 (2014).

19. Viale, A., et al. Oncogene ablation-resistant pancreatic cancer cells depend on mitochondrial function. *Nature* **514**, 628-632 (2014).

20. Shackelford, D. B., et al. LKB1 inactivation dictates therapeutic response of non-small cell lung cancer to the metabolism drug phenformin. *Cancer Cell* **23**, 143-158 (2013).

21. Nunnari, J.,et al. Mitochondria: In Sickness and in Health. *Cell* **148,** 1145-1159 (2012).

22. Boland, M., et al. Mitochondrial dysfunction in cancer. *Front Oncol* **3**, 1-28 (2013).

23. Sena, L.A., et al. Physiological roles of mitochondrial reactive oxygen species. *Mol Cell* **48,**158-167 (2012).

24. Hamanaka, R.B., et al. Mitochondrial reactive oxygen species regulate cellular signaling and dictate biological outcomes. *Trends Biochem Sci* **35**, 505-513 (2010).

25. Schumacker, P.T. Reactive oxygen species in cancer cells: live by the sword, die by the sword. *Cancer Cell* **10**, 175-176 (2006).

26. Majmundar, A.J., et al. Hypoxia-inducble factors and the response to hypoxic stress. *Mol Cell* **40**, 294-309 (2010).

27. Sandaltzopoulos, R., et al. Reactive oxygen species and HIF-1 signaling in cancer. *Cancer Letters* **266**, 12-20 (2008)

28. Zhao-ji, L., et al. Hypoxia-inducible factor 1 and breast cancer metastasis. *JZUS* **16**, 32-43 (2005).

29. Vander Heiden, M.G., et al. Understanding the Warburg effect: the metabolic requirements of cell prolieferation. *Science* **324**, 1029-1033 (2009).

30. Semenza, G.L. Molecular mechanisms mediating metastasis of hypoxic breast cancer cells. *Trends Mol Med* **18**, 534-546 (2012)

31. Du, R., et al. HIF1$\alpha$ induces the recruitment of bone marrow-derived vascular modulatory cells to regulate tumor angiogenesis and invasion. *Cancer Cell* **13**, 206–220 (2008).

32. Rundqvist, H., et al. Tumor oxygenation: implications for breast cancer prognosis. *J Intern Med* **274**, 105-112 (2013).

33. Glick, D., et al. Autophagy: cellular and molecular mechanisms. *J Pathol* **221**, 3-12 (2010).

34. Mizushima, N., et al. Autophagy fights disease through cellular self-digestion. *Nature* **8**, 1069-1075 (2008).

35. Green, D.R., et al. To be or not to? How selective autophagy and cell death govern cell fate. *Cell* **157**, 65-75 (2014).

36. Chourasia, A.H., et al. Mitophagy and cancer. *Cancer & Metabolism* **3**, 1-11 (2015).

37. Brady, A.H., Mitophagy programs: mechanisms and physiological implications of mitochondrial targeting by autophagy. *Cell Mol Life Sci* **73**, 775-795 (2015).

38. Twig, G., et al. Fission and selective fusion govern mitochondrial segregation and elimination by autophagy. *EMBO J* **27,** 433-446 (2008).

39. Gomes L. C., et al. During autophagy mitochondria elongate, are spared from degradation and sustain cell viability. *Nat Cell Biol* **13,** 589-598 (2011).

40. Rambold A. S., et al. Tubular network formation protects mitochondrial from autophagosomal degradation during nutrient starvation. *Proc Natl Acad Sci U S A* **108,** 10190-10195 (2011).

41. Narendra D., et al. Targeting mitochondrial dysfunction: role for PINK1 and Parkin in mitochondrial quality control. *Antioxid Redox Signal* **14,** 1929-1938 (2011).

42. Youle R. J., et al. Mechanisms of Mitophagy. *Nat Rev Mol Cell Biol* **12,** 9-14 (2011).

43. Narendra, P., et al. Mitochondrial quality control mediated by PINK1 and Parkin: links to parkinsonism. *Cold Spring Harb Perspect Biol* **4**, 1-19 (2012).

44. Wang X., et al. PINK1 and Parkin target Miro for phosphorylation and degradation to arrest mitochondrial motility. *Cell* **147**, 893-906 (2011).

45. Kane, L.A., et al. PINK1 phosphorylates ubiquitin to activate E3 ubiquitin ligase activity. *J Cell Biol* **205**, 143-53 (2014).

46. Chen, Y., et al. PINK1-phosphorylated Mitofusin-2 is a Parkin receptor for culling damaged mitochondria. *Science* **340,** 471-475 (2013).

47. Geisler, S., et al. PINK1/Parkin-mediated mitophagy is dependent on VDAC1 and p62/SQSTM1. *Nat Cell Biol* **12,** 119-131 (2010).

48. Novak, I., et al. Mitophagy: a complex mechanism of mitochondrial removal. *Antioxid Redox Signal* **17,** 794-802 (2012).

49. Hollville, E., et al. Bcl-2 family proteins participate in mitochondrial quality control by regulating Parkin/PINK1-dependent mitophagy. *Mol Cell* **55**, 451-66 (2014).

50. Cesari R., et al. Parkin, a gene implicated in autosomal recessive juvenile parkinsonism, is a candidate tumor suppressor gene on chromosome 6q25-q27. *Proc. Natl. Acad. Sci. U S A* **100,** 5956-5961 (2003).

51. Picchio, M.C., et al. Alterations of the tumor suppressor gene Parkin in non-small cell lung cancer. *Clin Cancer Res* **10**, 2720-4 (2004).

52. Fujiwara M., et al. Parkin as a tumor suppressor gene for hepatocellular carcinoma. *Oncogene* **27,** 6002-6011 (2008).

53. Zhang C., et al. Parkin, a p53 target gene, mediates the role of p53 in glucose metabolism and the Warburg effect. *Proc Natl Acad Sci U S A* **108,** 16259-16264 (2011).

54. Gong, Y., et al. Pan-cancer genetic analysis indentifies PARK2 as a master regulator of G1/S cyclins. *Nat Genet* **46**, 588-94 (2014).

55. Scarpulla, R.C. Transcriptional paradigms in mammalian mitochondrial biogenesis and function. *Physiol Rev* **88**, 611-638 (2008).

56. Huo, L., et al. Mitochondrial DNA instability and peri-implantation lethality associated with targeted disruption of nuclear respiratory factor 1 in mice. *Mol Cell Biol* **21**, 644-54 (2001).

57. Scarpulla, R. C., et al. Transcriptional integration of mitochondrial biogenesis. *Trends Endocrinol Metab* **23,** 459-466 (2012).

58. Baar, K., et al. Skeletal muscle overexpression of nuclear respiratotry fctor 1 increases glucose transport capacity. *FASEB J* **17**, 1666-73 (2003).

59. Haq, R., et al. Oncogenic BRAF Regulates Oxidative Metabolism via PGC1α and MITF. *Cancer Cell* **23,** 303-315 (2013).

60. Vazquez, F., et al. PGC1α Expression Defines a Subset of Human Melanoma Tumors with Increased Mitochondrial Capacity and Resistance to Oxidative Stress. *Cancer Cell* **23,** 287-301 (2013).

61. Lamb, R., et al. Antibiotics that target mitochondria effectively eradicate cancer stem cells across multiple tumor types: treating cancer like an infectious disease. *Oncotarget* **6**, 4569-4585 (2015).

62. Sahin, E., et al. Telomere dysfunction induces metabolic and mitochondrial compromise. *Nature* **470,** 359-365 (2012).

63. Hu, J., et al. Antitelomearse therapy provokes ALT and mitochondrial adaptive mechanisms in cancer. *Cancer Cell* **148**, 651-663 (2012).

64. Li, F., et al. Myc stimulates nuclearly encoded mitochondrial genes and mitochondrial biogenesis. *Mol Cell Biol* **25**, 6225-6234 (2005).

65. Morrish, F., et al. Myc and mitochondrial biogenesis. *Cold Spring Harb Perspect Med* **4**, 1-16 (2015).

66. Kim, J., et al. Global identification of Myc target genes reveals its direct role in mitochondrial biogenesis and its E-box usage in vivo. *PLOS One* **12**, e1798 *(*2008).

67. Seitz, V., et al. Deep sequencing of MYC DNA-binding sites in Burkitt lymphoma. *PLoS One* **6**, e26837 (2011).

68. Morrish, F., et al. The oncogene c-Myc coordinates regulation of metabolic networks to enable rapid cell cycle entry. *Cell Cycle* **7**, 1054-1066 (2008).

69. Bellance, N., et al. Oncosecretomics coupled to bioenergetics identifies α-amino adipic acid, isoleucine and GABA as potential biomarkers of cancer: Differential expression of c-Myc, Oct1 and KLF4 coordinates metabolic changes. *Biochim Biophys Acta* **1817**, 2060-2071 (2012).

70. Murphy, T.A., et al. Isotopically nonstationary 13C flux analysis of Myc-induced metabolic reprogramming in B-cells. *Metab Eng* **15**, 206-217 (2013).

71. Zhang, H., et al. HIF-1 inhibits mitochondrial biogenesis and cellular respiration in VHL-deficient renal cell carcinoma by repression of c-Myc activity. *Cancer Cell* **11,** 407-20 (2007).

72. Kim, J.W., et al. Evaluation of myc E-box phylogenetic footprints in glycolytic genes by chromatin immunoprecipitation assays. *Mol Cell Biol* **24**, 5923-5936 (2004).

73. Shim, H., et al. c-Myc transactivation of LDH-A: implications for tumor metabolism and growth. *Proc Natl Acad Sci USA* **94**, 6658-6663 (19997).

74. Gao, P., et al. c-Myc suppression of miR-23a/b enhances mitochondrial glutaminase expression and glutamine metabolism. *Nature* **458**, 762-765 (2009).

75. Osthus, R.C., et al. Deregulation of glucose transporter 1 and glycolytic gene expression by c-Myc. *J Biol Chem* **275**, 21797-21800 (2000).

76. Fan, Y., et al. Akt and c-Myc differentially activate cellular metabolic programs and prime cells to bioenergetic inhibition. *J Biol Chem* **285**, 7324-7333 (2010).

77. Stine, Z.E., et al. MYC, Metabolism, and Cancer. *Cancer Discov* **5**, 1024-1039 (2015).

78. Dang, C.V. Glutaminolysis. Supplying carbon or nitrogen or both for cancer cells? *Cell Cycle* **9**, 3884-3886 (2010).

79. Dang, C.V., et al. The c-Myc target gene network. *Semin Cancer Biol* **16**, 253-264 (2006).

80. McKeown, M.R., et al. Therapeutic strategies to inhibit MYC. *Cold Spring Harb Perspect Med* **4**, 1-16 (2014).

81. Meyer, M., et al. Reflecting on 25 years with MYC. *Nat Rev Cancer* **8**, 976-990 (2008).

82. Zhang, J., et al. Role of BNIP3 and NIX in cell death, autophagy, and mitophagy. *Cell Death Differ* **16**, 939-946 (2009).

83. Chinnadurai, G., et al. BNIP3 subfamily BH3-only proteins: mitochondrial stress sensors in normal and pathological functions. *Oncogene* 27, 114-127 (2009)

84. Boyd, J.M., et al. Adenovirus E1B 19 kDa and Bcl-2 proteins interact with a common set of cellular proteins. Cell 21, 341-51 (1994).

85. Ohi, N., et al. A novel adenovirus E1B19K-binding protein B5 inhibits apoptosis induced by Nip3 by forming a heterodimer through the C-terminal hydrophobic region. *Cell Death Differ* **6**, 314-25 (1999).

86. Hardwick, J. M., et al. Snapshot: Bcl2 proteins. *Cell* **23**, 404 (2009).

87. Vande Velde, C., et al. BNIP3 and genetic control of necrosis-like cell death through the mitochondrial permeability transition pore. *Mol Cell Biol* **20,** 5454-5468 (2000).

88. Sulistijo, E.S., et al. Sequence-specific dimerization of the transmembrane domain of the "BH3-only" protein BNIP3 in membranes and detergent. *J Biol Chem* **278,** 51950-51956 (2003).

89. Sulistijo, E.S., et al. Structural Basis for Dimerization of the BNIP3 Transmembrane Domain. *Biochem* **48**, 5106-5120 (2009).

90. Hanna, R.A., et al. Microtubule-associated protein light chain 3 (LC3) interacts with BNip3 protein to selectively remove endoplasmic reticulum and mitochondria via autophagy. *J Biol Chem* **287**, 19094-19104 (2012).

91. Kanki, T., et al. Atg32 is a mitochondrial protein that confers selectivity during mitophagy. *Dev Cell* **17,** 98-109 (2009).

92. Okamoto, K., et al. Mitochondrial-anchored receptor Atg32 mediates degradation of mitochondria via selective autophagy. *Dev Cell* **17,** 87-97 (2009).

93. Ray, R., et al. BNIP3 heterodimerizes with Bcl-2/Bcl-XL and induces cell death independent of a Bcl-2 homology 3 (BH3) domain at both mitochondrial and nonmitochondrial sites. *J Biol Chem* **275**, 1439-1448 (2000).

94. Zhu, Y., et al. Modulation of serines 17 and 24 in the LC3-interacting region of BNIP3 determines pro-survival mitophagy VS. apoptosis. *J Biol Chem* **288**, 1099-1113 (2012).

95. Li, Y., et al. Bnip3 mediates the hypoxia-induced inhibition on mTOR by interacting with Rheb. *J Biol Chem* **282**, 35803-35813 (2007).

96. Lee, Y.K., et al. Mitochondrial autophagy by Bnip3 involves Drp1-mediated mitochondrial fission and recruitment of Parkin in cardiac myocytes. *Am J Physiol Heart Circ Physiol* **301**, 1924-1931 (2011).

97. Quinsay, M.N., et al. BNip3-mediated mitochondrial autophagy is independent of the mitochondrial permeability transition pore. *Autophagy* **6**, 855-862 (2010).

98. Landes, T., et al. The BH3-only BNip3 binds to the dynamin Opa1 to promote mitochondrial fragmentation and apoptosis by distinct mechanisms. *EMBO Rep*. **11**, 459-465 (2010).

99. Glick, D., et al. BNip3 regulates mitochondrial function and lipid metabolism in the liver. *Mol Cell Biol* **32**, 2570-2584 (2012).

100. Zhang, H., et al. Mitochondrial autophagy is a HIF-1-dependent adaptive metabolic response to hypoxia. *J Biol Chem* **283**, 10892-10903 (2008).

101. Bruick, R.K. Expression of the gene encoding the proapoptotic Nip3 protein is induced by hypoxia. *Proc Natl Acad Sci USA* **97,** 9082-9087 (2000).

102. Guo K., et al. Hypoxia induces the expression of the pro-apoptotic gene BNIP3. *Cell Death Diff* **8**, 367-376 (2001).

103. Sowter, H.M., et al. Hif-1-dependent regulation of hypoxic induction of the cell death factors BNIP3 and NIX in human tumors. *Cancer Res* **61**, 6669-6673 (2001).

104. Tracy, K., et al. BNIP3 is an RB/E2F target gene required for hypoxia-induced autophagy. *Mol Cell Biol* **27**, 6229-6242 (2007).

105. Feng, X., et al. p53 directly suppresses BNIP3 expression to protect against hypoxia-induced cell death. *EMBO J* **30,** 3397-3415 (2011).

106. Baetz, D., et al. Nuclear factor-kappaB-mediated cell survival involves transcriptional silencing of the mitochondrial death gene BNIP3 in ventricular myocytes. *Circulation* **112**, 3777-85 (2005).

107. Shaw, J., et al. Antagonism of E2F-1 regulated Bnip3 transcription by NF-kappaB is essential for basal cell survival. *Proc Natl Acad Sci U S A* **105**, 20734-20739 (2008).

108. Mammucari, C., et al. FoxO3 controls autophagy in skeletal muscle in vivo. *Cell Metab* **6**, 458-471 (2007).

109. An, H-J., et al. Activation of Ras up-regulates pro-apoptotic BNip3 in nitric oxide-induced cell death. *J Biol Chem* **281**, 33939-33948 (2006).

110. Kalas, W., et al. H-ras upregulates expression of BNIP3. *Anticancer Res* **31**, 2869-2876 (2011).

111. Wu, S-Y., et al. Ras-related tumorigenesis is suppressed by BNip3-mediated autophagy through inhibition of cell proliferation. *Neoplasia* **13**, 1171-1182 (2011).

112. Sowter, H.M., et al. Expression of the cell death genes BNip3 and NIX in ductal carcinoma *in situ* of the breast; correlation of BNip3 levels with necrosis and grade. *J Pathol* **201**, 573-580 (2003).

113. Koop, E.A., et al. Expression of BNIP3 in invasive breast cancer: correlations with the hypoxic response and clinicopathological features. *BMC Cancer* **9**, 1-8 (2009).

114. Manka, D., et al. Bcl-2/Adenovirus E1B 19 kDa interacting protein-3 knockdown enables growth of breast cancer metastases in the lung, liver, and bone. *Cancer Res* **65**, 11689-11693 (2005).

115. Vijayalingam, S., et al. Overexpression of BH3-only protein BNIP3 leads to enhanced tumor growth. *Genes Cancer* **1**, 964-971 (2010).

116. Chen, X., et al. MicroRNA145 targets BNIP3 and suppresses prostate cancer progression. *Cancer Res* **70**, 2728-2738 (2010).

117. Murai, M., et al. Aberrant DNA methylation associated with silencing BNIP3 expression in hematopoietic tumors. *Br J Cancer* **92**, 1165-1172 (2005).

118. Murai, M., et al. Aberrant methylation and silencing of the BNIP3 gene in colorectal and gastric cancer. *Clin Cancer Res* **11**, 1021-1027 (2005).

119. Castro, M., et al. Multiplexed methylation profiles of tumor suppressor genes and clinical outcome in lung cancer. *J Transl Med* **8**, 1-11 (2010).

120. Calvisi, D.F., et al. Mechanistic and prognostic significance of aberrant methylation in the molecular pathogenesis of human hepatocellular carcinoma. *J Clin Invest* **117**, 2713-2722 (2007).

121. Erkan, M., et al. Loss of BNIP3 expression is a late event in pancreatic cancer contributing to chemoresistance and worsened prognosis. *Oncogene* **24**, 4421-4432 (2005).

122. Akada, M., et al. Intrinsic chemoresistance to Gemcitabine is associated with decreased expression of BNip3 in pancreatic cancer. *Clin Cancer Res* **11**, 3094-3101 (2005).

123. Okami, J., et al. Silencing of the hypoxia-inducible cell death protein BNIP3 in pancreatic cancer. *Cancer Res* **64**, 5338-5346 (2004).

124. Abe, T., et al. Upregulation of BNIP3 by 5-aza-2'-deoxycytidine sensitizes pancreatic cancer cells to hypoxia-mediated cell death. *J Gastroenterol* **40**, 504-510 (2005).

125. Yu, M., et al. Metabolic phenotypes in pancreatic cancer. *PLoS One* **10**, 1-23 (2015).

126. Bardeesy, N., et al. Pancreatic cancer biology and genetics. *Nat Rev Cancer* **2**, 897-909 (2002).

127. Siegel, R.L., et al. Cancer Statistics, 2016. *CA Cancer J Clin* **66**, 7-30 (2016).

128. Weigelt, B., et al. Breast cancer metastasis: markers and models. *Nat Rev Cancer* **5**, 591-602 (2005).

129. Vargo-Gogola, T., et al. Modeling breast cancer: one size does not fit all. *Nat Rev Cancer* **7**, 659-672 (2007).

130. Fantozzi, A., et al. Mouse models of breast cancer metastasis. *Breast Cancer Res* **8**, 1-11 (2006).

131. Lin, E., et al. Progression to malignancy in the polyoma middle T oncoprotein mouse breast cancer model provides a reliable model for human diseases. *Am J Pathol* **163**, 2113-2126 (2003).

132. Hidalgo, M. Pancreatic cancer. *N Engl J Med* **362**, 1605-1617 (2010).

133. Ryan, D.P., et al. Pancreatic adenocarcinoma. *N Engl J Med* **371**, 1039-1049 (2014).

134. Hezel, A.F., et al. Genetics and biology of pancreatic ductal adenocarcinoma. *Genes Dev* **20**, 1218-1249 (2006).

135. Wood, L.D. Pancreatic cancer genomes: toward molecular subtyping and novel approaches to diagnosis and therapy. *Mol Diagn Ther* **17**, 287-297 (2013).

136. Lowy, A.M., et al. Chapter 11-Molecular signaling pathways in pancreatic cancer. *Pancreatic cancer.*

137. Pasca di Magliano, M., et al. Roles for KRAS in pancreatic tumor development and progression. *Gastroenterology* **144**, 1220-1229 (2013).

138. Morris IV, J.P., et al. KRAS, Hedgehog, Wnt and the twisted developmental biology of pancreatic ductal adenocarcinoma. *Nat Rev Cancer* **10**, 683-695 (2010).

139. Leach, S.D. Mouse models of pancreatic cancer: the fur is finally flying! *Cancer Cell* **5**, 7-11 (2004).

140. Mazur, P.K., et al. Genetically engineered mouse models of pancreatic cancer: unraveling tumor biology and progressing translational oncology. *Gut* **61**, 1488-1500 (2012).

141. Yamagata, M., et al. Genetically engineered mouse models for pancreatic cancer: advances and current limitations. *World J Clin Oncol* **10**, 195-202 (2011).

142. Hingorani, S.R., et al. Preinvasive and invasive ductal pancreatic cancer and its early detection in the mouse. *Cancer Cell* **4**, 437-450 (2003).

143. Tuveson, D.A., et al. Ductal pancreatic cancer in humans and mice. Cold *Spring Harb Symp Quant Biol* **70**, 65-72 (2005).

144. Bardeesy, N., et al. Both p16INK4a and the p19Arf-p53 pathway constrain progression of pancreatic adenocarcinoma in the mouse. *Proc Natl Acad Sci U S A* **103**, 5947-5952 (2006).

145. Hingorani, S.R., et al. Trp53R172H and KrasG12D cooperate to promote chromosomal instability and widely metastatic pancreatic ductal adenocarcinoma in mice. *Cancer Cell* **7**, 469-483 (2005).

146. Diwan, A., et al. Inhibition of ischemic cardiomyocyte apoptosis through targeted ablation of Bnip3 restrains postinfarction remodeling in mice. *J Clin Invest* **117**, 2825-2833 (2007).

147. Debnath, J., et al. Morphogenesis and oncogenesis of MCF-10A mammary epithelial acini grown in three-dimensional basement membrane cultures. *Methods* **30**, 256-268 (2003).

148. Yuan, M., et al. A positive/negative ion-switching, targeted mass spectrometry-based metabolomics platform for bodily fluids, cells, and fresh and fixed tissue. *Nat Protoc* **7**, 872-881 (2012).

149. Dranka, B.P., et al. Assessing bioenergetic function in response to oxidative stress by metabolic profiling. *Free Radic Biol Med* **51**, 1621-1635 (2011).

150. Chourasia, A.H., et al. Mitophagy defects arising from BNip3 loss promote mammary tumor progression to metastasis. *EMBO Rep* **16**, 1145-1163 (2015).

151. Lehmann, B.D., et al. Identification of human triple-negative breast cancer subtypes and preclinical models for selection of targeted therapies. *J Clin Invest* **121**, 2750-2767 (2011).

152. Schindl, M., et al. Overexpression of hypoxia-inducible factor 1alpha is associated with an unfavorable prognosis in lymph node-positive breast cancer. *Clin Cancer Res* **8**, 1831-1837 (2002).

153. Gruber, G., et al. Hypoxia-inducible factor 1 alpha in high-risk breast cancer: an independent prognostic parameter? *Breast Cancer Res* 6, 191-198 (2004).

154. Schwab, L.P., et al. Hypoxia-inducible factor 1α promotes primary tumor growth and tumor-initiating cell activity in breast cancer. *Breast Cancer Res* **14**, R6 (2012).

155. Montagner, M., et al. SHARP1 suppresses breast cancer metastasis by promoting degradation of hypoxia-inducible factors. *Nature* **487**, 380-384 (2012).

156. Erler, J.T., et al. Lysyl oxidase is essential for hypoxia-induced metastasis. *Nature* **440**, 1222-1226 (2006).

157. Wong, C.C., et al. Hypoxia-inducible factor 1 is a master regulator of breast cancer metastatic niche formation. *Proc Natl Acad Sci U S A* **108**, 16369-16374 (2011).

158. Javadov, S., et al. Mitochondrial permeability transition and cell death: the role of cyclophilin d. *Front Physiol* **4**, 1-5 (2013).

159. Shoshan-Barmatz, V., et al. VDAC-1: from structure to cancer therapy. *Front Oncol* **2**, 1-34 (2012).

160. Plathow, C., et al. Tumor cell metabolism imaging. *J Nuc Med* **49**, 43-63 (2008).

161. O'Neil, R.G., et al. Uptake of a fluorescent deoxyglucose analog (2-NBDG) in tumor cells. *Mol Imaging Biol* **7**, 388-392 (2005).

162. Thompson, C. Rethinking the regulation of cellular metabolism. *Cold Spring Harb Symp Quant Biol* 76, 23-29 (2011).

163. Cairns, R.A., et al. Regulation of cancer cell metabolism. *Nat Rev Cancer* **11**, 85-95 (2011).

164. Keith, B., et al. HIF1α and HIF2α: sibling rivalry in hypoxic tumour growth and progression. *Nat Rev Cancer* **12**, 9-22 (2011).

165. Kong, D., et al. Echinomycin, a small-molecule inhibitor of hypoxia-inducible factor-1 DNA-binding activity. *Cancer Res* **65**, 9047-9055 (2005).

166. Forkink, M., et al. Live-cell assessment of mitochondrial reactive oxygen species using dihydroethidine. *Methods Mol Biol* **1264**, 161-169 (2015).

167. Iverson, F. *In vivo* studies on butylated hydroxyanisole. *Food Chem Toxicol* **37**, 993-997 (19991).

168. Galluzi, L., et al. Autophagy in malignant transformation and cancer progression. *EMBO J* **34**, 856-880 (2015).

169. Guo, J.Y., et al. Autophagy suppresses progression of K-ras-induced lung tumors to oncocytomas and maintains lipid homeostasis. *Genes Dev* **27**, 1447-1461 (2013).

170. Rosenfeldt, M.T., et al. p53 status determines the role of autophagy in pancreatic tumour development. *Nature* **504**, 296-300 (2013).

171. Pathania, D., et al. Opportunities in discovery and delivery of anticancer drugs targeting mitochondria and cancer cell metabolism. *Adv Drug Deliv Rev* **61**, 1250-1275 (2009).

172. Barth, S., et al. Autophagy: assays and artifacts. *J Pathol* **221**, 117-124 (2010).

173. Vervoorts, J., et al. The ins and outs of MYC regulation by posttranslational mechanisms. *J Biol Chem* **281**, 34725-34729 (2006).

174. Vervoorts, J., et al. Stimulation of c-MYC transcriptional activity and acetylation by recruitment of the cofactor CBP. *EMBO Rep* **4**, 484-490 (2003).

175. Gregory, M.A., et al. Phosphorylation by Glycogen Synthase Kinase-3 Controls c-Myc Proteolysis and Subnuclear Localization. *J Biol Chem* **278**, 51606-51612 (2003).

176. Soucek, L., et al. Modelling Myc inhibition as a cancer therapy. *Nature* **455**, 679-683 (2008).

177. Asano, T., et al. The PI3-kinase/Akt signaling pathway is activated due to aberrant Pten expression and targets transcription factors NF-κB and c-Myc in pancreatic cancer cells. *Oncogene* **23**, 8571-8580 (2004).

178. Schleger, C., et al. c-MYC activation in primary and metastatic ductal adenocarcinoma of the pancreas: incidence, mechanisms, and clinical significance. *Mod Pathol* **15**, 462-469 (2002).

179. Li, Y.J., et al. Beta-catenin up-regulates the expression of cyclinD1, c-myc and MMP-7 in human pancreatic cancer: relationships with carcinogenesis and metastasis. *World J Gastroenterol* **11**, 2117-2123 (2005).

180. Rikka, S., et al. Bnip3 impairs mitochondrial bioenergetics and stimulates mitochondrial turnover. *Cell Death Differ* **18**, 721-731 (2011).

181. Yin, X., et al. Low molecular weight inhibitors of Myc-Max interaction and function. Oncogene 22, 6151-6159 (2003).

182. Prochownik, E.V., et al. Therapeutic Targeting of Myc. *Genes Cancer* **1**, 650-659 (2010).

183. Kim, S., et al. Metabolic phenotypes in triple-negative breast cancer. *Tumour Biol* **34**, 1699-1712 (2013).

184. White, E., et al. Autophagy, metabolism, and cancer. *Clin Cancer Res* **21**, 5037-5046 (2015).

185. Thompson, J.W., et al. Bnip3 Binds and Activates p300: Possible Role in Cardiac Transcription and Myocyte Morphology. *PLoS One* **10**, e0136847 (2015).